POLITECNICO DI TORINO

SCUOLA DI DOTTORATO

Dottorato in Matematica per le Scienze dell'Ingegneria - XXVI Ciclo

Settore disciplinare: MATEMATICA - MAT/08

Thesis submitted for the degree of Doctor of Philosophy

"Multispecies" models to describe large neuronal networks

Relatori:
Prof. Claudio Canuto
Prof. Luigi Preziosi

Presentata da:
Anna Cattani

Marzo 2014

To my family

To a future wolf

Acknowledgements

My Ph.D. degree has been one of the most exciting events in the first 28 years of my life. I say exciting because, beyond the hard work of these three years, I have been involved in one of the most fascinating research subjects ever: the human brain.

Of course, apart from the exciting subject, the people I have shared these moments with have been those who have made this work not only possible but also very interesting. Below are some of them I would particularly like to thank. Of course, the people I have met during these years and who have helped me grow from scientific and human perspective are many more than those I am able to include here.

My first debt of gratitude must go to my advisor, Prof. Claudio Canuto. He patiently provided the vision, encouragement and advise necessary for me to proceed through the doctoral program and to complete my dissertation. Moreover, it was he who led me to work in this subject.

Special thanks to my co-advisor, Prof. Luigi Preziosi for his support, guidance and helpful suggestions. His guidance has served me well and I owe him my heartfelt appreciation.

I would like to express my deepest gratitude to several professors and researchers who provided me with precious suggestions about the work-in-progress thesis. Prof. Laura Sacerdote for her guidance concerning my first steps in the neuroscientific community and for providing me with international contacts. Prof. Henry Tuckwell for discussing with me about FitzHugh-Nagumo model features. I am proud to have communicated with such an important professor, and his help turned out to be absolutely priceless. Prof. Giovanni Naldi for initial suggestions. Ph.D. Sergio Solinas for his excellent guidance, care, patience, and for providing me with excellent input about doing research and imaging future developments. Prof. Piero Colli Franzone for helping me exploit the XPP AUT software. Ph.D. Paolo Bardella for helping me with Matlab issues. Prof.

Nicolas Brunel for his suggestions about exploiting non-regular grid in simulations. Prof.Rinaldo Colombo and Prof. Graziano Guerra for having let me sample research for the first time: it is thanks to them if I decided to do my Ph.D.

I would like to highlight that not only did these people give me precious technical advices, but I thank them all even more for their contagious passion for research. Moreover, together with the passion they feel for their work, they did not hesitate to share their knowledge and experiences with me. I am not exaggerating by saying that they have been models for me.

I shared the best and worst moments of my doctoral journey with many people I have been in touch with every day. It has been a great privilege to spend several years in the Department of Mathematical Sciences at Turin Polythecnic, and its members will always remain dear to me. In particular, my office-mates Moreno, Stefano and Chiara gave me incommensurable support in my work and in every day life. They are true friends.

I would like to thank my brother Davide for his help in overcoming problems concerning many diverse topics: from technical assistance to moral support to raise my spirits in moment of difficulties. Of course, he was always with me in the moment of joy, as well.

I would also like to thank my parents who have always supported me and encouraged me with their best wishes.

And finally, of course, I would like to thank all my friends.

Contents

Introduction

In recent years, brain studies have come onto the scene as a fascinating challenge. Beyond a thirst for knowledge itself, many practical reasons for unveiling brain features and mechanisms exist. In fact, unravelling brain architectures and functioning would mean we have the possibility of treating diseases that are crippling humanity, and achieving great technological advances. Both goals would unimaginably improve our quality of life.

Within this big picture, the art of modelling is an essential tool and mathematical theoretical insights give valuable contributions. These concern both the formalization of simplified models used for capturing complex brain structures and dynamics, the description of neural computation at different levels of brain organisation, and the characterization of brain functions which most imaging techniques record.

The brain is believed to be the most complex organ in the human body. A huge number of ingredients interact to give rise to its biological tissues and its functions. Indeed, there are about twenty billion neurons in the brain, each of them linked to as many as ten thousand others. Moreover, highly nonlinear dynamics underlying single cell behaviour and the interactions among them give rise to enormous complexity which we can only strive to manage by means of the famous Picasso quote:

> "Modelling is the lie that reveals the Truth."

This means that by exploiting mathematical instruments we are able to make a synthesis process from an extremely complex reality, and to make predictions to be later evaluated by experiments.

For modelling purposes, one can imagine the brain as a large network constituted by a collection of diverse smaller ones. Zooming into smaller areas, the same picture arises: several kinds of neuronal populations interact with each other. Of course, signal

transmissions among neurons within the same population also exist. In particular, we assume neurons belonging to the same population have the same features. Differently from other approaches for large-scale modelling, the present work attempts to describe brain areas without ignoring intrinsic differences among neuronal populations through what we call *multispecies models*. Such models are based on the assumption that differences in population densities, often by several orders of magnitude, let the single population be modelled by a discrete or a continuous model. Considering only two populations, for instance, a *multispecies model* consists in an ODEs system for each cell of the low-density population, combined with only one PDEs system for the whole high-density population.

The formalization of the *multispecies model* is the end product of my Ph.D. thesis, which follows a logical path of reasoning from the necessary starting concepts through the research results. Since the first step is the description of the single neuron in the network, Chapter 1 is concerned with the FitzHugh-Nagumo model, subsequently exploited in the whole thesis. More specifically, we start by deducing the model starting from the Hodgkin-Huxley system and continue by analysing its features and its limitations, as a means to define the type II neuron. Let us stress that replacing the FitzHugh-Nagumo model by another one of type II in literature, would lead to results qualitatively similar to those presented in the whole thesis. In order to describe a network, links among the single units are the second most important ingredient. Neurons interact with each other within a fully-organized ensemble which consists of two connection types: electrical and chemical synapses. Chapter 2 takes into account cells coupled by electrical synapses. Chapter 3 involves the more complex phenomena underlying chemical synapses. In both chapters, after setting mathematical models of idealized neurons with only electrical-type or chemical-type couplings among them, we carefully investigate the "passage to the limit", as the number of neurons tends to infinity while remaining confined in a fixed and bounded spatial region. Chapter 4 provides results concerning the more realistic network with both coupling types considered together. Referring to such a continuous model several simulations are performed in order to describe the membrane potential dynamics in such a network. In Chapter 5 we come to the formalization of the *multispecies model* by applying it to a concrete network: the Golgi-Granular loop in the Cerebellum. This model formalization is promising and should be explored in future by adding few more ingredients omitted in this work: the plasticity mechanism and the delay underlying synapses. Furthermore, since stochasticity is a fundamental issue in the mathematical description of biological system, parameters as random variables should be embedded in the model.

Modelling and computer simulations of complex networks with a huge number of nodes is a formidable challenge. The intrinsic difficulties concerning the high number of neurons may be alleviated to some extent by exploiting the *multispecies models* in which the presence of the continuous model allows simulation costs to be highly reduced. Indeed, by modelling the high-density population on the whole domain with only a PDEs model, we avoid the computationally prohibitive cost of describing the huge number of dense cells by ODEs. Moreover, since populations are supposed to interact with each other, multiscale peculiarities can emerge between the coefficients in the models, e.g., conductance coefficients can differ by several orders of magnitude between discrete and continuous models.

To conclude, identifying the suitable level of modelling for a specific problem is often difficult. Thanks to the *multispecies models*, which combine different levels, we are able to model networks maintaining differences among populations and, at the same time, to reduce the computational cost.

Chapter 1

Models in literature

In order to introduce the models which describe the dynamics of neurons, let us start to briefly explain the biological background. First of all, let us deepen the function and the structure of neuron which is the fundamental part of the nervous tissue. It allows the spikes reception and diffusion and the communication with the nervous system which controls everything, from movement and speech to breathing and digestion. In particular, the nervous system takes in sensory information, processes it, and then tells the body how to respond. From the central nervous system's control centered in the brain and spinal cord, information is constantly moving to and from the network of nerve cells in the peripheral nervous system.

As described in Figure 1.1, neurons are constituted by a cell body, called *soma*, *dendrites* which are thin structures that arise from the cell body and an *axon* which is a nerve fiber that conducts electrical impulses away from the soma. The impulses from other cells are led to the axon which in turn leads them to muscles or other cells. At the cellular level these messages are passed from neuron to neuron by way of electrical impulses and chemical signals. When a neuron fires, an electrical impulse, known as an *action potential*, travels along its axon. From one neuron to another this signal must cross the small space, called the *synapse*, between the end of one nerve cell's axon and the dendrites of another cell. Because the action potential cannot pass over this gap, when it reaches the end of the axon, chemicals called *neurotransmitters* are released into the synaptic cleft close to the dendrites of the next neuron, and eventually cause that neuron fires. In order that the action potential begins to move down the axon, ion channels in the cells membrane must be opened, allowing the voltage between the inside and the outside of the cell to rise above its resting state at -75 millivolts. While at rest only potassium ions can pass through the cell membrane, at the moment in

which the resting potential grows an action potential begins to travel along the axon by opening sodium ion channels along the way. The result of this process is that the cell rapidly becomes more positive than the outside in a stage known as *depolarization*. This depolarizing effect travels along the front of the action potential as it moves down the axon. After that, the cell repolarizes when potassium ions rush outward across the membrane restoring it to its resting potential. The almost instantaneous change in potential produced by depolarization and repolarization creates a pattern called *spike discharge*. When the action potential reaches the end of the axon, it opens calcium ion channels thus increasing the concentration of calcium ions inside the cell. This increase in calcium ions triggers the release of neurotransmitters into the synaptic cleft, and in so doing triggers a nerve impulse in a neighboring neuron.

Some of the models concerning action potential generation in neurons we decide to focus on the Hodgkin-Huxley [26] and FitzHugh-Nagumo [17] ones. In order to cite several alternatives, many other models which will not be analysed here are the following: integrate-and-fire [37, 51], Brette-Gerstner [10], Morris-Lecal [40], Hindmarsh-Rose [25], Izhikevich [30]. Thanks to these models, different levels of details are possible to be obtained but in general, with except for the Hodgkin-Huxley model, the cited ones present minimal dynamics range which reduces the real variety of neuronal behaviour. All models in literature can be collected in categories. Thus, the *conductance-based models* are characterized by a reasonable description of the neuronal dynamics but they are expensive by computational perspective and near to impossible for analytical treatments, the Hodgking-Huxley model is one of them. Going toward the direction of reduce the complexity, the *generic bifurcation models* provide a qualitative description of a wide range of neuronal behaviour. The FitzHugh-Nagumo models belongs in this category. The *threshold models* are marked by a threshold in the voltage which, if is overcame, cause a spike. By exploiting models like these, the informations concerning the spike, as the height and the form of the spike are lost. This is due to the fact that just after the voltage reaches the threshold is reset to the quiescent value of the voltage. A complete explanation of the threshold models are performed in [21]. Finally, the *rate models*, which are the less computationally demanding, describe only the spike rate or the frequency.

1.1 The Hodgkin-Huxley equations

Neurons, in particular the squid giant axon, are the object of study of Alan Hodgkin and Andrew Huxley during the '50s, whose model is presented in [26]. The main purpose

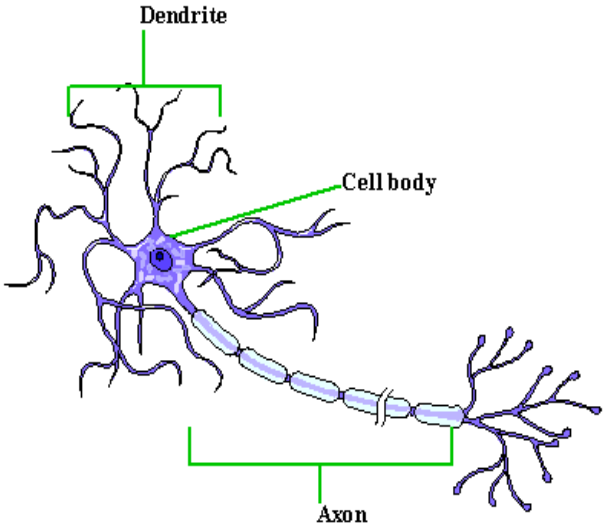

Figure 1.1: Structure of a single neuron.

of Hodgkin and Huxley is to understand and describe the action potential generation in a neuron starting from the idea that a neuron can be studied as other cells enclosed by a membrane which separates the interior of the cell from the extracellular space. Due to the distribution of ions and the permeability of the cell membrane, between the inside and outside of a cell, there is always a potential difference. As described at the beginning of this chapter, the cell will undergo an action potential when it is sufficiently depolarized. This is a temporary change in the potential difference over the membrane. In order to explain how Hodgkin and Huxley derived their model, let us stress that the most important properties of the membrane can be collected in the electric circuit shown in Figure 1.2, from [26]. This circuit is appropriate for simple membrane systems like the squid giant axon or other axonal membranes. In the model there is a capacitor C_M, to represent the lipid bilayer membrane, a sodium resistance R_{Na}, potassium resistance R_K and a leakage resistance R_l. The membrane potential v is the potential inside the cell minus the potential outside and there can be a current I injected into the cell from an electrode or from other parts of the cell. The model in Figure 1.2 represents a patch of membrane, i.e., a small area of membrane which is isopotential, meaning that the membrane potential v is constant across the patch. In models like this, two things are assumed. Firstly, the number of channels is large enough that individual gating events are averaged out and the sodium (Na^+) and potassium (K^+) currents are smooth population currents. Secondly, the channels are not arranged in any way which allows special local interactions among small numbers of channels. In

this model, the channels interact only through v.

The subsequent step consists of expressing the circuit in Figure 1.2 as a set of equations using the laws by Ohm and Kirchhoff. To obtain the Hodgkin-Huxley equations, we follow the approach by J. Murray in [41]. See [34, 52] for full references. The cur-

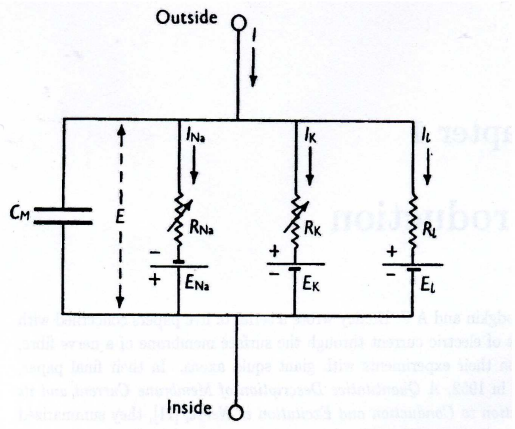

Figure 1.2: Electrical circuit model of the cell membrane.

rent $I(t)$ is made up by the currents due to ions which pass through the membrane and the contribution from the time variation in the transmembrane potential, that is, the membrane capacitance contribution. Thus we have,

$$I(t) = C_M \frac{\mathrm{d}v}{\mathrm{d}t} + I_i, \tag{1.1}$$

where v is the voltage, C_M the membrane capacity and I_i the ionic currents. Based on Ohm and Kirchhoff laws, Hodgkin and Huxley imposed

$$I_i = I_{Na} + I_K + I_L = \bar{g}_{Na} m^3 h (v - v_{Na}) + \bar{g}_K n^4 (v - v_K) + \bar{g}_L (v - v_L), \tag{1.2}$$

where the ionic current is specified into components carried out by sodium (I_{Na}), potassium (I_K) and the residual (I_L) where L stands for leakage. In the second equality, each current is then associated with a conductance and a driving force which is due to the different concentrations of ions in the intracellular and extracellular media of the cell, where v_{Na}, v_K and v_L are the Nernst potentials of each channel. Let us stress that the Nernst potential proper to each channel is the potential value at which that specific

ionic current vanishes. Furthermore, we define the ionic conductances as follows:

$$\begin{aligned} g_{Na} &= \bar{g}_{Na} m^3 h, \\ g_K &= \bar{g}_K n^4. \end{aligned} \tag{1.3}$$

Let us underline that the conductances in Eq. (1.3) are linked to the resistances in Figure 1.2 by the following relations: $g_{Na} = 1/R_{Na}$, $g_K = 1/R_K$ and $g_L = 1/R_L$. By going further, the ingredients m, n and h in (1.3) are variables, bounded by 0 and 1, which are determined by the following differential equations:

$$\begin{aligned} \frac{\mathrm{d}m}{\mathrm{d}t} &= \alpha_m(1-m) - \beta_m m, \\ \frac{\mathrm{d}n}{\mathrm{d}t} &= \alpha_n(1-n) - \beta_n n, \\ \frac{\mathrm{d}h}{\mathrm{d}t} &= \alpha_h(1-h) - \beta_h h. \end{aligned} \tag{1.4}$$

In particular, the variables m and h describe the activation and the inactivation of the Na^+ channel, respectively. While n rules the opening and closing of K^+ gates. Thus, the equations (1.3) are formalized by Hodgkin-Huxley by modelling the ionic channels as consisting of multiple subunits, each of which obeys a simple two-state model. The Na^+ gating equations derive from the assumption that the Na^+ channel consists of three "m" gates and one "h" gate, each of which can be either closed or open. Since the gates operate independently, then the fraction of open Na^+ channel is m^3h, where m and h obey the equation of the two-state channel model. Similarly, since there are four "n" gates per K^+ channel, all of which must be open for K^+ to flow, then the fraction of open K^+ channels is n^4.

In [34], the expressions of the α and β functions, in units of $(\mathrm{ms})^{-1}$, are presented. They are:

$$\begin{aligned} \alpha_m &= 0.1 \frac{25 - v}{\exp\left(\frac{25-v}{10}\right) - 1}, \\ \beta_m &= 4 \exp\left(\frac{-v}{18}\right), \\ \alpha_h &= 0.07 \exp\left(\frac{-v}{20}\right), \\ \beta_h &= \frac{1}{\exp\left(\frac{30-v}{10}\right) + 1}, \end{aligned}$$

and,

$$\alpha_n = 0.01\frac{10-v}{\exp\left(\frac{10-v}{10}\right)-1},$$
$$\beta_n = 0.125\exp\left(\frac{-v}{80}\right),$$

while the remaining parameters are

$$\bar{g}_{Na} = 120, \quad \bar{g}_K = 36 \quad \text{and} \quad \bar{g}_L = 0.3.$$

Let us stress that these parameters enable to determine the conductances g_{Na}, g_K in (1.3), which are in units of mS/cm^2.

Another recurrent form of Eq. (1.4) is the following:

$$\begin{aligned}\frac{\mathrm{d}m}{\mathrm{d}t} &= \frac{m_\infty(v)-m}{\tau_m(v)},\\ \frac{\mathrm{d}n}{\mathrm{d}t} &= \frac{n_\infty(v)-n}{\tau_n(v)},\\ \frac{\mathrm{d}h}{\mathrm{d}t} &= \frac{h_\infty(v)-h}{\tau_h(v)},\end{aligned} \tag{1.5}$$

which depend on $x_\infty(v)$ and $\tau_x(v)$ (for $x = m, n, h$) as functions of the membrane potential only. In particular, the $x_\infty(v)$ are the steady state values of m, n and h at a particular membrane potential and the $\tau_x(v)$ functions are the time constants at which m, n and h change in responses to changes in v.

Now, if an applied current $I_{app}(t)$ is imposed, using Eq. (1.2), Eq. (1.1) becomes:

$$C_m\frac{\mathrm{d}v}{\mathrm{d}t} = -\bar{g}_K n^4(v-v_K) - \bar{g}_{Na}m^3h(v-v_{Na}) - \bar{g}_L(v-v_L) + I_{app}. \tag{1.6}$$

The system constituted by (1.4)-(1.6), or equivalently (1.5)-(1.6), is the so-called Hodgkin-Huxley model, which we reproduce here:

$$\begin{aligned}C_m\frac{\mathrm{d}v}{\mathrm{d}t} &= -\bar{g}_K n^4(v-v_K) - \bar{g}_{Na}m^3h(v-v_{Na}) - \bar{g}_L(v-v_L) + I_{app},\\ \frac{\mathrm{d}m}{\mathrm{d}t} &= \alpha_m(1-m) - \beta_m m,\\ \frac{\mathrm{d}n}{\mathrm{d}t} &= \alpha_n(1-n) - \beta_n n,\\ \frac{\mathrm{d}h}{\mathrm{d}t} &= \alpha_h(1-h) - \beta_h h.\end{aligned} \tag{1.7}$$

The equations (1.7) are supplemented by suitable initial conditions.

1.2 Qualitative analysis of Hodgkin-Huxley equations

During the 60's FitzHugh provided an useful qualitative analysis of Eq. (1.7). As presented in [34], it has an elegant qualitative description that allows a better understanding of the model behavior. In FitzHugh's article, [17], on Hodgkin-Huxley equations, is underlined that the phase space (V, m, n, h) can be divided in two subsystems: (v, m) constituted by the fast variables and (n, h) constituted by the slow ones. Considering only two of the four variables, the full four-dimensional phase space can be reduced and simplified.

1.2.1 Fast phase plane analysis

The presence in Eq. (1.7) of the slow variables leads to the fact that during the initial phase of the action potential, n and h remain essentially unchanged while m and v vary. This allows to simplify the full four-dimensional phase space by fixing the slow variables and considering the behavior of the model as a function of only the two fast variables. Of course, this analysis is valid only for the initial stages of the action potential. In fact, as soon as the slow variables n and h start to change, this system becomes invalid.

In order to provide this qualitative description, let us fix the slow variables n and h at their resting states, respectively n_0 and h_0, and consider how is the response of m and v after a stimulus. The fast phase plane is described by the following differential equations which can be studied in the (m, v) phase plane:

$$\begin{aligned} C_m \frac{\mathrm{d}v}{\mathrm{d}t} &= -\bar{g}_K n_0^4 (v - v_K) - \bar{g}_{Na} m^3 h_0 (v - v_{Na}) - \bar{g}_L (v - v_L) + I_{app}, \\ \frac{\mathrm{d}m}{\mathrm{d}t} &= \alpha_m (1 - m) - \beta_m m \ . \end{aligned} \tag{1.8}$$

Specifically, Figure 1.3 shows the nullclines $\mathrm{d}v \,/\, \mathrm{d}t = 0$, $\mathrm{d}m \,/\, \mathrm{d}t = 0$ and two sample trajectories. The m and v nullclines intersect each other in three points called, according to the notation in [34], v_r, v_s and v_e which mean *resting*, *saddle* and *excited* point, respectively. These points represent the steady states of Eq. (1.8) but not of the full model in Eq. (1.7). In particular, v_r and v_e are stable states while v_s is a saddle point. The one-dimensional stable manifold described by v_s, shown in Figure 1.3, divides the (m, v)-plane in two regions. Trajectories having initial membrane potential just on the left and just on the right of this threshold follow the unstable manifolds, ending in one or the other stable equilibrium potential. However, as pointed out before, the behavior of the reduced system depends on the values chosen for the variable states that are held constant. First of all, let us note that since $v_e > v_r$, then $h_\infty(v_e) < h_\infty(v_r)$ and

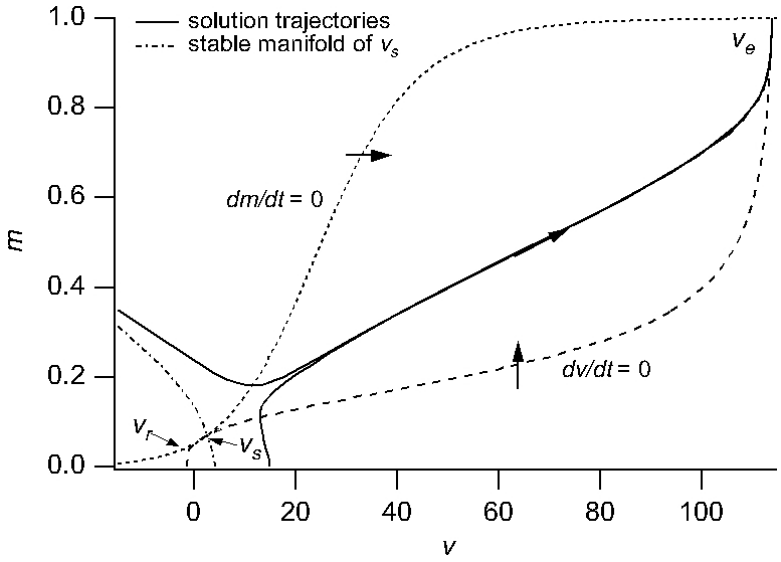

Figure 1.3: The Hodgkin-Huxley fast phase plane. Nullclines $\mathrm{d}v\,/\,\mathrm{d}t = 0$ and $\mathrm{d}m\,/\,\mathrm{d}t = 0$ are shown with two sample trajectories. The saddle point v_s describes a manifold which is also represented. This figure is generated by considering $h_0 = 0.596$ and $n_0 = 0.3176$.

$n_\infty(v_e) > n_\infty(v_r)$. Hence, while v is at the excited state, h begins to decrease, thus inactivating the Na^+ conductance, and n starts to increase thus activating the K^+ conductance. Furthermore, let us remember that v nullclines are not independent of n and h as shown in Figure. 1.4. Specifically, as h decreases, the v nullcline moves vertically upward. The result is that the saddle node moves to the right along the m nullcline. As the saddle moves, the downward-pointing stable manifold is dragged along. Since this manifold is the threshold separatrix, a threshold increasing arises. This behaviour in the phase plane physiologically corresponds to the fact that, as h decreases, sodium channels are inactivated and therefore unavailable to participate in action potentials. The limit case is that, as n increases and h decreases, v_e and v_s move toward each other and they collapse. The new point will be a saddle-node bifurcation and v_r remains the unique stable steady state reached by the solution. Otherwise, the combined effect of reducing n and increasing h is to move the v nullcline downward, eliminating the intersection of the nullcline near the rest potential. As a result, there is now no stable equilibrium point in the reduced system except for v_e. The effect is that the system undergoes a rapid depolarization which leads to an action potential in the full system.

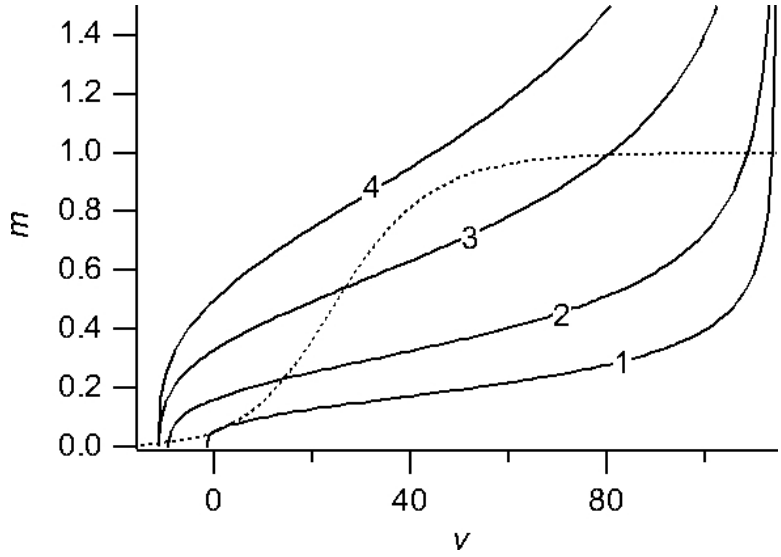

Figure 1.4: Slow variables affect the position of the v nullcline which is represented by solid line in four different cases. The figure shows the movement of v nullcline and the disappearance of the steady state. The four different v nullclines are generated by considering: (1) $h_0 = 0.596$, $n_0 = 0.3176$; (2) $h_0 = 0.4$, $n_0 = 0.5$; (3) $h_0 = 0.2$, $n_0 = 0.7$; (4) $h_0 = 0.1$, $n_0 = 0.8$.

1.2.2 Fast-slow phase plane analysis

Another reduced system can be constructed from the Hodgkin-Huxley model (see Eq. (1.7)) by eliminating m and h leaving v and n. This corresponds to assume that m is always at equilibrium, i.e., $m = m_\infty(v)$. Physiologically, it is equivalent to suppose that the activation of the Na^+ conductances is on a faster time scale than that of the voltage. Next, FitzHugh noted that n and $-h$ have the same shape in the numerical simulations. Specifically, $n + h \approx 0.8$ and thus h can be eliminated by imposing $h = 0.8 - n$. In other words, the model assumes that some sodium channels, $(0.8 - n)$, have lost their activation gates, so that their conductance is gated only by the activation gate m. The resulting model contains only two state variables and can be written as

$$\begin{aligned} C_m \frac{\mathrm{d}v}{\mathrm{d}t} &= -\bar{g}_K n_0^4 (v - v_K) - \bar{g}_{Na} m^3 (0.8 - n)(v - v_{Na}) - \bar{g}_L (v - v_L) + I_{app}, \\ \frac{\mathrm{d}n}{\mathrm{d}t} &= \alpha_n (1 - n) - \beta_n n \ . \end{aligned} \tag{1.9}$$

To tackle the phase plane analysis for this system, let us introduced the function $f(v,n)$ and $g(v,n)$ as in the case of the system with both fast variables. In particular,

$$-f(v,n) = \bar{g}_K n_0^4 (v - v_K) + \bar{g}_{Na} m^3 (0.8 - n)(v - v_{Na}) + \bar{g}_L (v - v_L).$$

The v nullcline, defined by $f(v,n) = 0$, has a cubic shape while n nullcline is monotonically increasing. Nullclines are shown in Figure 1.5, respectively with dashed and dotted lines. There is a unique intersection between these two curves and thus, for this system, there is a single steady state. Precisely, the curve $f(v,n) = 0$ is called *slow manifold* since the solution of Eq. (1.9), shown in Figure 1.5 with full line, is almost horizontal except where $f(v,n) \approx 0$. Therefore, along the slow manifold the solution moves slowly accordingly to the sign of $\mathrm{d}n\,/\,\mathrm{d}t$ but away from the slow manifold it moves quickly in a horizontal direction.

To complete this analysis, let us underline the close relationship between the fast and the fast-slow phase plane analysis. Recall that, by imposing $n = n_0$ and $h = h_0$ in the fast phase plane, the v and m nullclines have three intersection points called v_r, v_s and v_e. In the case of fast-slow phase plane, when n is fixed at n_0, the equation $f(v, n_0) = 0$ has exactly three possible solutions which correspond to that mentioned before.

As discussed in the next section, the formulation of Hodgkin-Huxley equations in terms of two variables, one fast and one slow, is the basis of the fundamental FitzHugh-Nagumo model.

1.3 FitzHugh-Nagumo Model Reduction

The FitzHugh-Nagumo model extracts the previously explained Hodgkin-Huxley fast-slow phase plane and presents it in a simplified form. Thus, the model is constituted by two equations in two variables v and r. The first is the fast variable called *excitatory* while the second is the slow one called *recovery variable*. Being a two-dimensional fast/slow system, it has the following form:

$$\begin{aligned} \frac{\mathrm{d}v}{\mathrm{d}t} &= f(v,r) \\ \frac{\mathrm{d}r}{\mathrm{d}t} &= \epsilon \tilde{g}(v,r)\ , \end{aligned} \tag{1.10}$$

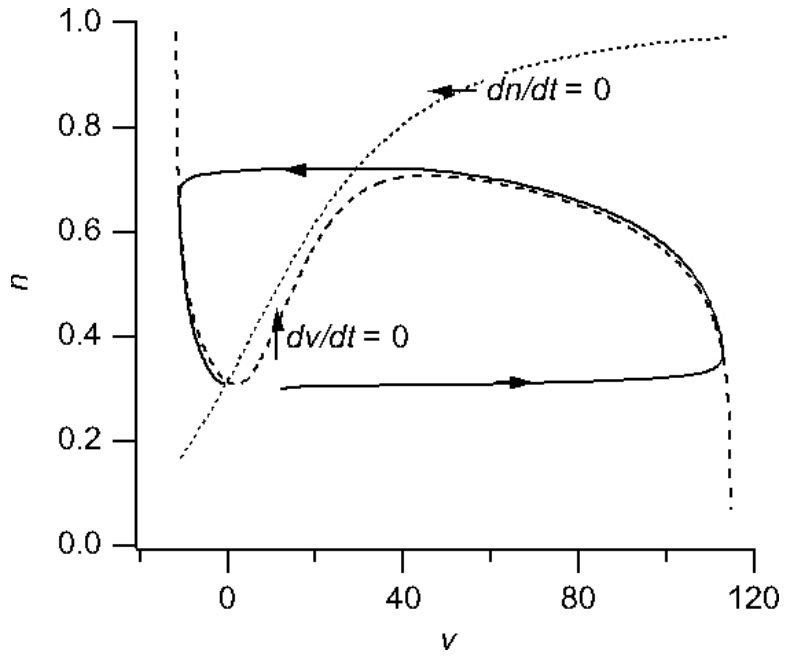

Figure 1.5: The Hodgkin-Huxley fast-slow phase plane with $I = 0$. Nullclines $\mathrm{d}v\,/\,\mathrm{d}t = 0$ and $\mathrm{d}n\,/\,\mathrm{d}t = 0$ are shown with one sample solution.

where the parameter $0 < \epsilon \ll 1$ describes the ratio of time scales of the variable v and r. Using the notation in [41], the FitzHugh-Nagumo equations are as follows:

$$\begin{aligned} \frac{\mathrm{d}v}{\mathrm{d}t} &= -v(a-v)(1-v) - r + I \\ \frac{\mathrm{d}r}{\mathrm{d}t} &= bv - cr \ . \end{aligned} \tag{1.11}$$

where, a, b, $c \in \mathbb{R}^+\backslash\{0\}$ and $I \in \mathbb{R}^+$ are the parameters of the model. One of the interesting aspects of this model is that it can be studied using phase-plane technique whose first step consists in determining the steady states $(\bar{v}, \bar{r})$. These are obtained by imposing the nullcline intersection $f(\bar{v}, \bar{r}) = g(\bar{v}, \bar{r}) = 0$, where $f(v, r)$ and $g(v, r)$ are the right-hand side in Eq. (1.11):

$$\begin{aligned} f(v, r) &= -v(a-v)(1-v) - r + I \\ g(v, r) &= bv - cr \ . \end{aligned} \tag{1.12}$$

In the sequel, let us consider a framework in which a unique equilibrium point exists. In particular, the following condition, that holds for all I, can be imposed:

Proposition 1.1. Under the condition:

$$\frac{b}{c} > \frac{1}{3}(a^2 - a + 1)\,, \tag{1.13}$$

there exists a unique equilibrium point.

Proof. In order to have only one equilibrium point, the $g(v, r)$ slop has to be greater than the maximum gradient of $f(v, r)$. The calculations are straightforward and hence omitted. □

Fixing specific values of the parameters satisfying (1.13), Figure 1.6 represents the nullclines and the equilibrium point at the intersection of the curves.

1.3.1 Stability and bifurcation analysis

Under the hypothesis (1.13) and according to the equilibrium point $(\bar{v}, \bar{r})$ coordinates (see Figure 1.6), there are two possible characteristic phase portraits. Indeed, if the steady state lies on either the left or right branch of $f(v, r)$, then the solution is stable, as shown in Figure 1.7. Otherwise, if it lies in the curve branch between its extremal values, the solution becomes a periodic orbit which is a stable limit cycle. This phase plane portrait is described in Figure 1.8.

In order to provide a precise analysis of the model (1.11), let us firstly introduce some essential definitions and theorems well formalized in, beyond many others, [8, 24, 29].

1.3.1.1 Preliminary concepts

Definition 1.1 (Equilibrium point)**.** Consider the autonomous system of ordinary differential equations

$$\frac{\mathrm{d}\mathbf{u}}{\mathrm{d}t} = \mathbf{f}(\mathbf{u})\,,$$

where $\mathbf{u}$, $\mathbf{f} \in \mathbb{R}^n$. The states $\mathbf{u}_e$ such that

$$\mathbf{f}(\mathbf{u}_e) = \mathbf{0}$$

are called *equilibrium points*. If $\mathbf{u}(t_0) = \mathbf{u}_e$, then $\mathbf{u}(t) = \mathbf{u}_e$ for all times.

Definition 1.2 (Stability and instability of the equilibrium points)**.** The equilibrium states $\mathbf{u}_e$ is said to be *stable* if for any $\varepsilon > 0$ it is possible to find a $\delta(\varepsilon) > 0$ such that for any initial condition $\mathbf{u}(0)$ with

$$\|\mathbf{u}(0) - \mathbf{u}_e\| < \delta(\varepsilon),$$

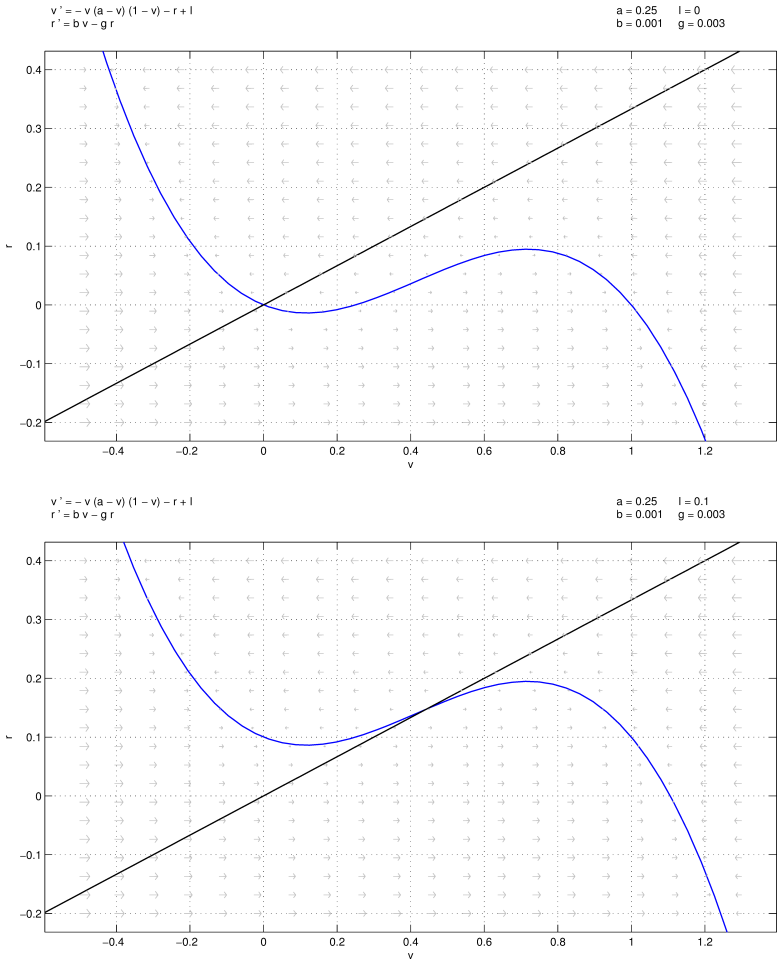

Figure 1.6: The nullclines provided by imposing $f(v, r) = g(v, r) = 0$ in Eq. (1.12) with parameters $a = 0.25$, $b = 0.001$ and $c = 0.003$. Top, the current $I = 0$ leads to nullclines intersecting in the left branch of $f(v, r) = 0$. Bottom, the current $I = 0.1$ leads to their intersection lying between the extremal values of $f(v, r) = 0$.

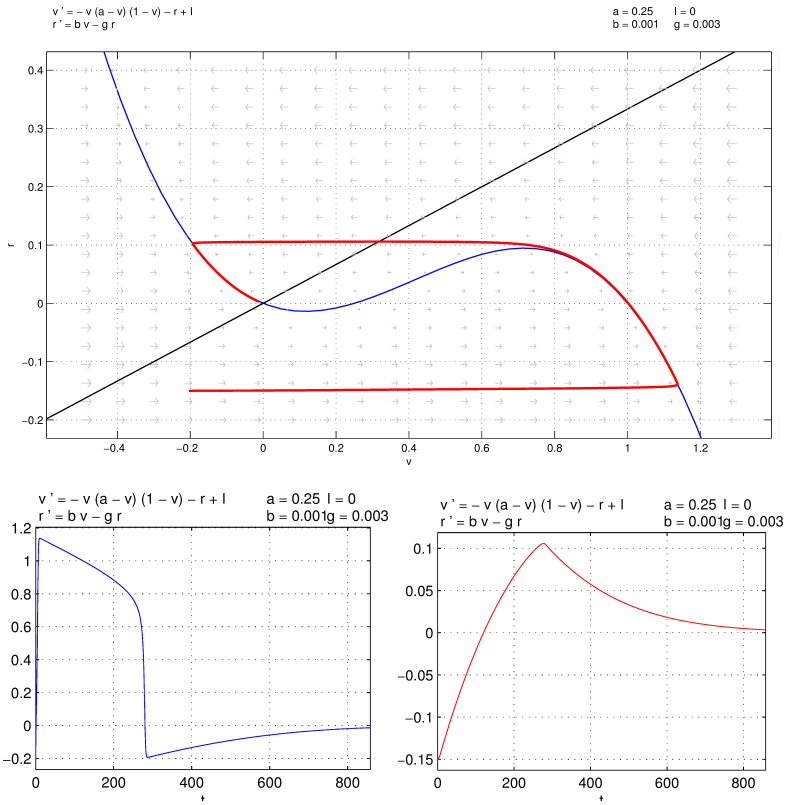

Figure 1.7: Top, phase portrait for the FitzHugh-Nagumo equations (Eq. (1.11)) with parameters $a = 0.25$, $b = 0.001$, $c = 0.003$ and $I = 0$. The system has a unique globally stable rest point at the nullcline intersection. The red curve is the forward solution with the initial datum $(v_0, r_0) = (-0.2, -0.15)$.
Down, the graphs which show the action potential v as a function of time (left) and the recovery variable r as a function of time (right).

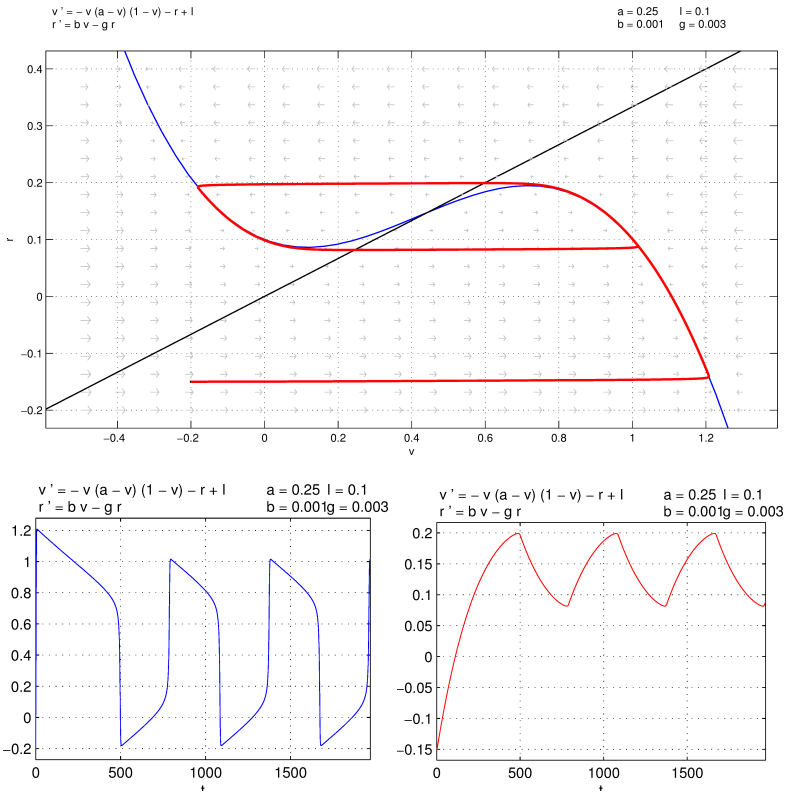

Figure 1.8: Top, phase portrait for the FitzHugh-Nagumo equations (Eq. (1.11)) with parameters $a = 0.25$, $b = 0.001$, $c = 0.003$ and $I = 0.1$. The system has a unique unstable rest point at the nullcline intersection and then there is a globally stable periodic orbit. The red curve is the forward solution with the initial datum $(v_0, r_0) = (-0.2, -0.15)$.
Bottom, two graphs which show the action potential v as a function of time (left) and the recovery variable r as a function of time (right). Both graphs underline the periodicity of the solution.

one has that

$$\|\mathbf{u}(t) - \mathbf{u}_e\| < \varepsilon, \quad \forall t \geq 0.$$

An equilibrium state that is not stable is called *unstable*.

Definition 1.3 (Asymptotic stability)**.** A stable equilibrium point $\mathbf{u}_e$ is also *asymptotically stable* if there is a neighborhood $\mathcal{D}_e$ of $\mathbf{u}_e$ such that for $\mathbf{u}(0) \in \mathcal{D}_e$; one has

$$\lim_{t \to +\infty} \|\mathbf{u}(t) - \mathbf{u}(0)\| = 0.$$

Theorem 1.4 (Linear stability)**.** *If $\mathbf{f}(\mathbf{u})$ is twice continuously differentiable, denoting with λ_i the eigenvalues of the Jacobian matrix evaluated at the equilibrium state, one has:*

- *If $\forall i$ $\mathrm{Re}(\lambda_i) < 0$, then $\mathbf{u}_e$ is asymptotically stable;*
- *If $\exists i$ such that $\mathrm{Re}(\lambda_i) > 0$, then $\mathbf{u}_e$ is unstable.*

By considering a system of two ordinary differential equations, a characterization of the equilibrium points by analysing the eigenvalues λ_i can be performed. In this case one may have the following nondegenerated situations:

- $\lambda_1, \lambda_2 \in \mathbb{R}$. *If $\lambda_1, \lambda_2 < 0$, then*

  $$\lim_{t \to +\infty} \mathbf{u}(t) = \mathbf{0}\ ,$$

  and this equilibrium point is called a stable node. If instead one of the eigenvalue is positive, then

  $$\lim_{t \to +\infty} \mathbf{u}(t) = +\infty\ .$$

  If both eigenvalues are positive, the equilibrium point is called unstable node. Otherwise, it is called saddle point.

- $\lambda_1 = \lambda + iw$, $\lambda_2 = \lambda - iw$ *complex conjugate. If $\lambda = Re(\lambda_1) = Re(\lambda_2) < 0$, then*

  $$\lim_{t \to +\infty} \mathbf{u}(t) = \mathbf{0}\ ,$$

  and the equilibrium point is called stable focus. If $\lambda = Re(\lambda_1) = Re(\lambda_2) > 0$, then

  $$\lim_{t \to +\infty} \mathbf{u}(t) = +\infty\ ,$$

and the equilibrium point is called unstable focus.
Finally, if $\lambda = Re(\lambda_1) = Re(\lambda_2) = 0$*, then* $\mathbf{u}(t)$ *stays bounded and the equilibrium state is a vortex point.*

Let us stress that for systems of two differential equations, the eigenvalues of the Jacobian matrix J *are*

$$\lambda = \frac{trJ}{2} \pm \sqrt{\frac{(trJ)^2}{4} - detJ}\ . \tag{1.14}$$

Let us now consider the following system of ordinary differential equations:

$$\frac{\mathrm{d}\mathbf{u}}{\mathrm{d}t} = \mathbf{f}(\mathbf{u}, \alpha).$$

Definition 1.5 (Bifurcation point)**.** An equilibrium solution $\mathbf{u}_e$ *bifurcates* from another at $\alpha = \alpha_b$ if there are two distinct branches $\hat{\mathbf{u}}_e(\alpha)$ and $\check{\mathbf{u}}_e(\alpha)$ continuous in α, such that $\hat{\mathbf{u}}_e(\alpha) = \check{\mathbf{u}}_e(\alpha)$. The common value α_b such that $(\alpha_b, \hat{\mathbf{u}}_e(\alpha_b)) = (\alpha_b, \hat{\mathbf{u}}_e(\alpha_b))$ is called *bifurcation point.*

It may happen that for $\alpha > \alpha_b$, the solution tends to a time-periodic orbit. The system then undergoes a bifurcation in which trajectories will not spiral toward a new stable equilibrium point, but will tend to a limit cycle. This is called *Hopf bifurcation.* In other words, an Hopf bifurcation is the birth of a limit cycle from an equilibrium in dynamical systems generated by ODEs, when the equilibrium changes stability via a pair of purely imaginary eigenvalues.

Definition 1.6 (Limit cycle)**.** An orbit $\mathbf{u}(t)$ tends to a closed curve Γ called *limit cycle* if there exists a period $T > 0$ such that the sequence of points $\mathbf{u}(t + nT)$ tends to a point of Γ as the integer n goes to infinity.

A cycle Γ is asymptotically stable if there exists a neighborhood $\mathcal{U}_\Gamma$ of Γ such that, if $\mathbf{u}(0) \in \mathcal{U}_\Gamma$, then $\mathbf{u}(t)$ tends to Γ.

Theorem 1.7 (Hopf theorem)**.** *Focus on the dependence of the equilibrium configuration* $\mathbf{u}_e$ *on a parameter* α*, and assume that there is a critical value* α_b*, such that* $\mathbf{u}_e(\alpha)$ *is asymptotically stable for* $\alpha < \alpha_b$ *and unstable for* $\alpha > \alpha_b$*. If at criticality the Jacobian* J *of* $\mathbf{f}$ *has a simple pair of purely imaginary eigenvalues*

$$\lambda(\alpha_b)) = \pm i\Omega,$$

and all the other eigenvalues have a negative real part and, furthermore, for α *close to* α_b

$$\lambda(\alpha) = \mu(\alpha) \pm i\omega(\alpha), \quad \textit{with} \quad \frac{\mathrm{d}\mu}{\mathrm{d}\alpha}(\alpha = \alpha_b) > 0, \tag{1.15}$$

then for α sufficiently near the critical value α_b, there exists a limit cycle with initial period $T = 2\pi/\Omega$. If, in addiction, at criticality the equilibrium configuration $\mathbf{u}(\alpha = \alpha_b)$ is locally asymptotically stable, then the limit cycle is stable.

1.3.2 FitzHugh-Nagumo analysis

In order to introduce the FitzHugh-Nagumo model analysis, let us first consider the model (1.11) without injected current, i.e., $I = 0$. Thus, the point

$$(\bar{v}, \bar{r}) = (0, 0) \tag{1.16}$$

is the trivial stationary solution and it is the unique equilibrium point since Eq. (1.13) holds.

Proposition 1. *$\forall a$, b, $g \in \mathbb{R}^+ \setminus \{0\}$, such that (1.13) holds, the steady state $(\bar{v}, \bar{r}) = (0, 0)$ is stable.*

Proof. The linearization of Eq. (1.11) on the trivial equilibrium point (1.16) is

$$\begin{bmatrix} \dot{v} \\ \dot{r} \end{bmatrix} = \begin{bmatrix} -a & -1 \\ b & -c \end{bmatrix} \begin{bmatrix} v \\ r \end{bmatrix}.$$

The corresponding characteristic equation is

$$\lambda^2 + (a + c)\lambda + ac + b = 0$$

which provides the eigenvalues of the linearized system:

$$\lambda_{1,2} = \frac{-(a + c) \pm \sqrt{(a - c)^2 - 4b}}{2}.$$

As $\forall a$, b, $g \in \mathbb{R}^+$ is $\mathrm{Re}(\lambda_{1,2}) < 0$, then we conclude that $(\bar{v}, \bar{r}) = (0, 0)$ is stable. □

Now, let us come back to the system (1.11) in which a current $I \neq 0$ appears in the first equation, and let us consider a generic equilibrium point $(\bar{v}, \bar{r})$ which varies as a function of I. Since the FitzHugh-Nagumo model is a widely studied one, we know there exist two Hopf bifurcations which characterize two current critical values. These two values characterize the equilibrium point passage from stability to instability or vice versa. In this configuration, the current I is the bifurcation parameter.

Proposition 1.2. $\forall a,\, b,\, g \in \mathbb{R}^+\backslash\{0\}$ and $I \in \mathbb{R}^+$, two critical points arise when the bifurcation parameter takes the values:

$$\begin{aligned} I_1^* &= \bar{v}_1^*(a - \bar{v}_1^*)(1 - \bar{v}_1^*) + b/c\bar{v}_1^* \\ I_2^* &= \bar{v}_2^*(a - \bar{v}_2^*)(1 - \bar{v}_2^*) + b/c\bar{v}_2^* \end{aligned} \tag{1.17}$$

for

$$\begin{aligned} (v_1^*, r_1^*) &= (1/3(-\sqrt{a^2 - a + 1 - 3c} + a + 1), b/(3c)(-\sqrt{a^2 - a + 1 - 3c} + a + 1)) \\ (v_2^*, r_2^*) &= (1/3(\sqrt{a^2 - a + 1 - 3c} + a + 1), b/(3c)(\sqrt{a^2 - a + 1 - 3c} + a + 1)) \,. \end{aligned} \tag{1.18}$$

which are Hopf bifurcation points.

Furthermore, for $I < I_1^* \vee I > I_2^*$, i.e., $(\bar{v}, \bar{r}) < (\bar{v}_1^*, \bar{r}_1^*) \vee (\bar{v}, \bar{r}) > (\bar{v}_2^*, \bar{r}_2^*)$, then the equilibrium point $(\bar{v}, \bar{r})$ is stable. Otherwise, it is unstable and a limit circle arises.

Proof. As stated in Theorem 1.4, we can determine the nature of the equilibrium point $(\bar{v}, \bar{r})$ by considering the eigenvalues of the Jacobian matrix. Thus, let us introduce

$$J = \begin{bmatrix} -a + 2(a+1)\bar{v} - 3\bar{v}^2 & -1 \\ b & -c \end{bmatrix} . \tag{1.19}$$

We remark that for systems constituted by two equations, the eigenvalues of J can be determined by exploiting (1.14). Since the trace of the Jacobian matrix is the sum of the eigenvalues and the determinant is those product, the equilibrium point loses stability via an Hopf bifurcation when

$$\begin{aligned} \operatorname{tr} J &= 0 \\ \det J &> 0. \end{aligned}$$

The first equation gives us the coordinates of the critical points $(\bar{v}_{1,2}^*, \bar{r}_{1,2}^*)$:

$$(\bar{v}_{1,2}^*, \bar{r}_1^*) = \Big(\frac{1}{3}(\pm\sqrt{a^2 - a - 3c + 1} + a + 1), \frac{b}{3c}(\pm\sqrt{a^2 - a - 3c + 1} + a + 1)\Big) \,.$$

Otherwise, since $b/c > 1/3(a^2 - a + 1)$ (see condition (1.13)), the inequality is always satisfied. Thanks to this, we can state that $(\bar{v}_{1,2}^*, \bar{r}_{1,2}^*)$ are two Hopf bifurcations. The corresponding values of the bifurcation parameters $I_{1,2}^*$ can be determined in the following manner. By recalling that for the second equation in (1.11) $r = b/gv$, it holds

that

$$I^*_{1,2} = \bar{v}^*_{1,2}(a - \bar{v}^*_{1,2})(1 - \bar{v}^*_{1,2}) + b/c\bar{v}^*_{1,2} \ . \tag{1.20}$$

Furthermore, by exploiting Theorem 1.4, for $(\bar{v}, \bar{r})$ such that $\mathrm{Tr}J < 0$, i.e., $(\bar{v}, \bar{r}) < (\bar{v}^*_1, \bar{r}^*_1) \vee (\bar{v}, \bar{r}) > (\bar{v}^*_2, \bar{r}^*_2)$, then the equilibrium point is stable. Otherwise, it is unstable. □

The presence of the Hopf bifurcations, instead of saddle-node ones, leads the FitzHugh-Nagumo model to belong to the *Class II of neural excitability*, where the criterion for classifying excitability was suggested by Hodgkin in [26]. Through experiments, he observed that by injecting strong current into excitable membrane, spike trains with a certain oscillation frequency arose. The spike train frequency, as a function of the current I, led to the classification. Two are the major classes that have been formalized, and they are described in [27, 29]. The FitzHugh-Nagumo model (1.11) belongs to the class II and it is characterized by a frequency band of the spike trains that is quasi-independent to the input strength (when it is enough to produce spikes). What remains dependent to the injected current is the duration of the burst phenomenon. A different neuronal behaviour is described, for example, by exploiting the Hodgkin-Huxley model where the presence of a saddle equilibrium point leads the frequency to start from zero and to increase smoothly. It follows that the Hodgkin-Huxley model belongs to the class I.

The bifurcation diagram in Figure 1.9 collects several information about the FitzHugh-Nagumo model. In particular, beyond the results presented in Proposition 1.2, it underlines that the Hopf bifurcation are subcritical. Moreover, as specified above, without any external contribution, the equilibrium point is stable. But if the injected current overcomes the I^*_1 value, it joins a periodic limit circle. In that situation, a *burst* happens with a quasi-constant frequency for all $I^*_1 < I < I^*_2$. An exhaustive analysis of this can be found in [29]. The injected current variation in time leads the neuron to exhibit several behaviours which include the quiescent state, the single spike and the burst. Nonetheless the FitzHugh-Nagumo model is not a fixed threshold model, it holds a quasi-threshold which is a canard trajectory, i.e., a trajectory that follows the unstable manifold. This means that with precise parameter choices, intermediate sized spikes can arise. However, the precision needed is so great that an approximation of a real threshold can be made. It follows that sub-threshold oscillations are severely limited in the FitzHugh-Nagumo model.

With the choice of parameters $a = 0.25$, $b = 0.001$ and $c = 0.003$, which satisfy the

condition (1.13), the bifurcation parameters are

$$I_1^* = 0.05302 \text{ and } I_2^* = 0.14373 \ , \tag{1.21}$$

and the corresponding potential values are:

$$\bar{v}_1^* = 0.11787 \text{ and } \bar{v}_2^* = 0.715461 \ . \tag{1.22}$$

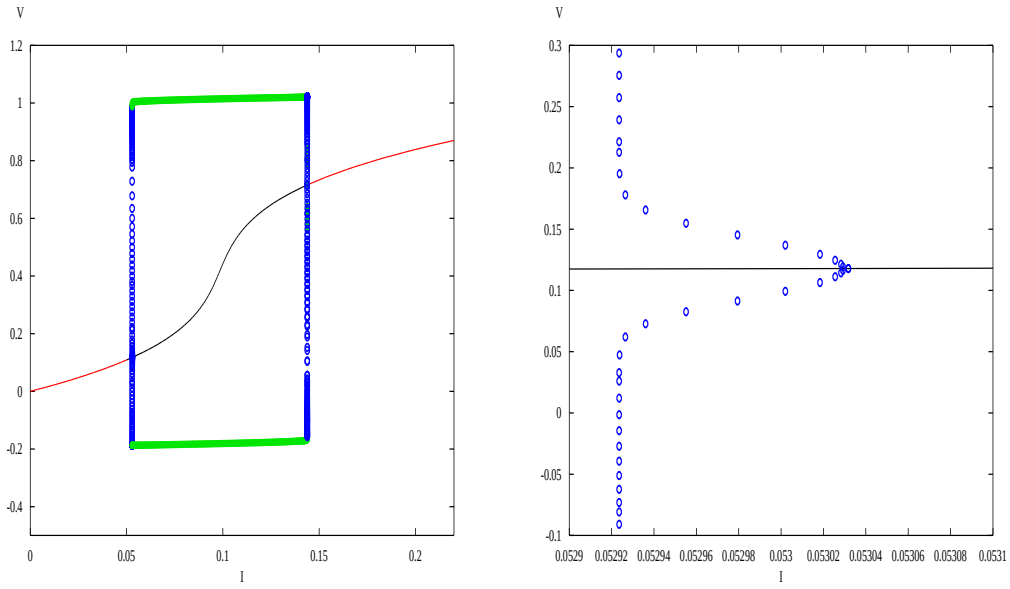

Figure 1.9: Bifurcation diagram made with XPPAUT by Bard Ermentrout. On the left, le complete bifurcation diagram is presented. The line which cross the domain describes the equilibrium point curve as I varies. Outside the limit circle, i.e., on the extreme left and right branches of the equilibrium point curve, they are stable. Otherwise, on the center branch, they are unstable and originate limit cycles. In the plot, open circles represent unstable limit cycles while green line represent stable ones. On the right, a zoom on the first bifurcation point is shown and it can be demonstrated that it is a subcritical one

1.3.3 FitzHugh-Nagumo model and the travelling waves

At this stage, let us underline that the FitzHugh-Nagumo model shown in Eq. (1.11) is proper for the homogeneous (with respect to the current) situation, i.e. the membrane potential is enforced to be space-homogeneous. For the general case, one may think of a chain of coupled homogeneous elements, but now the potential can "diffuse" through the membrane to the neighboring elements. In other words, the potential diffuses along a membrane ions and hence along the neuron's axon. Accordingly, let us make more

general the Eq. (1.11) and add a diffusion term to the first equation:

$$\begin{aligned} \frac{\partial v}{\partial t} &= -v(a-v)(1-v) - r + I + d\frac{\partial^2 v}{\partial x^2} \\ \frac{\partial r}{\partial t} &= bv - cr, \end{aligned} \tag{1.23}$$

where x is the space variable which allows to consider the axon as spatially distributed while a, b, c and D are parameters with $D \geq 0$. Equations (1.23) are in the form presented by Murray in [41]. Note that the diffusive term is only in the first equation since we are only interested in the diffusion of the action potential v.

Chapter 2

Electrically coupled neuronal networks

Despite in the past years almost all networks have been represented as constituted by neurons that are interconnected by chemical synapses, electrical synapses are largely present in the nervous system. In the sequel, we will use indifferently the terms *electrical synapses* and *gap junctions*. However, for the sake of completeness, gap junctions are the morphological equivalent of electrical synapses. In particular, as specified in [34], gap junctions exist between near-neighbour neurons and they allow low-resistance electrical transmissions. Indeed, at an electrical synapse a current I_{gap} is generated which is proportional to the difference between the action potentials v of the post-synaptic and pre-synaptic neurons (see, e.g., [15] eq. (7.12)); explicitly, we have for some $d > 0$

$$I_{\text{gap}} = d(v_{\text{post}} - v_{\text{pre}}) \, . \tag{2.1}$$

This establishes a *diffusive coupling* between neighbouring neurons. Let us stress that in Chapter 5, (2.1) will be exploited to describe the interesting mechanism underlying the *ephaptic coupling*.

Unfortunately, the analysis of electrical synapses *in situ* presents severe technical difficulties and therefore their specific roles are still largely unexplored. Nevertheless, in the past ten years, the topic concerning gap junction networks has been object of several investigations, sometimes leading to paradoxical results (see e.g. [19, 38, 53]).

In order to build up the sample network we will consider, several ingredients are taken into account. First of all, we model each single cell as an excitable element by exploiting the FitzHugh-Nagumo model in (1.11). The excitable feature means that neurons may not fire intrinsically without any synaptic inputs. Furthermore, we suppose each cell belongs to the same functional class, avoiding the presence of

heterogeneity. This agrees with authors in [19] who stress that electrical synapses exist exclusively between neurons of the same class. In particular, despite many works underline the presence of electrical synapses between inhibitory neurons (see e.g. [19]), the existence of electrical connections between excitatory neurons is demonstrated in the early postnatal stages (see [53]). Finally, as we will specify, we consider the presence of both bidirectional (non-rectifying) and unidirectional (rectifying) synapses as claimed in [38].

In this chapter, after setting our mathematical model of an idealized neuronal network with electrical-type coupling between neurons, we carefully investigate the "passage to the limit" as the number of neurons tends to infinity, while they remain confined in a fixed and bounded spatial region. We identify two different manners of increasing the population of the network so that a non-trivial continuum limit is obtained. The first one assumes a fixed topology of the network (nearest-neighbour connections) but makes the proportionality coefficient in (2.1) to depend upon the total number of neurons according to a specific law; conversely, the second manner keeps this coefficient fixed but suitably increases the number of connections per neuron. Both methods lead to equivalent continuous models, in which the action potential is the solution of a reaction-diffusion partial differential equation (or a reaction-convection-diffusion equation if connections are not symmetric, i.e., if rectifying synapses are allowed). Our arguments apply in any spatial dimension, although we detail them in 1D and we sketch their extension to 2D. Clear numerical evidence confirms all theoretical results. At last, an example of random connections is also presented.

2.1 Diffusive coupling within the network

We suppose that our network contains N neurons, identified by integer labels $i = 1, \cdots, N$; labels refer to the physical position of the neurons in the network. Electrical-type connections in the neuronal network are easily described by basic concepts from graph theory (see, e.g., [5]). Let us consider a graph $G = (V, E)$, where $V = \{1, \cdots, N\} \subset \mathbb{N}$ is the set of vertices and $E \subset V \times V$ is the set of edges. The so-called *adjacency matrix* $A_G = (a_{ij})$ is an $N \times N$ matrix whose entries are:

$$a_{ij} = \begin{cases} w_{ij} & \text{if } (i,j) \in E(G) \\ 0 & \text{else}, \end{cases} \tag{2.2}$$

where i, $j = 1, \cdots, N$ and the weights are strictly positive.

Exploiting the adjacency matrix, and assuming the gap-junction law (2.1) for the interaction between adjacent neurons, we define the FitzHugh-Nagumo model with diffusive coupling as follows:

$$\begin{aligned} \dot{v}_i &= f(v_i, r_i) + \sum_{j \neq i} a_{ij}(v_j - v_i) \ , \\ \dot{r}_i &= g(v_i, r_i) \ , \end{aligned} \tag{2.3}$$

where functions f and g are as in (1.12). Specifically, the summation describes the influence on the $i-$th neuron by all neurons linked to it: it produces a diffusion effect within the network. The simplest example is given by the expression in (2.7), which models nearest-neighbour interactions in a chain of neurons.

Introducing the diagonal *degree matrix* $D_G := \mathrm{diag}(d_i)$ with $d_i = \sum_{j \neq i} a_{ij}$, and the *Laplacian matrix* $L_G := D_G - A_G = (l_{ij})$, the previous system can be written as

$$\begin{aligned} \underline{\dot{v}} &= \underline{f}(\underline{v}, \underline{r}) - L_G \underline{v} \ , \\ \underline{\dot{r}} &= \underline{g}(\underline{v}, \underline{r}) \ , \end{aligned}$$

where $\underline{v} = (v_i)$, $\underline{r} = (r_i)$ and $\underline{f}(\underline{v}, \underline{r}) = (f(v_i, r_i))$, $\underline{g}(\underline{v}, \underline{r}) = (g(v_i, r_i))$.

In the sequel, referring to the present chapter, we assume that all weights w_{ij} are equal and precisely $w_{ij} = d$ for some $d > 0$, which we will call the *diffusion coefficient*. Let us introduce the set $\mathcal{Q}(i)$ of all indices q such that neuron $i + q$ is linked to neuron i, i.e., $a_{i,i+q} \neq 0$. Then, the model (2.3) can be written as

$$\begin{aligned} \dot{v}_i &= f(v_i, r_i) + d \sum_{q \in \mathcal{Q}(i)} (v_{i+q} - v_i) \ , \\ \dot{r}_i &= g(v_i, r_i) \ . \end{aligned} \tag{2.4}$$

In most cases, we shall consider $\mathcal{Q}(i) = \mathcal{Q}$ independent of i, thus assuming a homogeneous network topology.

We are interested in describing the behaviour of the network as the number of neurons increases, identifying conditions on the model which lead to non-trivial asymptotic patterns in the limit $N \to \infty$. We assume that the network is contained in a bounded region B (independent of N) of the Euclidean space $\mathbb{R}^m$, for some $1 \leq m \leq 3$; let us denote by $x_i \in B$ the physical position of the $i-$th neuron. Then, we assume that the distance of any point $\hat{x} \in B$ from the network tends to zero as $N \to \infty$, and the distance of each neuron from its neighbours in the network has a similar behaviour.

If interactions between neurons are local, we can give an expression of the diffusive

term in (2.4) which is based on the Taylor expansion of the differences $\Delta v_{i,q} = v_{i+q} - v_i$. Precisely, let us assume that at each time there exists a sufficiently smooth function v defined in B such that $v_i = v(x_i)$ for $i = 1, \cdots, N$. Then, setting $\Delta x_{i,q} = x_{i+q} - x_i$, we have

$$\Delta v_{i,q} = \nabla v(x_i)\Delta x_{i,q} + \frac{1}{2}\Delta x_{i,q}^T Hv(x_i)\Delta x_{i,q} + \text{h.o.t.}\,, \tag{2.5}$$

where ∇v denotes the gradient vector of v, whereas Hv denotes the Hessian matrix of v. Substituting this expression into (2.4), we obtain a representation of the diffusive term by which we can find the conditions on the coefficient d and/or the sets $\mathcal{Q}(i)$ (depending on the network) yielding a non-trivial limit as $N \to \infty$. We will detail our analysis assuming a specific distribution of neurons in the one-dimensional case first, and then we will consider the multi-dimensional extension.

2.2 One-dimensional dynamics

We consider neurons disposed over a closed chain, i.e., a ring. Each neuron occupies a specific physical position x_i in the interval $B = [0, 1]$ given by

$$x_i = (i-1)\Delta x = \frac{i-1}{N} \quad \text{with } 1 \le i \le N\,, \tag{2.6}$$

where N is the number of elements equally distributed along the chain and, consequently, $\Delta x = 1/N$ is the distance between any two adjacent ones. Since the chain is closed, we assume periodic boundary conditions, i.e., we set $v_0 = v_N$ and $v_{i+kN} = v_i$ for any $k \in \mathbb{Z}$.

2.2.1 Nearest-neighbour interactions

Let us first consider two symmetric nearest-neighbour interactions for each neuron. This translates in considering the set of connections per neuron $\mathcal{Q}(i) = \mathcal{Q} = \{\pm 1\}$. In this case, the diffusive coupling assumes the following form:

$$-(L_G v)_i = d \sum_{q=\pm 1} (v_{i+q} - v_i) = d[(v_{i+1} - v_i) + (v_{i-1} - v_i)] = d(v_{i+1} - 2v_i + v_{i-1})\,. \tag{2.7}$$

An interesting dynamics produced by (2.4), which will represent a test case for the subsequent discussion, is obtained by applying an initial stimulus to the central neuron ($i = N/2$, assuming N even) of the line. Specifically, its action potential is initially set to the value 2, whereas all the other variables are set to 0. Considering the diffusion

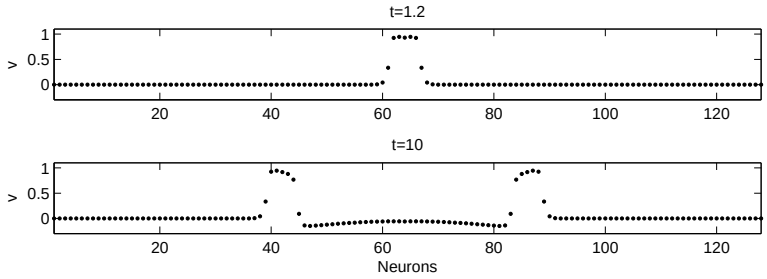

Figure 2.1: Propagation of an initial pulse along a closed ring of $N = 128$ neurons

coefficient $d = 0.05$ (see [52]), the resulting dynamics is constituted by two pulses that travel in opposite directions in the whole set of neurons (see e.g. [34] for the analysis of travelling pulses). A sample dynamics is shown in Figure 2.1. We observe for further reference that a similar dynamics is obtained starting from an initial stimulus of the action potential given by a Gaussian function concentrated around the central neuron. In all cases, at the end of dynamics, neurons return to the quiescent state. In fact, neurons are modelled as excitable units and then, after the excitation, they undergo a long refractory period. In this period they are blind to any stimulus. This is the reason why two travelling pulses that collide depress their signals.

We now focus on how the dynamics produced by our model depends upon N. The first observation is that, if the diffusion parameter d is kept fixed, then the diffusive effect tends to vanish as $N \to \infty$. This can be seen in two ways. On the one hand, if neurons get close to each other and the action potential varies in a smooth manner, then the differences on the right-hand side of (2.7) tends to zero, implying the vanishing of the diffusion term $L_G v$ in each node. On the other hand, considering the test case introduced above, it is easily seen that the effect of, say, doubling N is equivalent to have a chain of neurons with the same spacing but with double length; this means that on the original chain, waves have half the length and propagate with half the speed.

In order to obtain non-trivial diffusion effects in the limit, one possibility - that we call Approach I - consists in letting the parameter d grow with N, i.e., $d = d_N$. The precise dependence can be found by exploiting the Taylor expansion (2.5), which in the present setting becomes

$$\Delta v_{i,q} = q\Delta x v'(x_i) + \frac{1}{2}q^2\Delta x^2 v''(x_i) + \text{h.o.t.}\,, \tag{2.8}$$

where the prime indicates differentiation with respect to the spatial variable x. There-

fore, the following expression holds for the diffusive term:

$$-(L_G v)_i = d_N \left[(v_{i+1} - v_i) + (v_{i-1} - v_i)\right] = d_N[\Delta x^2 v''(x_i) + \text{h.o.t.}] \,. \tag{2.9}$$

We choose d_N in such a way that $d_N \Delta x^2$ is independent on N, say

$$d_N \Delta x^2 = d^* \tag{2.10}$$

for a fixed constant $d^* > 0$. Hence, we obtain

$$d_N = \frac{d^*}{\Delta x^2} = d^* N^2 \,, \tag{2.11}$$

i.e., d_N is proportional to the square of the number of neurons. The fact that d_N is proportional to N^2 is not surprising: the spectral gap of the Laplacian matrix, which is its smallest non-zero eigenvalue, has the same behaviour as $1/(N^2)$.

As $N \to \infty$, the discrete model

$$\begin{aligned} \dot{v}_i &= f(v_i, r_i) + d_N \left[(v_{i+1} - v_i) + (v_{i-1} - v_i)\right] \,, \\ \dot{r}_i &= g(v_i, r_i) \,, \end{aligned} \tag{2.12}$$

"converges" to a continuous model. To support this statement, we observe that the quantity h.o.t. in (2.9) is given by

$$\text{h.o.t.} = \frac{1}{12} \Delta x^4 v^{(iv)}(\bar{x}_i) \,,$$

where $\bar{x}_i \in (x_{i-1}, x_{i+1})$ and $v^{(iv)}$ is assumed continuous in $[0, 1]$. Thus, we have

$$\begin{aligned} -(L_G v)_i &= \frac{d^*}{\Delta x^2} \left[(v_{i+1} - v_i) + (v_{i-1} - v_i)\right] \\ &= d^* v''(x_i) + \frac{d^*}{12} \Delta x^2 v^{(iv)}(\bar{x}_i) \,. \end{aligned} \tag{2.13}$$

It follows that if we fix any point $\hat{x} \in [0, 1]$ and, for each N, we consider a neuron of index $i = i(N)$ such that

$$x_{i(N)} = \frac{i(N)}{N} \to \hat{x} \quad \text{as } N \to \infty \,,$$

then,

$$\lim_{N \to \infty} d_N \sum_{q \in \mathcal{Q}} (v_{i(N)+q} - v_{i(N)}) = d^* v''(\hat{x}) \,.$$

We conclude that a continuum of neurons is the result of the limit process of letting $N \to \infty$, and

$$\begin{aligned} \frac{\partial v}{\partial t} &= f(v,r) + d^* \frac{\partial^2 v}{\partial x^2} \,, \\ \frac{\partial r}{\partial t} &= g(v,r) \,, \end{aligned} \tag{2.14}$$

is the system of nonlinear partial differential equations of incomplete parabolic type which describes the action potential and the recovery variable in the whole set of neurons. Note that the first equation is similar to the so-called cable equation, which describes the distribution of the potential along the axon of a single neuron (see, e.g. [15, 44]). Reaction-diffusion models like (2.14) are studied in, among others, [18, 46].

We observe that the discrete model (2.11)–(2.12) can be viewed as a numerical semi-discretization (in space) of the PDE system (2.14), obtained by using a second-order centered finite difference method on the equally-spaced (2.6). Thus, if the solution of (2.14) is sufficiently smooth as in the case of an initial Gaussian stimulus, we expect to have quadratic convergence in Δx of the discrete solutions, at any fixed time $t > 0$, as it can be deduced from the fact that the error term on the right-hand side of (2.13) is proportional to Δx^2.

We now give an example. Following the choice of parameters presented in [52], we set $d = 0.05$ and we consider the case $N = 128$ as a reference one, i.e., we impose $d_N = d$ for $N = 128$, which yields

$$d^* = \frac{0.05}{128^2} = 3.0518 \cdot 10^{-6} \,. \tag{2.15}$$

A comparison of several discrete solutions is presented in Figure 2.2. The (b) plots clearly document the convergence of the discrete dynamics towards a limit one. Note that these dynamics are generated by applying an initial stimulus $v_{i|t=0} = 2$ to a number of neurons proportional to N around the center of the chain; in the limit, the initial action potential takes the value 2 in an interval of positive length symmetrically placed around the point $x = 1/2$, and vanishes elsewhere.

For the sake of completeness, let us define the error between dynamics involving a couple of N and $2N$ neurons as follow:

$$\|v_N - v_{2N}\|_2 = \left(\frac{1}{N} \sum_{i=1}^{N} |v_{N,i}(t) - v_{2N,2i}(t)|^2 \right)^{1/2} \,. \tag{2.16}$$

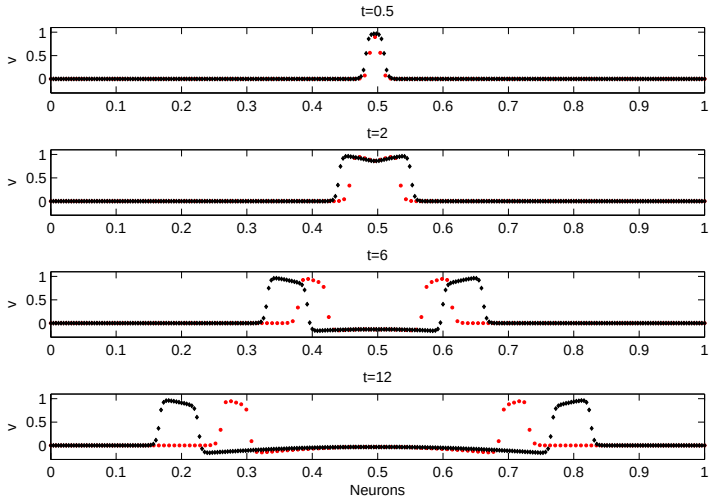

(a)

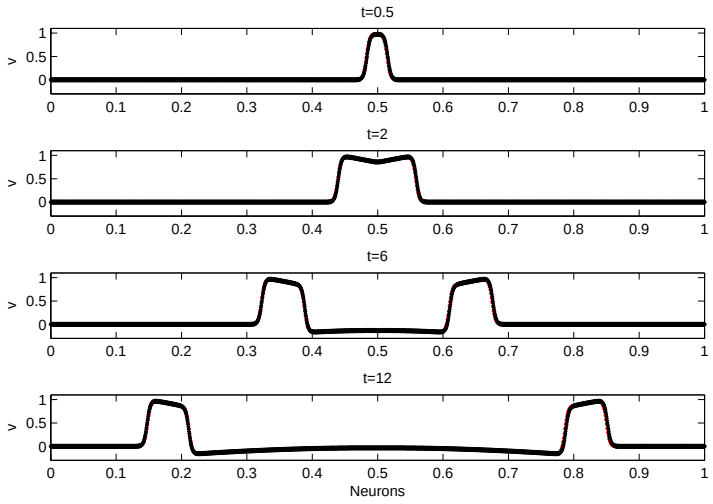

(b)

Figure 2.2: Convergence of the discrete model (2.12)-(2.11) (Approach I) as $N \to \infty$. Evolution of pulses (a) for $N = 128$ (red dots) and $N = 256$ (black dots), (b) for $N = 1024$ (red dots) and $N = 2048$ (black dots)

Remark 1. A more general situation considers $d = d_N$ in (2.7) also depending on i and q, i.e., the diffusive coupling law is replaced by

$$-(L_G v)_i = d_{i+1}(v_{i+1} - v_i) + d_{i-1}(v_{i-1} - v_i) \,, \tag{2.17}$$

where $d_{i\pm1} = N^2 d^*(x_{i\pm1})$ and d^* is a smooth function. In the limit, the diffusion term in (2.14) is replaced by $\frac{\partial}{\partial x}\left(d^* \frac{\partial v}{\partial x}\right)$. For simplicity, we confine ourselves to the constant-coefficient case.

2.2.2 Extended range interactions

We now introduce a second approach to reproduce the same limit dynamics emerged above, which avoids rescaling the diffusion coefficient with the square of the number of neurons. This alternative way - which we call Approach II - consists of increasing the number of connections per neuron according to a specific law (and just slightly adjust the diffusion coefficient).

Since the core idea is to consider a number of connections per neuron that varies as a function of N, let us define the following set:

$$\mathcal{Q} = \mathcal{Q}_N = \{\pm1, \pm2, \cdots, \pm Q_N\} \,, \tag{2.18}$$

where Q_N is a positive integer to be determined. Thus, neurons linked to the i-th one belong to the interval

$$I = [x_i - Q_N \Delta x, x_i + Q_N \Delta x] \,. \tag{2.19}$$

Using again Taylor expansions, the sum in the diffusive coupling becomes

$$\sum_{q \in \mathcal{Q}} (v_{i+q} - v_i) = \left(\sum_{q=1}^{Q_N} q^2 \right) \Delta x^2 v''(x_i) + \text{h.o.t.} \,.$$

Introducing the function $\phi : \mathbb{R}^+ \to \mathbb{R}^+$ defined as

$$\phi(x) = \frac{x(x+1)(2x+1)}{6} \tag{2.20}$$

and invoking the identity

$$\sum_{q=1}^{n} q^2 = \phi(n) \quad \forall n \geq 1 \,,$$

we obtain,

$$-(L_G v)_i = d \sum_{q \in \mathcal{Q}_N} (v_{i+q} - v_i) = d[\phi(Q_N)\Delta x^2 v''(x_i) + \text{h.o.t.}] \,. \tag{2.21}$$

We would like to choose Q_N in such a way that $d\phi(Q_N)/N^2$ is independent on N, say

$$d\frac{\phi(Q_N)}{N^2} = d^* \,, \tag{2.22}$$

for a fixed constant $d^* > 0$. This equation admits a unique solution, say Q_N^r, which however need not be an integer. Therefore, we choose Q_N as the nearest integer to Q_N^r.

Proposition 2.1. The number of neurons linked to any given one grows proportionally to the power $N^{2/3}$ of the total number of neurons. Indeed[1],

$$Q_N \sim Q_N^r \sim \left(\frac{3d^*}{d}N^2\right)^{1/3} = cN^{\frac{2}{3}} \,.$$

Proof. By definition, Q_N^r satisfies

$$d\frac{\phi(Q_N^r)}{N^2} = d^* \,. \tag{2.23}$$

The result follows recalling that $\phi(x) \sim \frac{x^3}{3}$ for $x \to \infty$. □

Let us underline that, although the number of neurons linked to any given one grows with N, interactions remain local, i.e., these neurons belong to a neighbourhood whose size decays with N. Indeed, considering the $i-$th neuron and recalling (2.19), we have

$$|I| \simeq Q_N \Delta x \simeq N^{-1/3} \,. \tag{2.24}$$

Thus, we expect that the limit model, as $N \to \infty$, be again described by partial differential equations.

As specified above, the slight shift from Q_N^r to Q_N provokes the necessity of slightly

[1] For any two non-negative sequences A_N and B_N and for $N \to \infty$, we will use the symbols

$$\begin{aligned} A_N \sim B_N \quad &\Longleftrightarrow \quad A_N/B_N \to 1 \,, \\ A_N \simeq B_N \quad &\Longleftrightarrow \quad cB_N \le A_N \le c'B_N \quad \text{with } c, c' > 0 \,, \\ A_N \lesssim B_N \quad &\Longleftrightarrow \quad A_N \le cB_N \quad \text{with } c > 0. \end{aligned}$$

modifying the diffusion coefficient. Precisely, we define d_N so that the identity

$$d_N \frac{\varphi(Q_N)}{N^2} = d^* \tag{2.25}$$

is satisfied. An alternative possibility, which will be explored later on and which leads to similar effects, would be to define d_N^* so that

$$d \frac{\varphi(Q_N)}{N^2} = d_N^* \, . \tag{2.26}$$

The coefficient d_N is really a small perturbation of d, as the next proposition indicates.

Proposition 2.2. Let d_N be the diffusion coefficient defined in (2.25). Then, one has

$$|d_N - d| \lesssim N^{-\frac{2}{3}} \, .$$

Proof. From (2.23) and (2.25), we obtain the following equality:

$$d_N \frac{\phi(Q_N)}{N^2} = d \frac{\phi(Q_N^r)}{N^2} \, . \tag{2.27}$$

Since Q_N is defined as the nearest integer to Q_N^r,

$$|Q_N^r - Q_N| \leq \frac{1}{2} \, , \tag{2.28}$$

and then, $Q_N = Q_N^r + \varepsilon_N$ with a proper choice of ε_N, such that $|\varepsilon_N| \leq 1/2$. Writing $\phi(Q_N^r) = \phi(Q_N) + \phi(Q_N^r) - \phi(Q_N)$ and substituting in (2.27), we get

$$|d_N - d| = \frac{|\phi(Q_N^r) - \phi(Q_N)|}{\phi(Q_N)} d \, . \tag{2.29}$$

Using (2.28) and omitting computations, we conclude that $|\phi(Q_N^r) - \phi(Q_N)| \lesssim N^{4/3}$ while $\phi(Q_N) \simeq N^2$. This gives the desired estimate. □

In order to obtain the continuous model as a limit of the discrete model for $N \to \infty$, we observe that, if the fourth derivative of v is continuous in $[0,1]$, the diffusion term (2.21) takes the form

$$\begin{aligned} -(L_G v)_i &= d_N \Big[\varphi(Q_N) \Delta x^2 v''(x_i) + \text{h.o.t.} \Big] \\ &= d^* v''(x_i) + \frac{d_N}{12} \Delta x^4 \sum_{q=1}^{Q_N} q^4 v^{(iv)}(\bar{x}_{i,q}) \, , \end{aligned} \tag{2.30}$$

where $\bar{x}_{i,q}$ are suitable points in the interval (x_{i-q}, x_{i+q}). Since $\sum_{q=1}^{Q_N} q^4 \sim \frac{1}{5} Q_N^5$, using Property 2.1 and Proposition 2.2, we deduce that

$$d_N \Delta x^4 \sum_{q=1}^{Q_N} q^4 \simeq N^{\frac{10}{3}-4} = N^{-\frac{2}{3}} \to 0 \text{ as } N \to \infty \,. \tag{2.31}$$

Therefore, proceeding as in Section 2.2.1, if we fix any point $\hat{x} \in [0,1]$ and we consider a neuron of index $i = i(N)$ such that $x_{i(N)} \to \hat{x}$ as $N \to \infty$, we conclude that

$$-(L_G v)_{i(N)} \to d^* v''(\hat{x}) \text{ as } N \to \infty \,.$$

This means that Approach II yields in the limit the same system (2.14) of partial differential equations, that we got from Approach I.

We now illustrate the asymptotic behaviour of the quantities defined above, for the same test case considered in the previous subsection. We choose again $d = 0.05$, and we enforce that for $N = N_0 = 128$ we have $Q_{N_0} = Q_{N_0}^r = 1$, which corresponds to the nearest-neighbour interaction previously considered; we also enforce $d_{N_0} = d$, and consequently we get

$$d^* = \frac{d}{N_0^2} \,,$$

which is precisely (2.15). Increasing N by powers of 2, i.e., setting $N = N_0 2^p$ with $p \geq 1$, the algorithm presented above produces the values of Q_N and d_N shown in Table 2.1. The last column of this table, as well as Figure 2.3 (left), quantitatively support the asymptotic estimates proven in Propositions 2.1 and 2.2 (ignoring few values of p that give superconvergence effects). Some representative dynamics obtained with Approach II are documented in Figure 2.4; they should be compared to those given in Figure 2.2. The evolutions of the action potentials produced by the discrete model with $N = 1024$, and by a very accurate solution of the continuous model (2.14) are documented in Figure 2.5. While the shapes of the pulses are already well captured, their speed of propagation is less accurately reproduced; this should be related to the fourth-order error term on the right-hand side of (2.30), whose decay is slower than in Approach I as indicated by (2.31) compared to (2.13).

2.2.3 Comparison between approaches

After having described Approaches I and II, the main result consists to show that they produce equivalent limit dynamics. The frames in Figures 2.6–2.7–2.8–2.9–2.10 describe the dynamics obtained with a fixed number of neurons N. Obviously, as

Table 2.1: Number of connections per neuron Q_N, diffusion coefficient d_N and relative error as a function of $N = N_0 2^p$ with $N_0 = 128$.

p	$N = N_0 2^p$	Q_N	d_N	$\lvert d_N - d\rvert / d$
0	128	1	0.0500	0
1	256	2	0.0400	$2.0{\cdot}10^{-1}$
2	512	3	0.0571	$1.4{\cdot}10^{-1}$
3	1024	5	0.0582	$1.6{\cdot}10^{-1}$
4	2048	9	0.0490	$1.0{\cdot}10^{-1}$
5	4096	14	0.0504	$8.7{\cdot}10^{-3}$
6	8192	23	0.0473	$5.3{\cdot}10^{-2}$
7	16384	36	0.0505	$1.1{\cdot}10^{-2}$
8	32768	58	0.0491	$1.8{\cdot}10^{-2}$
9	65536	92	0.0496	$6.3{\cdot}10^{-3}$
10	131072	146	0.0500	$4.9{\cdot}10^{-4}$
11	262144	232	0.0500	$1.2{\cdot}10^{-3}$
12	524288	369	0.0500	$2.3{\cdot}10^{-3}$
13	1048576	586	0.0500	$2.1{\cdot}10^{-3}$
14	2097152	930	0.0500	$4.3{\cdot}10^{-4}$
15	4194304	1476	0.0500	$7.4{\cdot}10^{-4}$
16	8388608	2344	0.0500	$1.6{\cdot}10^{-4}$
17	16777216	3721	0.0500	$3.0{\cdot}10^{-5}$
18	33554432	5907	0.0500	$2.3{\cdot}10^{-5}$
19	67108864	9377	0.0500	$2.9{\cdot}10^{-7}$
20	134217728	14885	0.0500	$7.1{\cdot}10^{-5}$

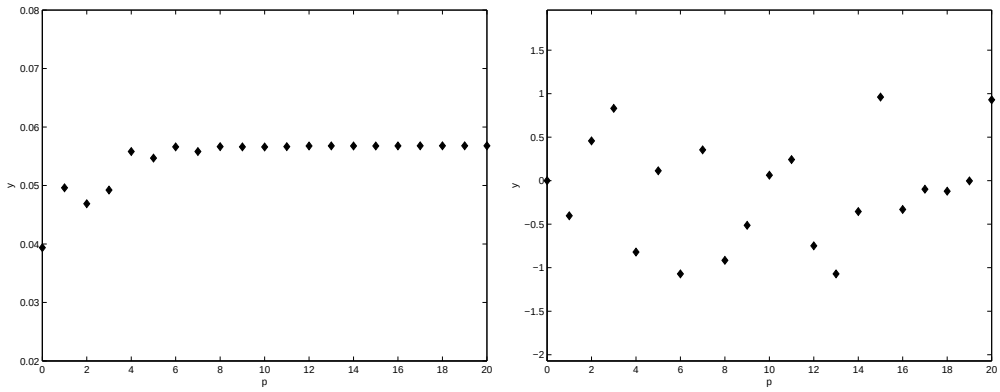

Figure 2.3: Plots of $Q_N/N^{2/3}$ (left) and $(d_N - d)/N^{-2/3}$ (right) vs p, where $N = N_0 2^p$

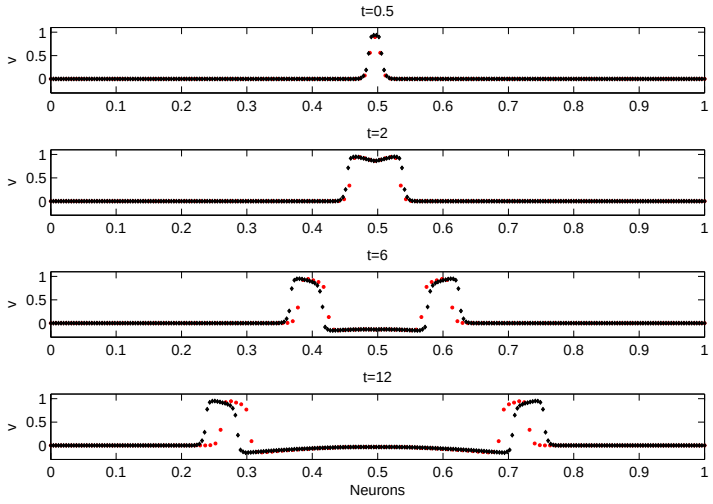

(a)

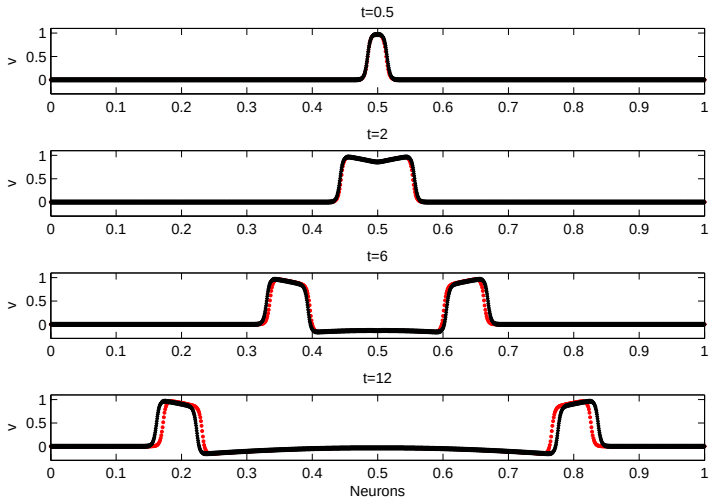

(b)

Figure 2.4: Convergence of the discrete model (2.4)-(2.18)-(2.22) (Approach II) as $N \to \infty$. Evolution of pulses (a) for $N = 128$ (red dots) and $N = 256$ (black dots), (b) for $N = 1024$ (red dots) and $N = 2048$ (black dots)

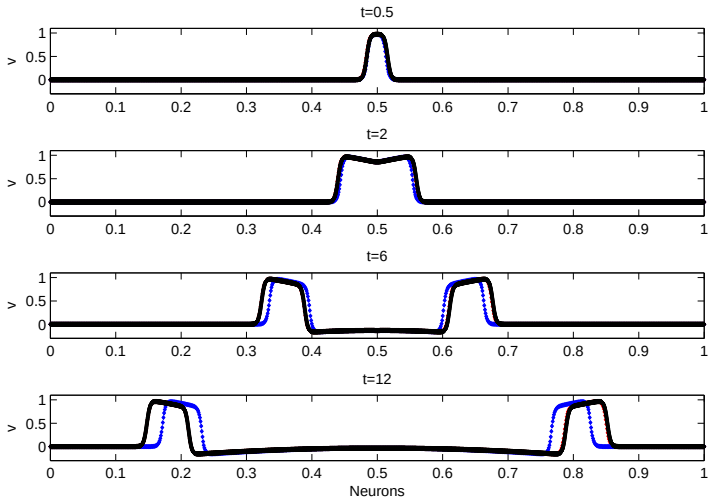

Figure 2.5: Comparison of the dynamics produced by Approach II with $N = 1024$ (blue dots) and by the continuous model (2.14) (black dots)

$N = 128$ represents the sample case, dynamics obtained by exploiting Approaches I and II coincides, see Figure 2.6. Doubling N, two dynamics which are clearly different arise and they are shown in Figure 2.7. The difference between dynamics reduces as N increases, as can be seen in Figure 2.8–2.9–2.10.

In order to quantify the difference between the solutions considering N fixed, we decide to compute the following L-2 norm:

$$\|v^* - v^{**}\|_2 = \left(\frac{1}{N} \sum_{i=1}^{N} |v^*_{N,i}(t) - v^{**}_{N,i}(t)|^2 \right)^{1/2} , \tag{2.32}$$

where v^* represents the solutions obtained by exploiting Approach I while v^{**} by exploiting Approach II.

2.2.4 Non-symmetric interactions

A more general configuration of the network admits non-symmetric links for each neuron, which correspond to unidirectional connections (the so-called rectifying synapses). A natural extension of the symmetric case consists in choosing

$$\mathcal{Q} = \mathcal{Q}_N = \mathcal{Q}_N^D \cup \mathcal{Q}_N^C , \tag{2.33}$$

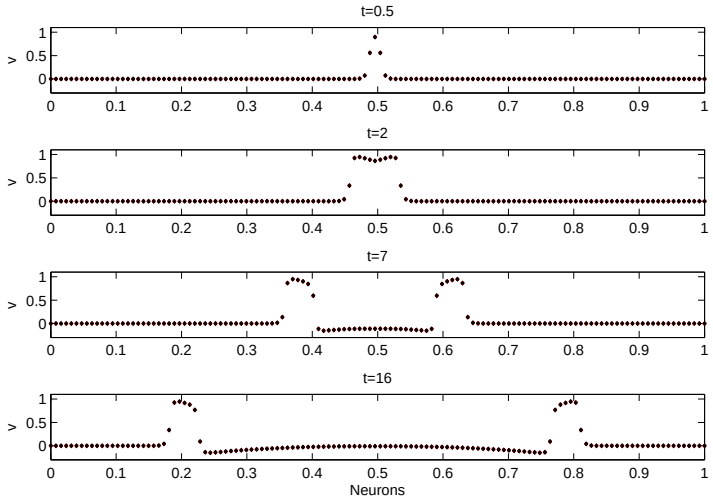

Figure 2.6: Having chosen $N = 128$, a comparison between Approaches I and II is shown.

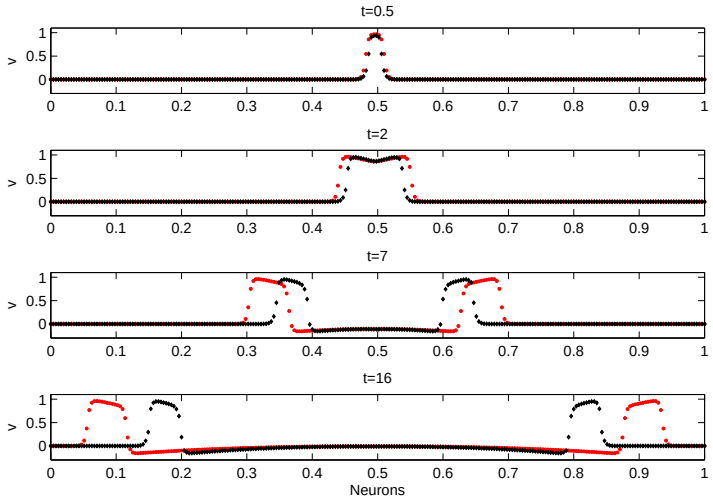

Figure 2.7: With $N = 256$, comparison between Approaches I and II is shown.

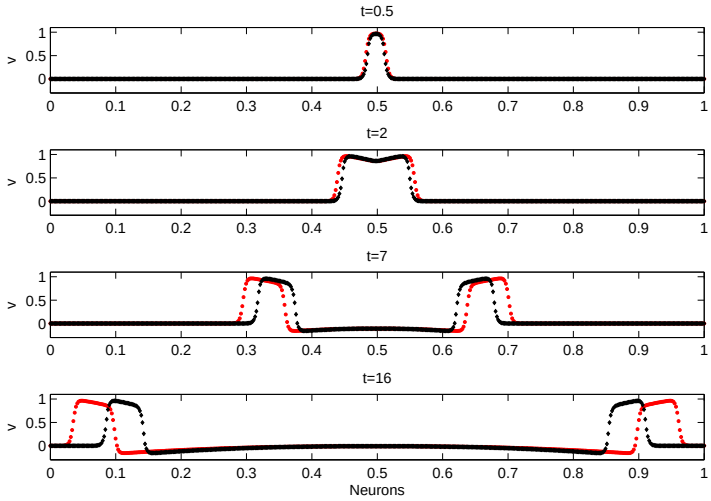

Figure 2.8: $N = 512$ neurons. A comparison between Approaches I and II is shown.

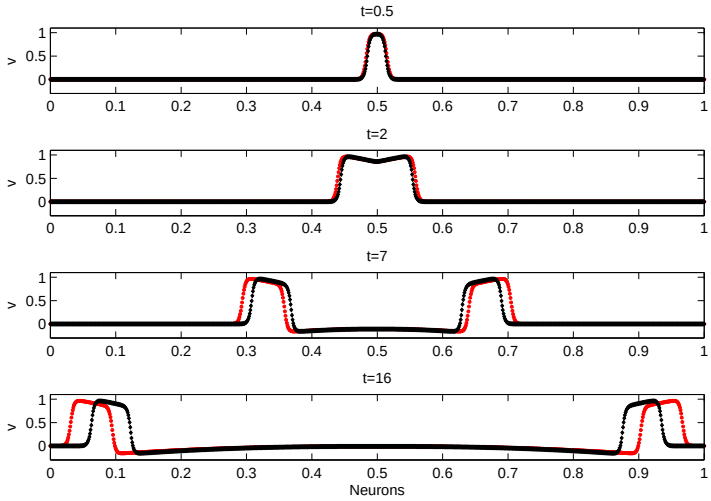

Figure 2.9: $N = 1024$ neurons. A comparison between Approaches I and II is shown.

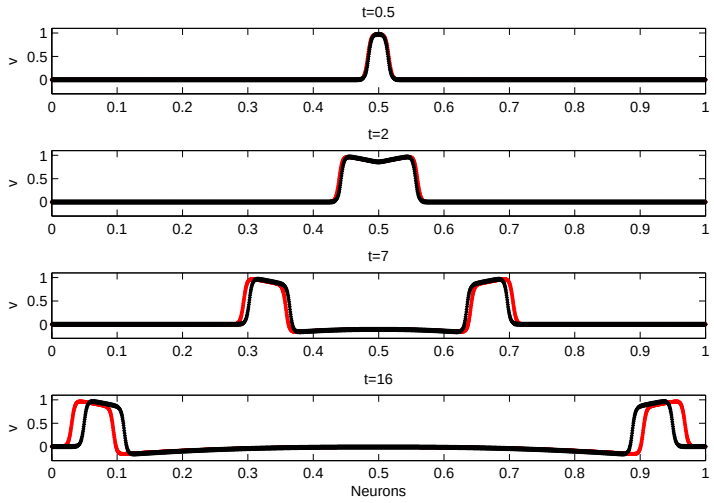

Figure 2.10: $N = 2048$ neurons. A comparison between Approaches I and II is shown.

where

$$\mathcal{Q}_N^D = \{\pm 1, \cdots, \pm Q_N^D\}\,, \quad \mathcal{Q}_N^C = \{Q_N^D + 1, \cdots, Q_N^C\}\,.$$

for some integers $Q_N^D \geq 1$ and $Q_N^C > Q_N^D$. (Choosing $-\mathcal{Q}_N^C$ instead of $\mathcal{Q}_N^C$ would be an obvious alternative.) We will prove that a suitable choice of Q_N^C depending on N leads to modify the limit model (2.14), by adding a first order term to the action potential equation.

With our definitions, the sum in the diffusive coupling becomes

$$\sum_{q\in\mathcal{Q}_N} (v_{i+q} - v_i) = \sum_{q=-Q_N^D}^{Q_N^D} (v_{i+q} - v_i) + \sum_{q=Q_N^D+1}^{Q_N^C} (v_{i+q} - v_i)\,. \tag{2.34}$$

Exploiting the Taylor expansion (2.8), we obtain

$$\begin{aligned}&\sum_{q\in\mathcal{Q}_N} (v_{i+q} - v_i) = \\ &\left(\sum_{q=Q_N^D+1}^{Q_N^C} q\right)\Delta x v'(x_i) + \left(\sum_{q=1}^{Q_N^D} q^2 + \frac{1}{2}\sum_{q=Q_N^D+1}^{Q_N^C} q^2\right)\Delta x^2 v''(x_i) + \text{h.o.t.}\,.\end{aligned} \tag{2.35}$$

Recalling the definition (2.20) of the function φ, and introducing the function $\psi : \mathbb{R}^+ \to \mathbb{R}^+$ defined as

$$\psi(x) = \frac{x(x+1)}{2} \tag{2.36}$$

and such that $\sum_{q=1}^{n} q = \psi(n)$, it is easily seen that the diffusive coupling takes the form

$$\begin{aligned} -(L_G v)_i = d \Big[& (\psi(Q_N^C) - \psi(Q_N^D))\Delta x v'(x_i) \\ & + \frac{1}{2}(\varphi(Q_N^D) + \varphi(Q_N^C))\Delta x^2 v''(x_i) + \text{h.o.t} \Big] \ . \end{aligned} \tag{2.37}$$

Ideally, we would like to find integers Q_N^D and $Q_N^C > Q_N^D$ satisfying the system

$$\begin{cases} \dfrac{1}{2} d(\phi(Q_N^D) + \phi(Q_N^C)) \dfrac{1}{N^2} = d^* \\ d(\psi(Q_N^C) - \psi(Q_N^D)) \dfrac{1}{N} = c^* \ , \end{cases} \tag{2.38}$$

for fixed constants $d^*, c^* > 0$. At first, we discuss the existence of real solutions $Q_N^{D,r}$ and $Q_N^{C,r}$.

Proposition 2.3. Set $A_N = 2\frac{d^*}{d} N^2$ and $B_N = \frac{c^*}{d} N$. If

$$\varphi(\psi^{-1}(B_N)) \leq A_N \ , \tag{2.39}$$

there exists a unique solution $(Q_N^{D,r}, Q_N^{C,r}) \in \mathbb{R}_+^2$ of the previous system.

Proof. For simplicity, let us set $\hat{x} = Q_N^{D,r}$ and $\hat{y} = Q_N^{C,r}$. They should satisfy

$$\begin{cases} \varphi(\hat{x}) + \varphi(\hat{y}) = A_N \\ \psi(\hat{y}) - \psi(\hat{x}) = B_N \ . \end{cases} \tag{2.40}$$

Recalling that both φ and ψ are strictly increasing bijections from $[0, +\infty)$ into itself, the second equation yields

$$\hat{y} = \psi^{-1}(\psi(\hat{x}) + B_N) \ ,$$

which, substituted into the first equation, yields

$$\varphi(\hat{x}) + \varphi(\eta(\hat{x})) = A_N \ , \tag{2.41}$$

with $\eta(\hat{x}) := \psi^{-1}(\psi(\hat{x}) + B_N)$. Now the function $\chi = \varphi + \varphi \circ \eta$ is again strictly increasing, and maps $[0, +\infty)$ into $[\chi(0), +\infty) = [\varphi(\psi^{-1}(B_N)), +\infty)$. Thus, condition (2.39) is equivalent to the existence of a unique solution of (2.41), whence the result. □

We observe that, given any arbitrary d^* and c^*, there always exists an integer N^* such that condition (2.39) is satisfied for all $N \geq N^*$.

Definition 2.1. Under the assumption (2.39), we define Q_N^D and Q_N^C, resp., to be the nearest integers to $Q_N^{D,r}$ and $Q_N^{C,r}$, resp., which are the unique solutions of the system

$$\begin{cases} \dfrac{1}{2} d(\phi(Q_N^{D,r}) + \phi(Q_N^{C,r}))\dfrac{1}{N^2} = d^* \\ d(\psi(Q_N^{C,r}) - \psi(Q_N^{D,r}))\dfrac{1}{N} = c^* \ . \end{cases} \tag{2.42}$$

Proposition 2.4. The following asymptotic behaviour of the integers Q_N^D and Q_N^C holds:

$$Q_N^D \simeq N^{\frac{2}{3}}, \qquad Q_N^C \simeq N^{\frac{2}{3}} \quad \text{with} \quad Q_N^C - Q_N^D \simeq N^{\frac{1}{3}}.$$

Proof. It is enough to estimate $\hat{x} = Q_N^{D,r}$ and $\hat{y} = Q_N^{C,r}$. We recall that they satisfy (2.40). With the ansatz $\hat{y} \simeq N^\alpha$, we have $\varphi(\hat{y}) \simeq N^{3\alpha}$. On the other hand, the inequality $\hat{x} < \hat{y}$ and the monotonicity of φ yield $\varphi(\hat{y}) \leq \varphi(\hat{x}) + \varphi(\hat{y}) \leq 2\varphi(\hat{y})$. Since $A_N \simeq N^2$, we deduce that $\varphi(\hat{y}) \simeq N^2$, whence $\alpha = 2/3$. On the other hand, $\psi(\hat{y}) \simeq N^{\frac{4}{3}}$ so that $\psi(\hat{x}) = \psi(\hat{y}) + B_N \simeq N^{\frac{4}{3}} + N \simeq N^{\frac{4}{3}}$, which implies $\hat{x} \simeq N^{\frac{2}{3}}$. Finally, by Lagrange's theorem,

$$N \simeq B_N = \psi(\hat{y}) - \psi(\hat{x}) = \psi'(\hat{z})(\hat{y} - \hat{x})$$

for some $\hat{x} < \hat{z} < \hat{y}$; since $\psi'(\hat{z}) = \hat{z} + 1/2 \simeq N^{\frac{2}{3}}$, we conclude that $\hat{y} - \hat{x} \simeq N^{\frac{1}{3}}$. □

Even for the present model, interactions are local. Indeed, all neurons linked to the $i-$th one belong to the interval

$$I = [x_i - Q_N^D \Delta x, x_i + Q_N^C \Delta x] \ ,$$

whose length shrinks to 0 as $N \to \infty$ since $Q_N^D \Delta x$, $Q_N^C \Delta x \simeq N^{-\frac{1}{3}}$.

In order to accommodate the effect of the slight shift from $(Q_N^{D,r}, Q_N^{C,r})$ to (Q_N^D, Q_N^C), we introduce perturbations (d_N^*, c_N^*) of (d^*, c^*). They are defined in such a way that (Q_N^D, Q_N^C) is the solution of the system

$$\begin{cases} \dfrac{1}{2} d(\phi(Q_N^D) + \phi(Q_N^C))\dfrac{1}{N^2} = d_N^* \\ d(\psi(Q_N^C) - \psi(Q_N^D))\dfrac{1}{N} = c_N^* \ . \end{cases} \tag{2.43}$$

The size of the perturbation can be estimated as follows.

Proposition 2.5. The perturbed coefficients d_N^* and c_N^* introduced above satisfy

$$|d_N^* - d^*| \lesssim N^{-\frac{2}{3}}, \quad |c_N^* - c^*| \lesssim N^{-\frac{1}{3}} .$$

Proof. Using (2.42) and (2.43), we get

$$\begin{aligned} d_N^* - d^* &= \frac{d}{2N^2}\left[(\varphi(Q_N^D) - \varphi(Q_N^{D,r})) + (\varphi(Q_N^C) - \varphi(Q_N^{C,r}))\right] , \\ c_N^* - c^* &= \frac{d}{N}\left[(\psi(Q_N^D) - \psi(Q_N^{D,r})) - (\psi(Q_N^C) - \psi(Q_N^{C,r}))\right] . \end{aligned}$$

As in the proof of Proposition 2.2, we have $|\varphi(Q_N^D) - \varphi(Q_N^{D,r})| \lesssim N^{\frac{4}{3}}$, $|\varphi(Q_N^C) - \varphi(Q_N^{C,r})| \lesssim N^{\frac{4}{3}}$, and $|\psi(Q_N^D) - \psi(Q_N^{D,r})| \lesssim N^{\frac{2}{3}}$, $|\psi(Q_N^C) - \psi(Q_N^{C,r})| \lesssim N^{\frac{2}{3}}$, which gives the result. □

Finally, we study the limit behaviour of our model as $N \to \infty$. To this end, we make use of the following expression for the higher order terms in (2.37):

$$\text{h.o.t.} = \frac{1}{12}\sum_{q=1}^{Q_N^D} q^4 \Delta x^4 v^{(iv)}(\bar{x}_{i,q}) + \frac{1}{6}\sum_{q=Q_N^D+1}^{Q_N^C} q^3 \Delta x^3 v'''(\bar{\bar{x}}_{i,q}) ,$$

which holds under the assumption that the fourth derivative of v is continuous in $[0,1]$, for suitable points $\bar{x}_{i,q} \in (x_{i-q}, x_{i+q})$ and $\bar{\bar{x}}_{i,q} \in (x_i, x_{i+q})$. Then, we observe that

$$\sum_{q=1}^{Q_N^D} q^4 \Delta x^4 \simeq (Q_N^D)^5 \Delta x^4 \simeq N^{\frac{10}{3}-4} = N^{-\frac{2}{3}}$$

and

$$\sum_{q=Q_N^D+1}^{Q_N^C} q^3 \Delta x^3 \simeq \left[(Q_N^C)^4 - (Q_N^D)^4\right] \Delta x^3 \simeq N^{\frac{7}{3}-3} = N^{-\frac{2}{3}} .$$

Thus, we obtain the following result.

Theorem 2.2. *Fix any point $\hat{x} \in [0,1]$ and for each N, consider a neuron $i = i(N)$ such that $x_{i(N)} \to \hat{x}$ as $N \to \infty$. Assuming the continuity of the fourth derivative of v in $[0,1]$, we have*

$$-(L_G v)_{i(N)} \to d^* v''(\hat{x}) + c^* v'(\hat{x}) \quad \text{as } N \to \infty .$$

Therefore, the discrete model (2.4) *with $\mathcal{Q}$ given by* (2.33) *and Q_N^D, Q_N^C defined in*

Definition 2.1 leads for $N \to \infty$ to the continuous model

$$\begin{aligned} \frac{\partial v}{\partial t} &= f(v,r) + d^* \frac{\partial^2 v}{\partial x^2} + c^* \frac{\partial v}{\partial x} \,, \\ \frac{\partial r}{\partial t} &= g(v,r) \,, \end{aligned} \tag{2.44}$$

which describes the behaviour of a continuum of neurons disposed along a closed ring.

□

Remark 2. A few comments are in order.

i) Observe that having a larger number of neurons influencing a given neuron from its right rather than from its left results in a convective term, whose coefficient c^* is positive; this corresponds to a negative speed of convective propagation, i.e., waves moving from right to left, as documented by Fig. 2.11. Obviously, choosing $c^* = 0$ yields $\mathcal{Q}_N^C = \emptyset$, so one is back to the symmetric case considered in Sect. 2.2.2.

ii) The same limit model can be obtained with a nearest-neighbour interaction that extends the one considered in Sect. 2.2.1, i.e.,

$$-(L_G v)_i = d_N[(v_{i+1} - v_i) + (v_{i-1} - v_i)] + c_N(v_{i+2} - v_i) \,, \tag{2.45}$$

with $d_N = d^* N^2$ and $c_N = c^* \frac{N}{2}$.

iii) A generalization to variable coefficients d^* and c^* similar to the one discussed in Remark 1 is also possible, yielding the two last terms on the right-hand side of (2.44) being replaced by the conservation form $\frac{\partial}{\partial x}\left(d^* \frac{\partial v}{\partial x}\right) + \frac{\partial}{\partial x}(c^* v)$.

We now provide some quantitative insights for our model. Extending the test case considered in the previous subsection, we choose $d = 0.05$ and we enforce that for $N = N_0 = 128$, we have $Q_{N_0}^D = Q_{N_0}^{D,r} = 1$ and $Q_{N_0}^C = Q_{N_0}^{C,r} = 2$, i.e., each neuron is influenced by its first neighbour on the left and by the two first neighbours on the right. Using (2.42), we obtain

$$\begin{aligned} d^* &= \frac{3 \cdot 0.05}{128^2} = 9.1553 \cdot 10^{-6} \,, \\ c^* &= \frac{2 \cdot 0.05}{128} = 7.8125 \cdot 10^{-4} \,. \end{aligned}$$

Then, we increase N by powers of 2 and we monitor the evolution of the quantities Q_N^D and Q_N^C, as well as the errors $d_N^* - d^*$ and $c_N^* - c^*$. The results, reported in

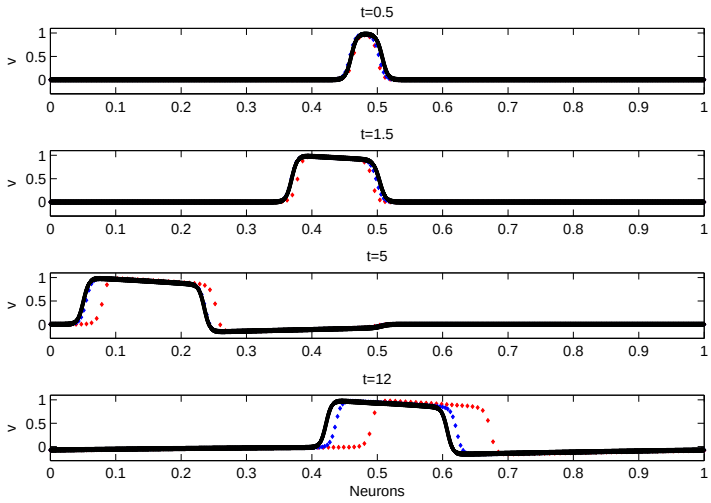

Figure 2.11: Convergence of the discrete model (2.4)-(2.33)-(2.42) as $N \to \infty$. Evolution of a pulse for $N = 128$ (red dots), $N = 256$ (blue dots) and $N = 8192$ (black dots)

Table 2.2, indicate an excellent agreement with the theoretical predictions given in Propositions 2.4–2.5. The evolutions of the action potentials produced by the discrete model with $N = 512$ and $N = 2048$, and by a very accurate solution of the continuous model (2.44) are documented in Figure 2.11.

2.3 Multi-dimensional dynamics

In this section, we extend the previous one-dimensional treatment, and in particular the material of Section 2.2.4, to describe the dynamics of a multi-dimensional agglomeration of neurons. We will focus on the main aspects of the analysis, leaving to the reader those details that are straightforward extensions of the one-dimensional results.

We assume that neurons form a periodic lattice contained in $B = [0,1]^m$, $m = 2$ or $m = 3$. Precisely, given any integer $n \geq 2$ and setting $h = 1/n$, each neuron is associated to a multi-index $l \in \{0, \cdots, n-1\}^m$, which identifies its physical position $x = hl \in B$. Thus we have $N = n^m$ distinct neurons in B, which are labelled by indices $i \in \{1, \cdots, N\}$ according to some rule; the $i-$th neurons has position $x_i = hl_i$, action potential v_i and recovery variable r_i. Periodicity means that we replicate the situation at $x = hl$ in any $y = h(l + nk)$ with $k \in \mathbb{Z}^m$.

We adopt again the diffusion model (2.4), with $\mathcal{Q}$ given by (2.33). The definition of $\mathcal{Q}_N^D$ and $\mathcal{Q}_N^C$ is as follows:

Table 2.2: Number of connections per neuron Q_D, Q_C, convection coefficient $\tilde{c}_N$ and diffusion coefficient $\tilde{d}_N$ as a function of N are shown.

p	$N = N = 2^p$	Q_N^D	Q_N^C	$N_0 d_N^*$	$\lvert d_N^* - d_N\rvert/d_N$	$N_0 c_N^*$	$\lvert c_N^* - c_N\rvert/c_N$
0	128	1	2	0.1500	0	0.1000	0
1	256	2	3	0.1188	$2.1{\cdot}10^{-1}$	0.0750	$2.5{\cdot}10^{-1}$
2	512	4	5	0.1328	$1.1{\cdot}10^{-1}$	0.0625	$3.75{\cdot}10^{-1}$
3	1024	7	9	0.1660	$1.1{\cdot}10^{-1}$	0.1063	$6.25{\cdot}10^{-2}$
4	2048	11	14	0.1485	$9.8{\cdot}10^{-3}$	0.1219	$2.2{\cdot}10^{-1}$
5	4096	19	22	0.1524	$2.0{\cdot}10^{-2}$	0.0984	$1.6{\cdot}10^{-2}$
6	8192	31	35	0.1546	$3.0{\cdot}10^{-2}$	0.1047	$4.7{\cdot}10^{-2}$
7	16384	50	55	0.1524	$1.6{\cdot}10^{-2}$	0.1035	$3.5{\cdot}10^{-2}$
8	32768	80	86	0.1486	$9.2{\cdot}10^{-3}$	0.0979	$2.1{\cdot}10^{-2}$
9	65536	129	136	0.1499	$7.6{\cdot}10^{-4}$	0.0909	$9.1{\cdot}10^{-2}$
10	131072	206	216	0.1506	$4.2{\cdot}10^{-3}$	0.1033	$3.3{\cdot}10^{-2}$
11	262144	329	341	0.1502	$1.4{\cdot}10^{-3}$	0.0983	$1.7{\cdot}10^{-2}$
12	524288	524	540	0.1501	$6.7{\cdot}10^{-4}$	0.1040	$4.0{\cdot}10^{-2}$
13	1048576	835	854	0.1499	$6.6{\cdot}10^{-4}$	0.0980	$2.0{\cdot}10^{-2}$
14	2097152	1329	1353	0.1499	$4.7{\cdot}10^{-4}$	0.0982	$1.7{\cdot}10^{-2}$
15	4194304	2114	2145	0.1500	$1.5{\cdot}10^{-4}$	0.1008	$7.5{\cdot}10^{-3}$
16	8388608	3361	3400	0.1499	$5.4{\cdot}10^{-5}$	0.1006	$6.0{\cdot}10^{-2}$
17	16777216	5342	5391	0.1499	$9.3{\cdot}10^{-5}$	0.1003	$3.2{\cdot}10^{-3}$
18	33554432	8489	8550	0.1500	$3.0{\cdot}10^{-5}$	0.0991	$8.7{\cdot}10^{-3}$
19	67108864	13485	13563	0.1500	$1.8{\cdot}10^{-5}$	0.1006	$6.0{\cdot}10^{-3}$
20	134217728	21420	21517	0.1500	$5.5{\cdot}10^{-7}$	0.0993	$7.0{\cdot}10^{-3}$

- given a radius $R_N^D := hQ_N^D$ with $Q_N^D > 0$ (to be determined later on), we set

$$\mathcal{Q}_N^D := \{q : \|x_{i+q} - x_i\| \leq R_N^D\} ; \tag{2.46}$$

- given a radius $R_N^C := hQ_N^C$ with $Q_N^C \geq Q_N^D$ (to be determined later on), and a unit vector $\nu \in \mathbb{R}^m$, we set

$$\mathcal{Q}_N^C := \{q : R_N^D < \|x_{i+q} - x_i\| \leq R_N^C \text{ and } (x_{i+q} - x_i) \cdot \nu \geq 0\} , \tag{2.47}$$

  i.e., $\mathcal{Q}_N^C$ identifies neurons sitting on semi-balls of suitable radii centered at x_i; these semi-balls are obtained by cutting the corresponding balls by the hyperplane containing x_i and perpendicular to ν, and retaining the halves oriented in the direction of ν (see Figure 2.12 for a pictorial representation of the sets $\mathcal{Q}_N^D$ and $\mathcal{Q}_N^C$ in two dimensions).

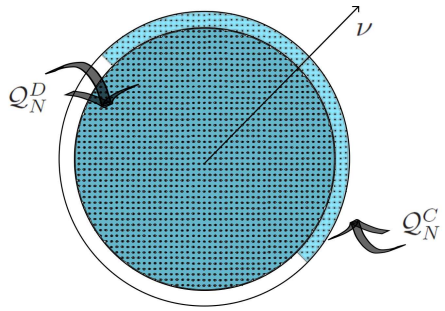

Figure 2.12: The sets $\mathcal{Q}_N^D$ and $\mathcal{Q}_N^C$ represented in a two-dimensional lattice

The effect of $\mathcal{Q}_N^D$ on the diffusion term $-(L_G v)_i$

Observe that $q \in \mathcal{Q}_N^D$ iff $x_{i+q} = hl_{i+q} = h(l_i + k)$ for some $k \in \mathcal{K}_N^D := \{k \in \mathbb{Z}^m : \|k\| \leq Q_N^D\}$. Thus, recalling (2.5), we have

$$\sum_{q \in \mathcal{Q}_N^D} (v_{i+q} - v_i) = \sum_{k \in \mathcal{K}_N^D} h\, k \cdot \nabla v(x_i) + \frac{1}{2} h^2 k^T H v(x_i) k + \text{h.o.t.} \,. \tag{2.48}$$

Now, writing

$$k^T H v(x_i) k = \sum_{\alpha=1}^{m} k_\alpha^2 D_{\alpha\alpha}^2 v(x_i) + \sum_{\substack{\alpha,\beta=1 \\ \alpha \neq \beta}}^{m} k_\alpha k_\beta D_{\alpha\beta}^2 v(x_i) \,,$$

we get

$$\sum_{k \in \mathcal{K}_N^D} k^T H v(x_i) k = \sum_{\alpha=1}^{m} \left(\sum_{k \in \mathcal{K}_N^D} k_\alpha^2 \right) D_{\alpha\alpha}^2 v(x_i) + \sum_{\substack{\alpha,\beta=1 \\ \alpha \neq \beta}}^{m} \left(\sum_{k \in \mathcal{K}_N^D} k_\alpha k_\beta \right) D_{\alpha\beta}^2 v(x_i) \,.$$

Now, it is easily seen that by the form of $\mathcal{K}_N^D$, the quantity

$$\varphi(Q_N^D) := \sum_{k \in \mathcal{K}_N^D} k_\alpha^2, \qquad \text{with } \alpha = 1, \cdots, m$$

is independent of α, whereas

$$\sum_{k \in \mathcal{K}_N^D} k = 0, \qquad \sum_{k \in \mathcal{K}_N^D} k_\alpha k_\beta = 0 \quad \text{if } \alpha \neq \beta \,,$$

since vectors in $\mathcal{K}_N^D$ can be arranged in couples that are symmetric with respect to each coordinate hyperplane. Thus,

$$\sum_{q\in\mathcal{Q}_N^D}(v_{i+q}-v_i)=\frac{1}{2}h^2\varphi(Q_N^D)\Delta v(x_i)+\text{h.o.t.}\,, \tag{2.49}$$

where $\Delta v=\sum_{\alpha=1}^m D_{\alpha\alpha}^2 v$ is the Laplacian of the function v. We observe for further reference that for any $Q>0$, denoting by $\mathcal{B}(0,Q)$ the ball of center 0 and radius Q in $\mathbb{R}^m$, one has for any given $\alpha=1,\cdots,m$

$$\varphi(Q)=\sum_{\|k\|\le Q}k_\alpha^2\sim\int_{\mathcal{B}(0,Q)}y_\alpha^2\,\mathrm{d}y\simeq Q^{2+m}\quad\text{as } Q\to\infty\,.$$

The effect of $\mathcal{Q}_N^C$ on the diffusion term $-(L_G v)_i$

Now, $q\in\mathcal{Q}_N^C$ iff $x_{i+q}=h(l_i+k)$ for some $k\in\mathcal{K}_N^C:=\{k\in\mathbb{Z}^m: Q_N^D<\|k\|\le Q_N^C \text{ and } k\cdot\nu>0\}$. At this point, we assume that $\nu=e_1$, the first element of the canonical basis in $\mathbb{R}^m$; this choice is not at all restrictive, but simplifies the following arguments. Indeed, referring to the analogue of (2.48) in which $\mathcal{Q}_N^D$, $\mathcal{K}_N^D$ resp., are replaced by $\mathcal{Q}_N^C$, $\mathcal{K}_N^C$ resp., we have

$$\sum_{k\in\mathcal{K}_N^C}k\cdot\nabla v(x_i)=\left(\sum_{k\in\mathcal{K}_N^C}k_1\right)\frac{\partial v}{\partial x_1}(x_i)=\left(\psi(Q_N^C)-\psi(Q_N^D)\right)\frac{\partial v}{\partial x_1}(x_i)\,,$$

with

$$\psi(Q):=\sum_{\substack{\|k\|\le Q\\ k_1\ge 0}}k_1\sim\int_{\mathcal{B}(0,Q)\cap\{y_1\ge 0\}}y_1\,\mathrm{d}y\simeq Q^{1+m}\quad\text{as } Q\to\infty\,.$$

On the other hand,

$$\sum_{k\in\mathcal{K}_N^C}k^T Hv(x_i)k=\sum_{\alpha=1}^m\left(\sum_{k\in\mathcal{K}_N^C}k_\alpha^2\right)D_{\alpha\alpha}^2 v(x_i)\,.$$

But now,

$$\sum_{k\in\mathcal{K}_N^C}k_\alpha^2=\frac{1}{2}\sum_{Q_N^D<\|k\|\le Q_N^C}k_\alpha^2=\frac{1}{2}\left(\varphi(Q_N^C)-\varphi(Q_N^D)\right)\,.$$

We conclude that, going back to the case of an arbitrary ν,

$$\sum_{q\in\mathcal{Q}_N^C}(v_{i+q}-v_i) = d\left[h\left(\psi(Q_N^C)-\psi(Q_N^D)\right)\nu\cdot\nabla v(x_i) + \frac{1}{4}h^2\left(\varphi(Q_N^C)-\varphi(Q_N^D)\right)\Delta v(x_i)+\text{h.o.t.}\right] . \tag{2.50}$$

The global effect of $\mathcal{Q}_N^C$

Summing up (2.49) and (2.50), we obtain

$$-(L_G v)_i = dh\left(\psi(Q_N^C)-\psi(Q_N^D)\right)\nu\cdot\nabla v(x_i) + \frac{d}{4}h^2\left(\varphi(Q_N^D)+\varphi(Q_N^C)\right)\Delta v(x_i)+\text{h.o.t.} .$$

At this point, given two constants $d^*>0$ and $c^*\geq 0$, we would like to find $Q_N^D>0$ and $Q_N^C\geq Q_N^D$ such that

$$\begin{cases} d\dfrac{h^2}{4}(\phi(Q_N^D)+\phi(Q_N^C)) = d^* \\ dh(\psi(Q_N^C)-\psi(Q_N^D)) = c^* . \end{cases} \tag{2.51}$$

This system is similar to (2.38) and we can discuss its solvability as done in Section 2.2.4. The conclusion is that for N large enough, the solution exists and satisfies

$$Q_N^D\simeq Q_N^C\simeq N^{\frac{2}{m(m+2)}} \quad\text{and}\quad Q_N^C-Q_N^D\simeq c^*N^{\frac{2-m}{m(m+2)}} ,$$

whereas the number of neurons that should be connected to a given neuron scales like $N^{\frac{2}{m+2}}$. We summarize our conclusions as follows.

Theorem 2.3. *The discrete model* (2.4)*, with* $\mathcal{Q}$ *given by* (2.33)-(2.46)-(2.47) *in which* Q_N^D *and* Q_N^C *are the solution of* (2.51)*, tends for* $N\to\infty$ *to the following continuous model of reaction-convection-diffusion type*

$$\begin{aligned} \frac{\partial v}{\partial t} &= f(v,r)+d^*\Delta v+\hat{c}^*\cdot\nabla v , \\ \frac{\partial r}{\partial t} &= g(v,r) , \end{aligned} \tag{2.52}$$

where the convective velocity is given by the vector $\hat{c}^*=c^*\nu$.

The well-posedness of this model, as well as its numerical discretization, can be studied by adapting the arguments given in [12] and [43].

An example of a two-dimensional dynamics produced by the model described above is given in Figure 2.13. We fix $d = 0.05$ as for the one-dimensional models; then, we choose d^* and c^* in such a way that (2.51) is satisfied for $n = 256$ by $Q_N^D = \sqrt{2}$ and $Q_N^C = 2$. This gives

$$d^* = 3.8147 \cdot 10^{-6} \quad \text{and} \quad c^* = 3.9063 \cdot 10^{-4} \, .$$

The vector ν is chosen to be e_1. Figure 2.13 shows the evolution of the action potential in the periodic box $B = [0, 1]^2$ for $n = 256$, starting from an initial stimulus $v_{|t=0} = 1$ applied to the neurons lying in the circle of radius $1/32$ around the center of the box. The stimulus propagates in all directions, but since $c^* > 0$ the speed of propagation is faster in the direction of $-\nu$.

2.3.1 Pseudo-random connections

While the models considered so far are fully deterministic, it is interesting to introduce a form of randomness and monitor its effects. In the simplest form, this can be accomplished by perturbing the model considered above via a (pseudo-)random removal of a fixed percentage of links among neurons. Connections to each neuron are turned-off with uniform distribution in the given percentage, independently of the other neurons; thus, the set $\mathcal{Q}(i)$ in (2.4) does depend upon i, in a (pseudo-)random manner. Compared to the dynamics in Figure 2.13, by turning off a certain number of connections leads to decreasing of the network activity. The signal propagation becomes more and more difficult, up to the limit case in which the travelling pulse vanishes and the whole network comes back to the equilibrium state.

As an example, we keep the same parameters $d = 0.05$, $Q_N^D = \sqrt{2}$, $Q_N^C = 2$ and $n = 256$, as well as the same initial datum as above, and we choose to turn 30% of connections off. In Figure 2.14, the resulting dynamics at the same time instants as in Figure 2.13 is shown. The random effects on the patterns are apparent. The reduction of active connections is reflected by a weaker propagation strength, i.e., a less travelling pulse velocity and a less number of excited neurons. Indeed, let us consider $t = 10$ as in the second snapshots in Figure 2.13 and 2.14. By qualitatively comparing these dynamics, a diminishing in velocity in the pseudo-random case is evident. Furthermore, it emerges that slightly less than one half of the neurons are still excited. Specifically, the number of active neurons at $t = 10$ in the deterministic dynamics is 2864, while it decreases to 1341 when 30% of connections are eliminated. Furthermore, contours are irregular and, in some realizations not shown here, even disconnected.

By increasing the percentage of turned-off links, what happens is that the travelling pulse having irregular contours propagates slower and slower and involves even less neurons. An observed limit case consists in 85% of connections off. Specifically, the active connections in the percentage of 15% are too few to guarantee the signal propagation and the pulse vanishes before reaching the domain boundaries.

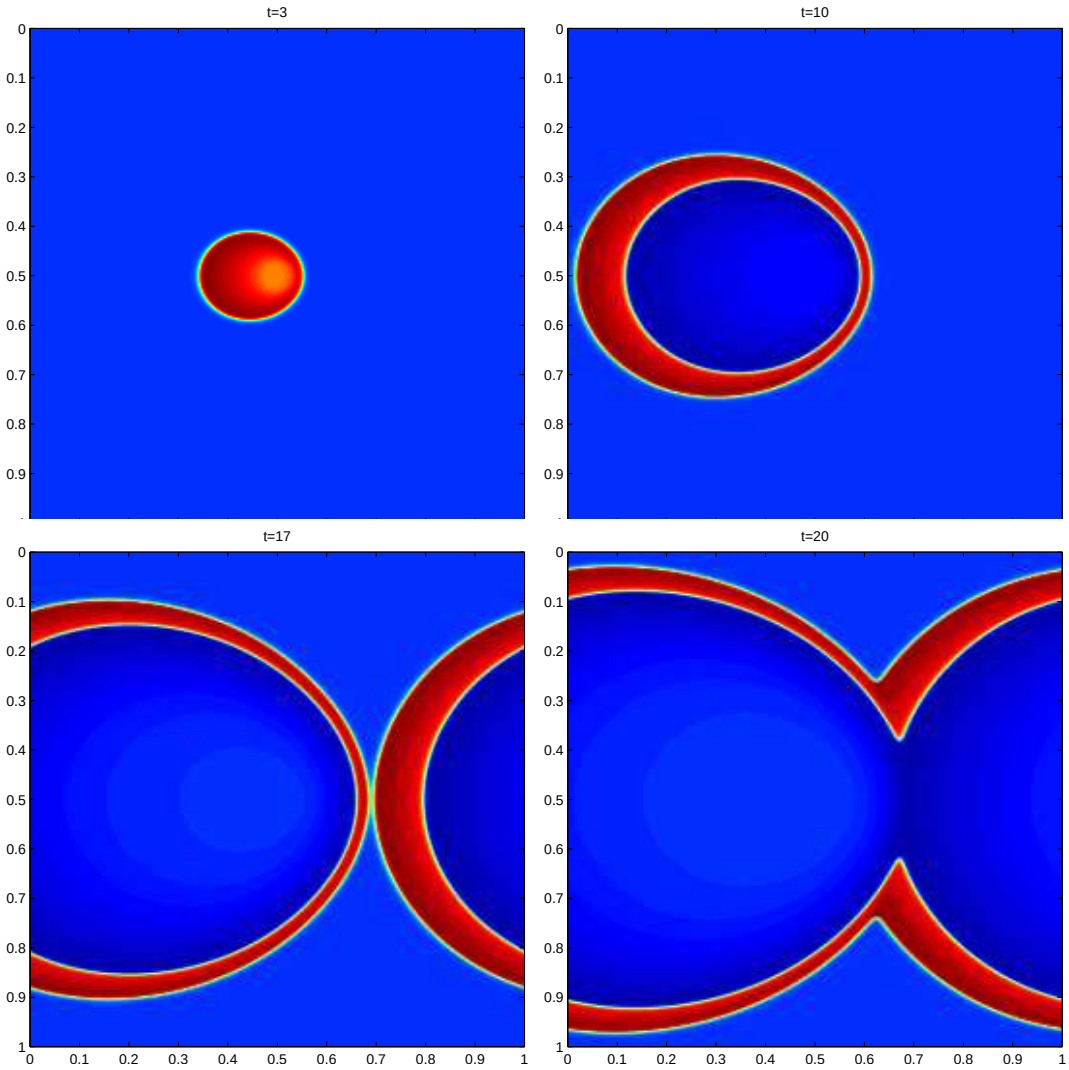

Figure 2.13: Two dimensional dynamics. Evolution of an initial stimulus by the discrete model of Theorem 2.3 in a $N = 256 \times 256$ lattice of neurons

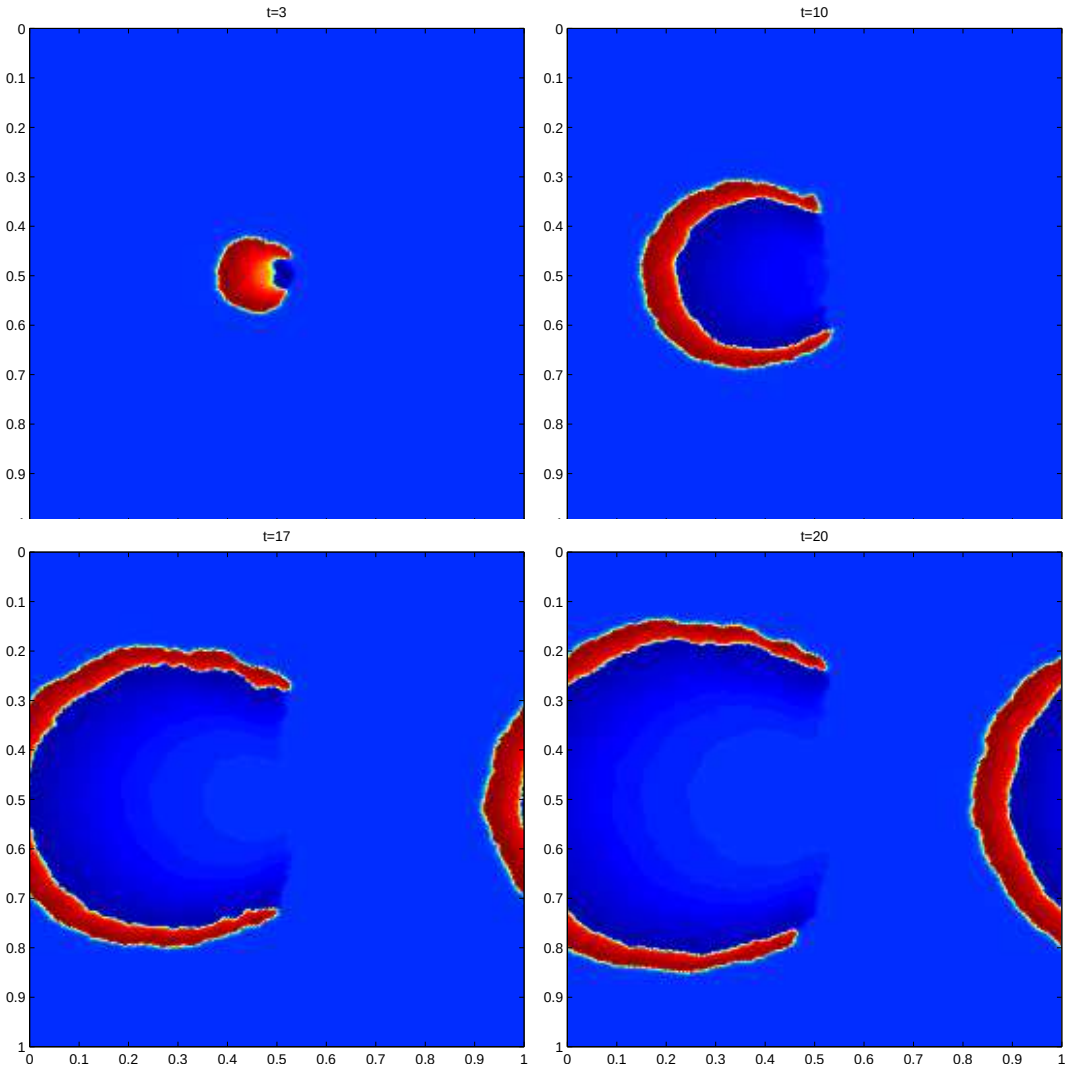

Figure 2.14: Evolution as in Fig. 2.13, but with 30% of the connections turned-off in a pseudo-random way

Chapter 3

Chemically coupled neurons

In the previous chapter we focussed on neuronal networks where neurons were only coupled by electrical synapses, i.e., gap junctions. Although this kind of networks have received increasing attention in recent years, chemical synapses are the most frequent ones in the central nervous system. Thus, after a brief introduction about chemical synapse properties, we will discuss network models in which connections are characterized by chemical synaptic transmission.

3.1 Biological and modelling background

In order to explain the mechanism underlying chemical synapses, let us focus on two chemically coupled neurons: the presynaptic and postsynaptic ones. Most frequently, synapse is located between the axon of the presynaptic cell and a dendrite of the postsynaptic one and it identifies the physical place in which the chemical reaction occurs. Unlike gap junctions, in chemical synapses the axon and the dendrite do not physically touch each other, i.e., there is a gap between them: the synaptic transmission takes place in this specialized site. Schematically, a chemical reaction occurs when a signal from the presynaptic neuron reaches the synapse, and it allows a potential variation in the postsynaptic membrane. Indeed, the action potential causes the depolarization of the axon's terminal which leads to the opening of the voltage gated Ca^{2+} channels. As a consequence of the increasing Ca^{2+} concentration inside the presynaptic membrane, the vesicles filled of neurotransmitters fuse with the presynaptic membrane and their content is released into the synaptic cleft. The neurotransmitters then passively diffuse through the synaptic cleft and finally bind up with postsynaptic receptors. Thanks to this binding between neurotransmitters and receptors, specialized postsynaptic channels

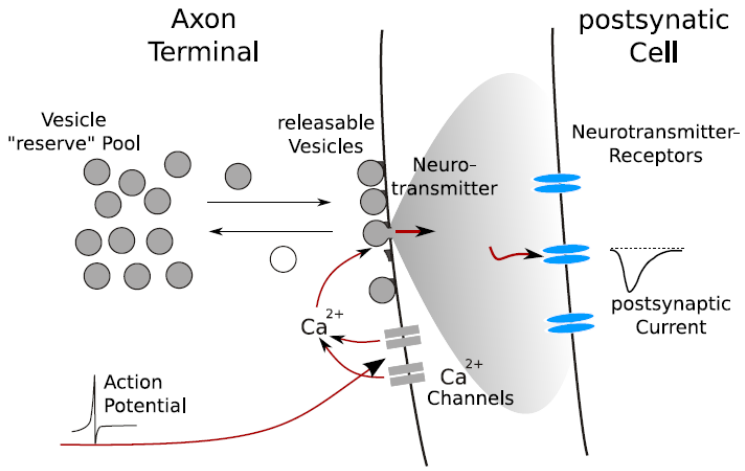

Figure 3.1: Presynaptic, in term of the axon terminal, and postsynaptic cells are depicted. The signal transmission in the synaptic cleft is carried out by neurotransmitters. Specifically, the action potential provokes the opening of the voltage-gated calcium channels (Ca^{2+}). Since the concentration of Ca^{2+} increases inside the presynaptic terminal, vesicles fuse with the terminal and they release neurotransmitters. By diffusion, they reach the postsynaptic cell provoking the opening of specific channels. Variation in potassium and sodium concentration in the postsynaptic cell translates in a change in the membrane potential

open. Accordingly, suitable ions flow through the postsynaptic membrane leading to a change in the postsynaptic membrane potential. Figure 3.1 schematically describes what happens in a synapse. Despite the response amplitude depends upon several factors, two are the main classes collecting the postsynaptic answers: the *excitatory postsynaptic potential* (EPSP) which describes a depolarization in the membrane potential, and the *inhibitory postsynaptic potential* (IPSP) when a membrane potential hyperpolarization occurs. The chief factor that determines the postsynaptic response is the combination of two ingredients: the kind of neurotransmitter released by the presynaptic neuron and the receptor type invoked in the postsynaptic one. Notably, there exist neurotransmitters, such as acetylcholine, for which both excitatory and inhibitory receptors exist and there are some types of receptors that activate complex metabolic pathways in the postsynaptic cell to produce effects that cannot appropriately be called either excitatory or inhibitory. In order to deal with this variegated phenomenon, we could consider postsynaptic neuron response as a direct function of the *synaptic reversal potential*, v_{syn}. This potential ideally takes into account both neurotransmitter and receptors. Nonetheless, it becomes apparent by experimental evaluations that most of neurotransmitters provoke a single type response. For example for the glutamate, the most important receptors all have excitatory effects. For other neurotransmitters, such

as GABA, the most important receptors all have inhibitory responses (although there is evidence that GABA is excitatory during early brain development). This is the reason why neurotransmitters are commonly described as *excitatory* or *inhibitory*. From the predominance of a single response-type, it follows that the postsynaptic potential can be modelled as a direct function of the presynaptic reversal potential, $v_{\text{syn,pre}}$. Despite we will consider this last approach, let us maintain in this introductory part the more general notation v_{syn}.

Authors in [13] propose to determine the current produced by a chemical synapses, I_{syn}, by considering the following linear $I_{\text{syn}} - v$ relationship:

$$I_{\text{syn}}(t) = g_{\text{syn}} s(t)(v(t) - v_{\text{syn}}) \ , \tag{3.1}$$

where $v(t)$ is the postsynaptic potential, $s(t)$ is the fraction of the open channels, $g_{\text{syn}} > 0$ is the maximum conductance and v_{syn} the reversal potential. Following the original approach in [13], the course-time variation of $s = s(t)$ follows by a simple kinetic scheme which takes into account that, when an action potential reaches the presynaptic terminal, it releases in the synaptic cleft the neurotransmitters molecules, T. Furthermore, these molecules bind to the postsynaptic receptors. This translates into considering the following first order kinetic scheme:

$$S + T \underset{\beta}{\overset{\alpha}{\rightleftharpoons}} TS^* \ ,$$

where S and TS^* characterize the bound and the unbound postsynaptic receptors, respectively, and $\alpha\,, \beta$ are the forward and backward rate constants for transmitters binding. Being s the fraction of open channels, i.e., the fraction of bound receptors, it is described by

$$\frac{\mathrm{d}s}{\mathrm{d}t} = \alpha[T](1 - s) - \beta s \ ,$$

where $[T]$ represents the neurotransmitter concentration in the synaptic cleft. We suppose $[T] = 1$ when a presynaptic impulse reaches the synapse, and for few times later. The neurotransmitter release span is determined by the presynaptic potential v_{pre} exceeding an *a priori* fixed threshold v_T. On the contrary we suppose $[T] = 0$ when the threshold is not outpaced. This translates into considering the s time-course as proposed in [15]:

$$\frac{\mathrm{d}s}{\mathrm{d}t} = \alpha(1 - s)H_\infty(v_{\text{pre}} - v_T) - \beta s \ , \tag{3.2}$$

where $H_\infty = H_\infty(x)$ is the Heaviside function such that $H_\infty = 0$ if $x < 0$ and $H_\infty = 1$

otherwise. Postsynaptic neurons could have a certain heterogeneity degree in α and β values. This allows us to describe different cell populations in a unique neuronal network, as proposed in [15]. For example, we could model populations characterized by gamma-aminobutyric acid $GABA_B$ synapses, which have slow opening and closing behaviours, and by $GABA_A$ and $AMPA$ synapses, which have a fast nature in opening and closing channels. In the sequel, if not otherwise specified, we suppose $\alpha > \beta$ according to the fast opening of the sodium channel as opposed to a slower activation of the potassium channel and deactivation of the sodium one. A rigorous treatment of these concepts specifically applied to motorneurons is proposed in [51]. In [13] and [15], a detailed classification of synaptic reversal potentials, linked to distinct neurotransmitter/receptor couples, are specified.

Let us recall that the threshold v_T did not appear in the FitzHugh-Nagumo model described in Chapter 1. The reason is that, as stressed before, the FitzHugh-Nagumo model is not a threshold type one. However, despite the spike generation in the presynaptic neuron being unrelated to a threshold, a bounded neurotransmitter release interval in the chemical synapse term is ensured by v_T in (3.2).

Before going on, a brief digression is now needed. The ordinary differential equation (3.2) is introduced by authors in [13] in order to avoid the necessity of considering a time-varying conductance $g_{\text{syn}} = g_{\text{syn}}(t)$ in (3.2), such as the alpha-function described in [42]:

$$g_{\text{syn}}(t) = \frac{t - t_0}{\tau} \exp\left[-\frac{\mathrm{t} - \mathrm{t}_0}{\tau}\right], \ \mathrm{t} \geq \mathrm{t}_0 \ , \tag{3.3}$$

where t_0 is the time of neurotransmitter release and τ is a time constant. Therefore, in order to take into account the specific time in activating neurotransmitter release and its subsequent time-course, exploiting (3.3) or introducing (3.2) becomes essential. Specifically, neurotransmitter release time in (3.2) coincides with the instant in which $v = v_T$. It means that, despite the presynaptic neuron has already left the quiescent state, as long as it does not reach the threshold v_T, neurotransmitters are not yet released. Of consequence, the postsynaptic neuron is not receiving any synaptic input. This gap in time in the presynaptic neuron dynamics, between the upstroke state and the threshold achieved, introduces a delay in transmission. Such a delay involves the physiological time lapse necessary to starting neurotransmitter release. It is important stressing that this delay cannot be assimilated to an axon conduction delay which would involve both presynaptic and postsynaptic neurons. In this latter case, the variable s in (3.1) would become

$$s_{ij} = s\left(t - \frac{|i - j|}{\nu}\right) \ , \tag{3.4}$$

where ν is the positive axonal velocity value and the timing of s depends upon the distance between the presynaptic neuron j and the postsynaptic one i. The equation (3.4) would rephrase the model that we are going to present in a system of delayed differential equations. Nonetheless axonal delays are not considered in the thesis, we recognize their importance in network description and we will introduce them in forthcoming works.

On the whole, the model which describes the action potential dynamics in a chemically coupled network is the following one, similar to those proposed in [15]:

$$\begin{aligned} \frac{\mathrm{d}v_i}{\mathrm{d}t} &= f(v_i, r_i) - g_{\mathrm{syn},i}\left(\sum_{j\neq i} a_{ij} s_j (v_i - v_{\mathrm{syn},j})\right) , \\ \frac{\mathrm{d}r_i}{\mathrm{d}t} &= g(v_i, r_i) , \\ \frac{\mathrm{d}s_i}{\mathrm{d}t} &= \alpha_i (1 - s_i) H_\infty (v_i - v_T) - \beta_i s_i , \end{aligned} \tag{3.5}$$

where the adjacency matrix $A_G = (a_{ij})$, defined in (2.2), describes the network architecture. For the sake of clarity, let us recall that the letter G identifies the graph, which stands for the network, and that the adjacency matrix entries are defined as follows:

$$a_{ij} = \begin{cases} w_{ij} & \text{if } (i,j) \in E(G) \\ 0 & \text{else} , \end{cases} \tag{3.6}$$

where i, $j = 1, \cdots, N$, the weights w_{ij} are strictly positive and $E(G)$ collects the edges of the graph G. In general, the adjacency matrix A_G could be sparse or dense, local or global. Nonetheless, in our case it is sparse since we assume each neuron is influenced only by those neurons occupying a small spatial area called $\mathcal{B}_i \subseteq B$, where B identifies the whole domain, depending on the neuron but which remains fixed as $N \to \infty$.

By using the Adjacency matrix definition in (3.6) and the notion of $\mathcal{B}_i$, let us rephrase the model (3.5) as follows:

$$\begin{aligned} \frac{\mathrm{d}v_i}{\mathrm{d}t} &= f(v_i, r_i) - g_{\mathrm{syn},i}\left(\sum_{j\in\mathcal{B}(i)} w_{ij} s_j (v_i - v_{\mathrm{syn},j})\right) , \\ \frac{\mathrm{d}r_i}{\mathrm{d}t} &= g(v_i, r_i) , \\ \frac{\mathrm{d}s_i}{\mathrm{d}t} &= \alpha_i (1 - s_i) H_\infty (v_i - v_T) - \beta_i s_i . \end{aligned} \tag{3.7}$$

The presence of a fixed area $\mathcal{B}(i)$ is the key difference between the model (3.7), involving chemical synapses, and the model treated in Chapter 2 where electrical synapses were taken into account. Since interactions involved in electrical synapses are mediated by diffusion, their contributions vanishes as $N \to \infty$ in a bounded domain. In order to avoid this cancellation of the coupling term, a rescaling of the diffusion coefficient or an increase in the number of connections for each neuron had been necessary. Nonetheless, the resulting continuum model was a local one described by a system of reaction-convection-diffusion equations (see Eq.(2.44)). On the contrary, as $N \to \infty$, the model (3.7) leads to the following integro-differential equations:

$$\begin{aligned}
\frac{\partial v}{\partial t} &= f(v(x,t), r(x,t)) - g_{\text{syn}} \int_{\mathcal{B}(x)} w(x,y) s(y,t) \Big(v(x,t) - v_{\text{syn}}(y) \Big) \, \mathrm{d}y \ , \\
\frac{\partial r}{\partial t} &= g(v(x,t), r(x,t)) \ , \\
\frac{\partial s}{\partial t} &= \alpha (1 - s(x,t)) H_\infty (v(x,t) - v_T) - \beta s(x,t) \ ,
\end{aligned}$$

where $\mathcal{B}(x)$ is the set collecting neurons, in the continuum framework, which influence the one placed at x. This model is similar to the system (9.7) in [15]. However, in order to highlight the fact that the reversal potential depends upon the presynaptic neuron, it is explicitly imposed $v_{\text{syn}} = v_{\text{syn}}(y)$ and, thus, the difference $v(x,t) - v_{\text{syn}}(y)$ is included in the integral operator.

Similarly, the discrete model (3.7) differs from (9.6) in [15] because we suppose that v_{syn} depends upon the presynaptic neuron, i.e., $v_{\text{syn},j}$, instead of depending upon the postsynaptic one which would be written $v_{\text{syn},i}$. In other words, the fact that the reversal potential is imposed to depend upon the neurons j, instead of i, means that the neuron which influences the postsynaptic neuron i is the presynaptic one, through the chemical synapses. When there exists a homogeneous reversal potential upon the whole network, i.e., $\forall j \ v_{\text{syn},j} = v_{\text{syn}}$, then the difference $(v_i - v_{\text{syn}})$ becomes independent from j and it can be pulled out of the summation. This assumption is considered in, for example, [4]. Moreover, focusing on the reversal potential in (3.7), we introduce the following notation:

$$v_{\text{syn}} = \begin{cases} v_{\text{syn}}^E \geq 0 \text{ if the presynaptic neuron is excitatory,} \\ v_{\text{syn}}^I < 0 \text{ if the presynaptic neuron is inhibitory.} \end{cases}$$

Specifically, considering a positive reversal potential, v_{syn}^E, the depolarization of the

postsynaptic membrane occurs. The depolarization is followed by, as usual, the hyperpolarization phenomenon until equilibrium is reached. This response in the postsynaptic membrane is due to the excitatory synapses. On the contrary, dealing with a negative value of the reversal potential, $v^I_{\rm syn}$, the hyperpolarization of the membrane suddenly appears. It is followed by the return towards equilibrium. This is the response of the membrane triggered by an inhibitory synapse. The possibility to differentiate these two kinds of synapses is a fundamental ingredient: it makes the model more meaningful from a biological perspective.

Let us stress that the description of a network constituted by heterogeneous neurons can be easily achieved by using parameters in the functions f and g, which depend on the neuron i, i.e., $f = f_i(v_i, r_i)$ and $g = g_i(v_i, r_i)$ in (1.11).

In order to make notations consistent with Chapter 2 where we defined the set $\mathcal{Q}(i)$, let us introduce the set $\mathcal{P}(i)$ which collects indexes p such that neuron $i+p$ is linked to neuron i via chemical synapses. Thus, the chemical coupling term in (3.7) is rephrased as

$$\sum_{p\in\mathcal{P}(i)} w_{i,i+p} s_{i+p}(v_i - v_{{\rm syn},i+p}) \ , \tag{3.8}$$

and the model (3.7) takes the following form:

$$\begin{aligned}
\frac{{\rm d}v_i}{{\rm d}t} &= f(v_i, r_i) - g_{{\rm syn},i}\left(\sum_{p\in\mathcal{P}(i)} w_{i,i+p} s_{i+p}(v_i - v_{{\rm syn},i+p})\right) \ , \\
\frac{{\rm d}r_i}{{\rm d}t} &= g(v_i, r_i) \ , \\
\frac{{\rm d}s_i}{{\rm d}t} &= \alpha_i(1-s_i)H_\infty(v_i - v_T) - \beta_i s_i \ .
\end{aligned} \tag{3.9}$$

Different definitions of the set $\mathcal{P}(i)$ can be considered. Each of them will give rise to a specific network architecture. An immediate choice consists to impose

$$\mathcal{P}(i) := \{p \in \mathbb{Z}\backslash\{0\} : \|x_{i+p} - x_i\| \le r_i\} \ , \tag{3.10}$$

by preliminarily fixing the ranges of interactions $r_i \in \mathbb{R}^+$. Let us underline that the range of interaction does not depend upon the number of neurons N in the domain. Moreover, if $r_i = r \quad \forall i = 1, \cdots, N$ thus, $\mathcal{P}(i) = \mathcal{P}$. It means there is no heterogeneity in the network topology with respect to each neuron.

In the sequel, we will tackle the issue of describing dynamics produced by (3.9) in one and more spatial dimensions.

3.2 One-dimensional dynamics

Firstly we detail the analysis of model (3.9) in the one-dimensional case. As in Chapter 2, neurons are identified by integer labels $i = 1, \cdots, N$. Each neuron occupies a specific physical position x_i in the interval $B = [0, 1)$ given by (2.6):

$$x_i = (i-1)\Delta x = \frac{i-1}{N} \quad \text{with } 1 \leq i \leq N \ ,$$

where N is the number of elements equally distributed along the chain and, consequently, $\Delta x = 1/N$ is the distance between any two adjacent ones. Furthermore, we assume periodic boundary conditions, thus the chain is closed, i.e., we set $v_0 = v_N$ and $v_{i+kN} = v_i$ for any $k \in \mathbb{Z}$.

Let us take into account a network without heterogeneity in the connection rule, i.e., $\mathcal{P}(i) = \mathcal{P}\ \forall i$, with $\mathcal{P}(i)$ as in (3.10). Elements $w_{i,i+p}$ in (3.9), which are the weights collected in the adjacency matrix (2.2), may assume different values according to a specific law chosen. In general, we assume that weights $w_{i,i+p}$ (i.e., w_{ij} in (2.2)) are determined as a function of the number of connections for each neuron. Specifically, let us introduce the scalar value ω which represents the number of connections among nearest-neighbour cells. For example, in this section, $\omega := 2$ (in general, $\omega := 2m$ where m is the space dimension). Thus,

$$w_{i,i+p} = \frac{\omega}{\#\mathcal{P}} \ . \tag{3.11}$$

Naively, carrying out dynamics which involve nearest-neighbour neurons only, weights are unitary. Otherwise, if the number of connections increases, the value of $w_{i,i+p}$ diminishes. In other words, the strength coupling is even up among all of them. Let us stress that each element $w_{i,i+p}$ is often interpreted as the probability to find a connection between cells i and $i + p$.

We first consider the case of all excitatory neurons. The model (3.9), with a suitable initial datum, generates a pulse-like dynamics, as shown in Figure 3.2 where $N = 256$. Specifically, such dynamics is originated by an initial stimulus applied to the central neuron ($i = N/2$) of the line: its action potential is initially set to the value 2, whereas all the other variable are set to 0. The parameters of the model are fixed as follows:

$$\alpha_i = 0.9, \quad \beta_i = 0.1, \quad g_{\mathrm{syn},i} = 0.1, \quad v^E_{\mathrm{syn},i} = 0.9, \quad v_T = 0.9, \quad r = 1/128 \quad \forall i \ . \tag{3.12}$$

Obviously, the choice of parameters characterizes the solution. A key role is played by

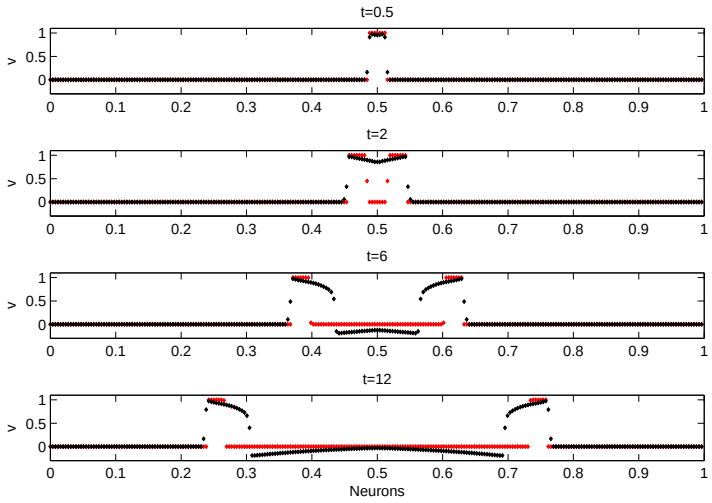

Figure 3.2: Dynamics obtained by exploiting the model (3.9) within a population of $N = 256$ neurons. Red dots with value 1 (0, resp.) indicate neurons such that $v_i \geq v_{\mathrm{T}}$, ($v_i < v_{\mathrm{T}}$)

the threshold v_T: it determines, together with the Heaviside function, the activation or deactivation of ion channels underlying the mechanism of the action potential. In Figure 3.2, the Heaviside function is shown simultaneous to the solution. Increase or decrease of the threshold leads to pulses with different velocities and thickness. Variations in velocity and thickness are documented in Figure 3.3. In every snapshot, $N = 256$. The only parameter that is changing is the value of the threshold v_T. In the first frame of Figure 3.3, $v_T = 0.7$. In the second one, $v_T = 0.8$, and in the last one, $v_T = 0.95$. These frames show dynamics at the same time instances. Note that the third snapshot in Figure 3.3 coincides with the last one in Figure 3.2. It is apparent that the threshold affects the dynamics: the lower is v_T, the bigger is the neuron number in the active state. Thus, the pulse is thicker and quicker. On the opposite, increasing v_T the pulse struggles to arise and to travel along the whole set of neurons.

In Figure 3.4, the evolution in time of the action potential produced by the discrete model (3.9) within populations with a different number of cells is documented. Focusing on both comparisons (between dynamics in populations of $N = 128$, $N = 256$ and $N = 2048$, $N = 4096$), the convergence of the solutions is documented.

Next, in order to embed a certain degree of heterogeneity in the network, let us consider two types of synapses: the inhibitory and the excitatory ones. Differently from (3.12), $v_T = 0.8$ and the inhibitory reversal potential is added, $v^I_{\mathrm{syn},i} = -0.1$. Figure 3.5 shows a dynamics where several neurons receive inhibitory synapses. Let us stress that, according to treatments in Paragraph 3.1, we characterize an inhibitory

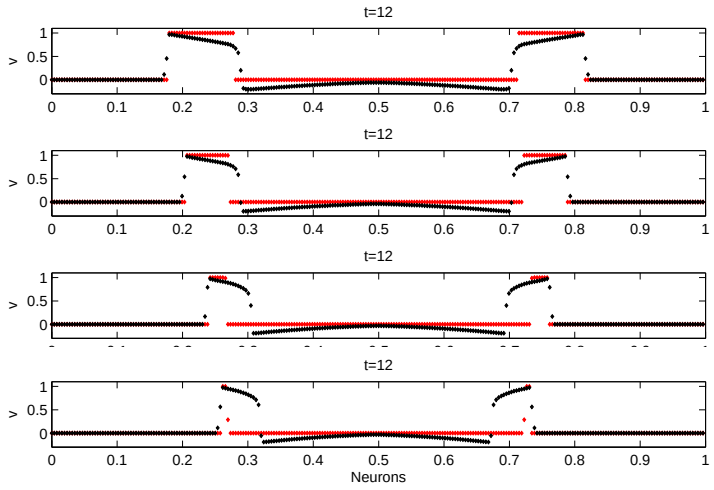

Figure 3.3: Snapshots at time $t = 12$ of dynamics within a population of $N = 256$ neurons coming from different choices of the threshold v_T. These results strengthen the expectation of a strong influence due to v_T. In the first frame $v_T = 0.7$, followed by $v_T = 0.8$ and $v_T = 0.9$, up to $v_T = 0.95$. As expected, by increasing v_T, the pulse becomes even thinner and slower

neuron with a negative reversal potential. In particular, we choose to fix a negative reversal potential to 5% of neurons uniformly distributed. The resulting dynamics has to be compared with the one in Figure 3.2. Coherently to biological attendance, neurons involved in inhibitory synapses are characterized by a membrane potential lower than the resting one during the whole dynamics. Nevertheless, all neurons return to the resting state at the end of the integration. Let us underline that the signal would abruptly disappear and neurons would suddenly return to the quiescent state, if we assumed that all synapses received from a neuron by one side are inhibitory. Figure 3.6 shows snapshots of dynamics originated in populations of neurons with different percentages of inhibitory neurons. Frames are collected at the same time instances. It is apparent that, while the number of inhibitory neurons increases, travelling pulses decrease in velocity.

3.3 Multi-dimensional dynamics

Let us now consider multi-dimensional dynamics. We first assume that neurons form a periodic lattice contained in $B = [0, 1)^m$, $m = 2$ or $m = 3$, as done in Chapter 2. Precisely, given any integer $n \geq 2$ and setting $h = 1/n$, each neuron is associated to a multi-index $l \in \{0, \cdots, n-1\}^m$, which identifies its physical position $x = hl \in B$. Thus we have $N = n^m$ distinct neurons in B, which are labelled by indices $i \in \{1, \cdots, N\}$

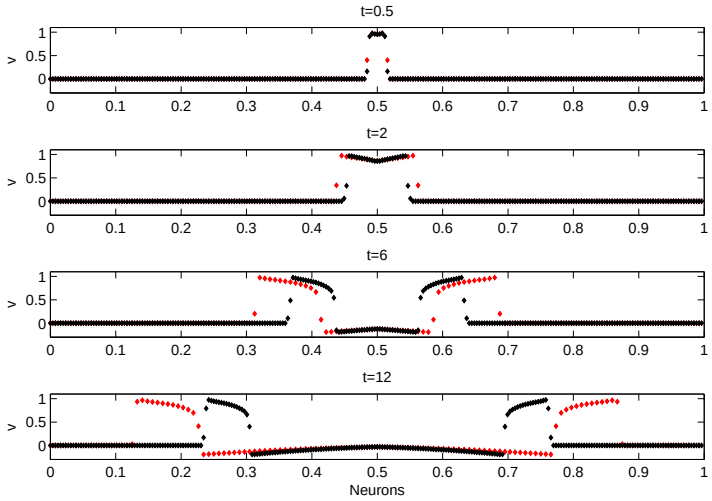

(a)

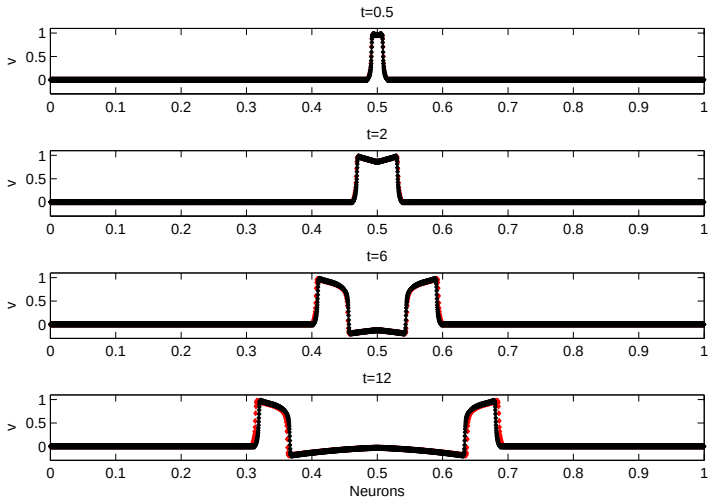

(b)

Figure 3.4: Convergence of the discrete model (3.9) as N increases. Evolution of pulses (a) for $N = 128$ (red dots) and $N = 256$ (black dots), (b) for $N = 2048$ (red dots) and $N = 4096$ (black dots)

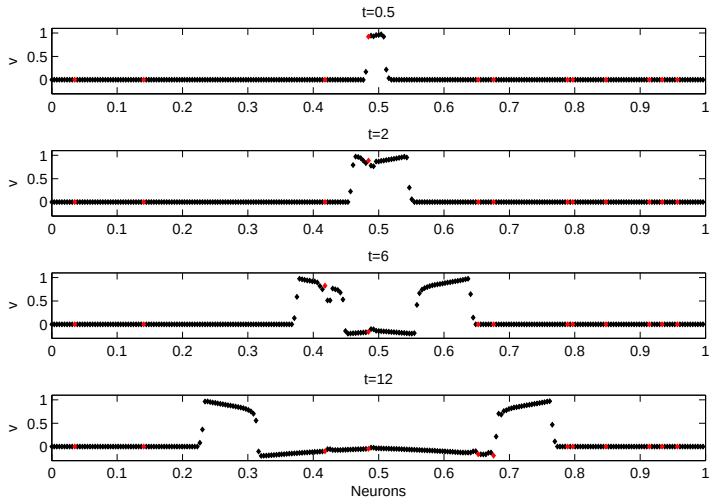

Figure 3.5: Dynamics obtained by exploiting the model (3.9). 5% of the $N = 256$ neurons are characterized by a $v^I_{\rm syn} = -0.1$ (red dots). On the contrary, cells described by black dots receive excitatory synapses. As above, $v^E_{\rm syn} = 0.9$, while the threshold is $v_T = 0.8$

according to some non-relevant rule; the $i-$th neuron has position $x_i = hl_i$, action potential v_i, recovery variable r_i and the synaptic variable s_i. These quantities are described by model (3.9) with periodic boundary conditions. By formula, periodicity means that we re-iterate the situation at $x = hl$ in any $y = h(l + nk)$ with $k \in \mathbb{Z}^m$.

According to the definition of $\mathcal{P}(i)$ in (3.10), neurons linked with the $i-$th one ($\forall i = 1, \cdots, N$) by chemical synapses belong to the *a priori* fixed area. As mentioned earlier, the number of links for each neuron, i.e., the cardinality of the set $\mathcal{P}$, affects the value of the non-zero elements of the adjacency matrix. Nonetheless, irrespective of the number of cells in the population, we select this area as a circle or a sphere with a fixed radius $r = 1/32 \simeq 0.0313$. If $n = 32$, this choice leads to four and six connections per neuron for $m = 2$ and $m = 3$, respectively; since we assume neurons to be disposed over a lattice, in all space dimensions each neuron is linked to the nearest-neighbours, as shown in Figure 3.7. Let us stress that, in the multi-dimensional case, the definition of $\mathcal{P}(i)$, stated in (3.10), is similar to that of $\mathcal{Q}^D_N$'s presented in Eq.(2.46). They do not coincide though, since as opposed to $\mathcal{P}(i)$, $|\mathcal{Q}^D_N|$ tends to zero as $N \to \infty$.

As in the one-dimensional case, the choice of parameters α, β, v_T, $g_{\rm syn}$ and r is crucial. Changing one parameter may radically modify the dynamics. We will see later on that, despite the conceptual differences they present, the range of interaction r and the threshold v_T cause similar changes in the dynamics (that becomes apparent by analysing Figures 3.9–3.10). In particular, effects on the velocity and on the thickness

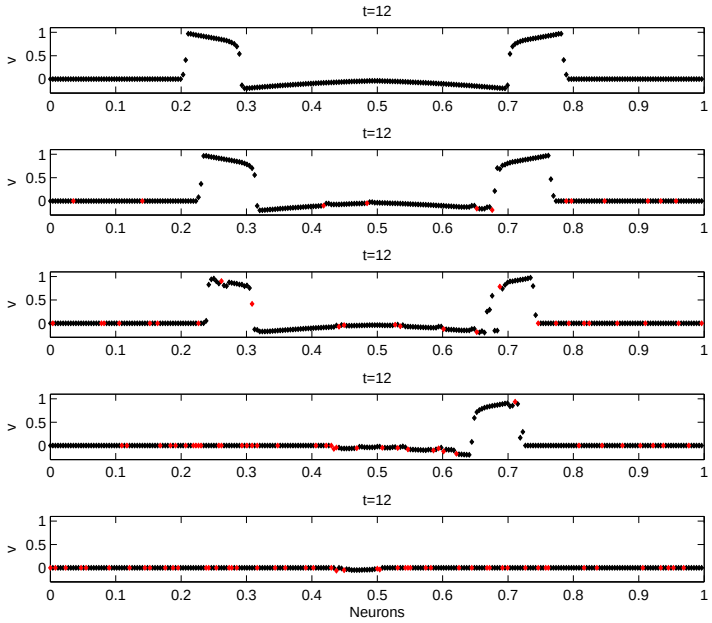

Figure 3.6: Snapshots at time $t = 12$ of dynamics within a population of $N = 256$ neurons with different percentage of inhibitory neurons. Specifically, from the top to the bottom, 0% (only excitatory neurons), 5%, 10%, 15% and 20% of inhibitory neurons are considered. While the percentage of inhibition increases, it is apparent that the velocity of the travelling pulse decreases. Moreover, the probability to have the wave diminishes. Indeed, hyperpolarization of the postsynaptic membrane due to the inhibitory synapse contrasts the wave propagation. This is the reason why in the last two snapshots one or two waves disappear. As in Figure 3.5, $v^E_{\text{syn}} = 0.9$, $v^I_{\text{syn}} = -0.1$ and $v_T = 0.8$

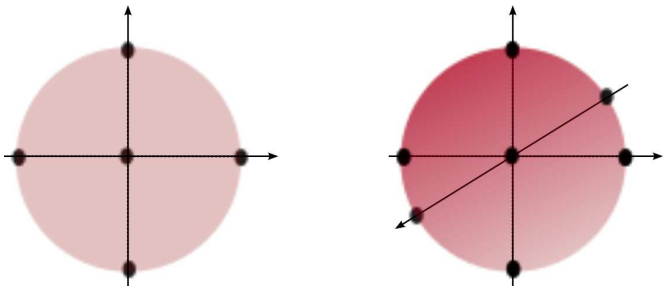

Figure 3.7: Neurons on the circumference (left) and on the surface of the sphere (right) are linked with the central node. Assuming in both cases the radius to be unitary, nearest-neighbour interactions are taken into account

of the pulses arise.

We first consider the case of excitatory neurons only. The parameters are fixed as follows:

$$\alpha_i = 0.9, \quad \beta_i = 0.1, \quad g_{\text{syn},i} = 0.1, \quad v^E_{\text{syn},i} = 0.9, \quad v_T = 0.9, \quad r = 1/32 \quad \forall i \ , \quad (3.13)$$

while the value of v^I_{syn} will be specified in the Section 3.3.3. In the sequel, possible parameter variations will be mentioned.

In order to investigate the dynamics produced by (3.9), in the following section we discuss several numerical results obtained by imposing (3.13). For the sake of simplicity, focusing on the case $m = 2$, i.e., let us consider the square box $B = [0, 1)^2$. In each numerical result, the initial stimulus $v_{t=0} = 1$ is applied to the neurons lying in the circle of radius 1/32 around the center of the box. In succession, the full-deterministic model as well as the model with stochastic parameters is taken into account.

3.3.1 Deterministic dynamics

The full-deterministic model is essential to completely understand solutions of model (3.9). Indeed, by avoiding any stochastic ingredient we are able to reveal specific features of solutions. In this section we examine three cases which concern networks' architectures at different levels of relevance from biological perspectives. Such cases allow us to qualitatively present the mathematical achievement related to the convergence of the solutions, as well as to show realistic dynamics within population of neurons.

Case A. Uniform distributed weights

Firstly, we deal with the set of connections $\mathcal{P}(i)$ defined in (3.10) such that $\mathcal{P}(i) = \mathcal{P}$ $\forall i$. Thus, we build up the adjacency matrix A_G, defined in (2.2) as a symmetric one with uniform weights values $a_{i,i+p}$ $\forall i$. As underlined before, this goes against the fundamental feature of the chemical synapses to be directional. Nonetheless, in order to qualitatively show the convergence of the solutions while the number of cells increases, we admit symmetric chemical reactions. In Figure 3.8, two-dimensional solutions of (3.9) are shown. Snapshots (a), (b) and (c) are taken at the same time instants and they differ by the number of neuron in the square box. We start in (a) with the benchmark case of $n = 32$ per side, going to $n = 64$ in (b) and up to $n = 256$ in (c). Since the connections are symmetric, the initial stimulus produces an isotropic dynamics. Let us underline that the solution is qualitatively similar to that originating from an electrical coupled network. Snapshots illustrate the initial excitation of the

cells closest to the initially stimulated points, while the farther cells are still at rest. As time passes, a steep wave front is generated and travels in the radial direction from the center to the boundaries. As described by the nonlinear term due to FitzHugh-Nagumo model, a repolarizing wave tail follows the wave front; it describes a travelling pulse. Furthermore, these plots qualitatively document the convergence of the discrete dynamics as n increases. As underlined before, the range of interactions r determines the properties and the evolution in time of the travelling pulses. Figure 3.9 shows the evolution of the travelling pulses by considering different ranges of interactions. In order to allow the comparison, snapshots are taken at the same time. Specifically, the radius are $r = 1/64$ and $r = 1/16$ in Figures 3.9 (a) and (b), respectively. These dynamics should be compared to that in Figure 3.8 (c). Since r is the only changing parameter, it is apparent how it qualitatively affects the evolution of the solutions. First of all, the larger is the radius r, the quicker is the travelling pulse. This is due to the fact that a larger number of linked neurons leads to a faster propagation of signals within the lattice. Moreover, the pulse involves greater excited neurons than in Figure 3.8 (c). In other words, the ring-shaped pulse becomes thicker. On the contrary, by considering half the radius as in (b), a slower pulse arises. The number of excited neurons involved are now less than in (b), thus we say the pulse becomes thinner. Similar effects on pulse's speed and shape can be obtained by considering different values of the threshold v_T, as documented in Figure 3.10.

In almost all dynamics of this chapter, we consider neurons placed over a regular grid in the domain. In the case of uniform distributed weights we anticipate a more realistic framework which will be used in the following chapters. Indeed, in order to make the neuron positions over a slice more realistic, we exploit a triangular decomposition of the domain which is borrowed from the FEM technique. Focusing on the two-dimensional domain, $B = [0, 1)^2$, we use a Matlab triangular mesh generator called BBTR described in [6]. Adopting a triangular mesh, two improvements are carried out. Fistly, distance between two nearest neighbour neurons, which are represented by the triangle vertices, is not constant. Secondly, domain subregions with different mesh refinement may be considered. This means that subregions with different density of neurons, as well as the absence of neurons, are affordable. In Figure 3.11, the same problem which leads to the dynamics shown in Figure 3.8 has been solved. In the case of the triangular domain decomposition, the number of neurons is 10319. Let us note that, despite we abandoned the regular grid in favour of an unstructured one, the solution converges to those in Figure (3.8) (c).

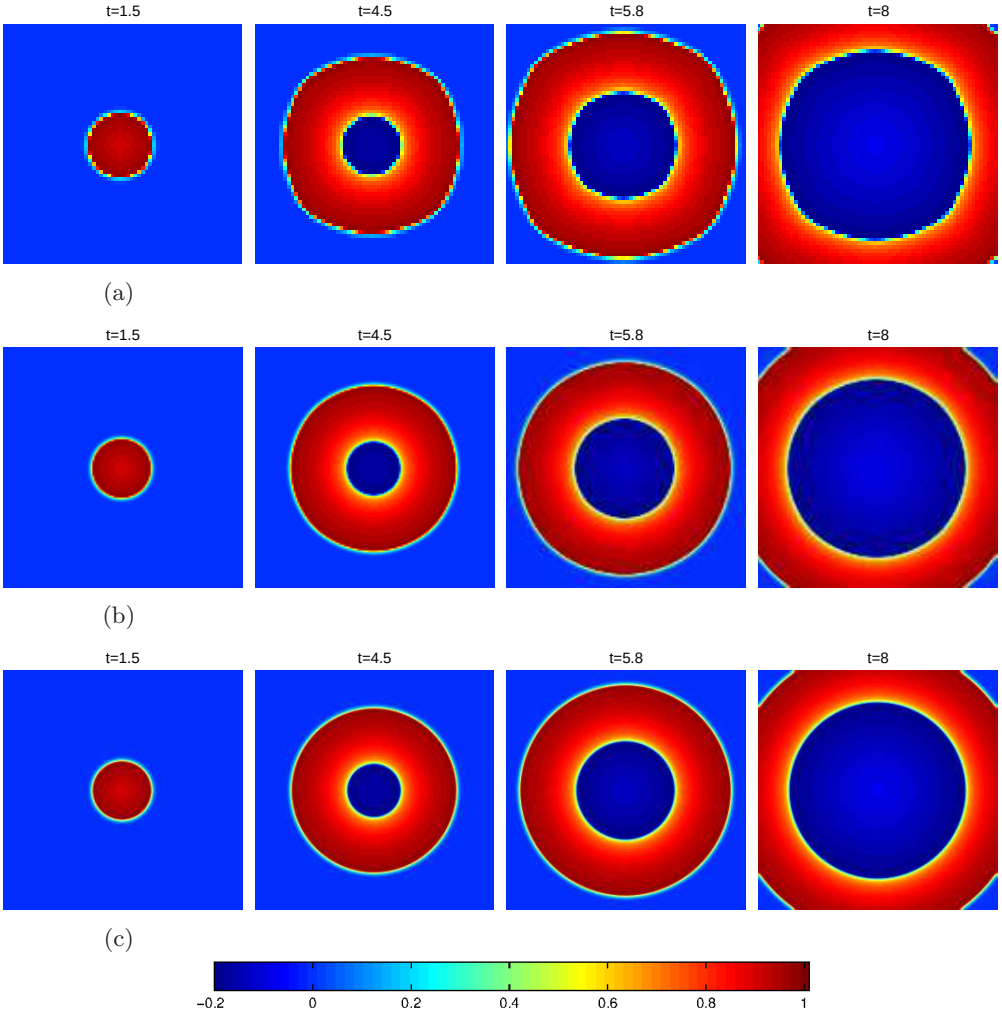

Figure 3.8: Convergence of the solutions of discrete model (3.9) by considering different $N = n^2$. Evolution of pulse (a) for $n = 32$, (b) for $n = 128$ and (c) for $n = 256$.

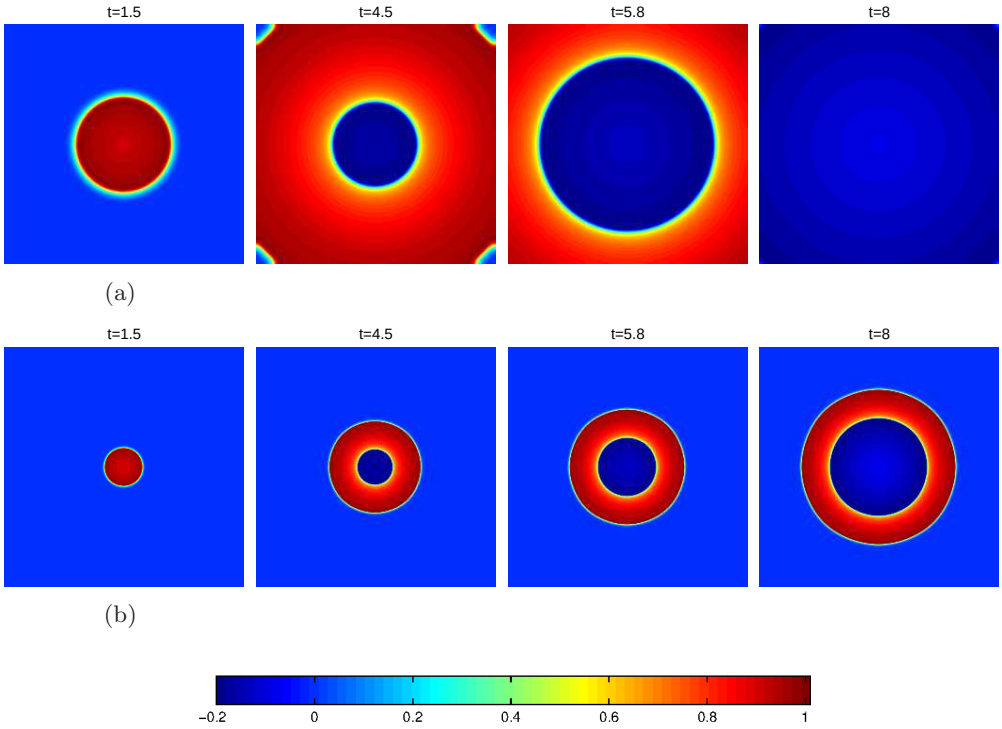

Figure 3.9: Evolution of the travelling pulse in the square lattice with $n = 256$. The only difference with Figure 3.8-(c) is a different value of r which was $r = 1/32$. Now, $r = 1/16$ in (a) while $r = 1/64$ in (b). Differences in velocity and thickness of the travelling pulse are evident

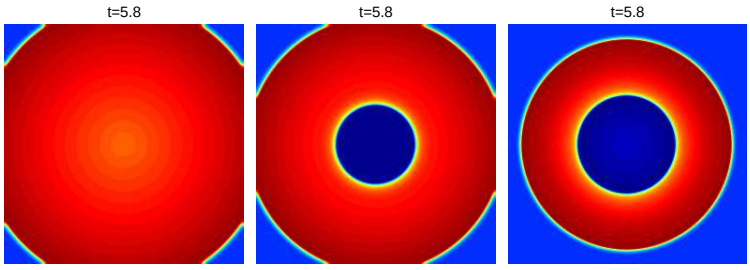

Figure 3.10: Dynamics at $t = 5.8$ obtained by choosing different threshold values. The first frame refers to $v_T = 0.7$, the second to $v_T = 0.8$ while the third one involves $v_T = 0.93$ as in Figure 3.8. It is apparent that changes in the threshold value provoke different thickness of the pulses. Despite the threshold value and radius of interactions are not similar from a conceptual perspective, comparing these snapshots with those in Figure 3.9, becomes evident that they produce rather similar effects on the travelling pulses

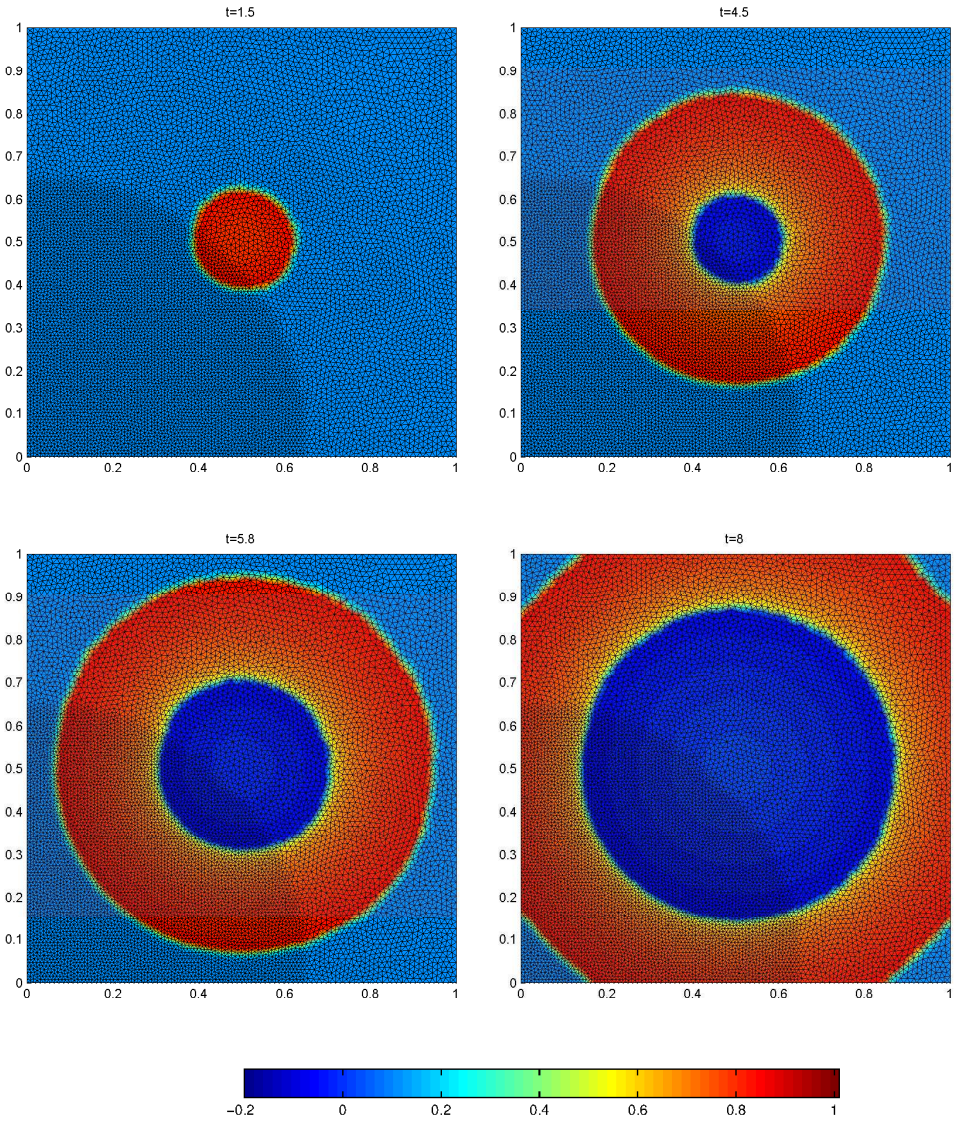

Figure 3.11: Development of the travelling pulse in the square block with 10319 neurons placed at the vertices of the triangles. Each neuron receives chemical input from those which belong a circle of radius 1/16 (of which it is the center). Two areas with different neuronal densities are considered. Despite this new approach, with in addition a non-uniform mesh, a qualitative comparison between this dynamics and those in Figure 3.8 (c) leads to the conclusion that these travelling pulse are similar. Thus, the triangular decomposition does not affects the solution

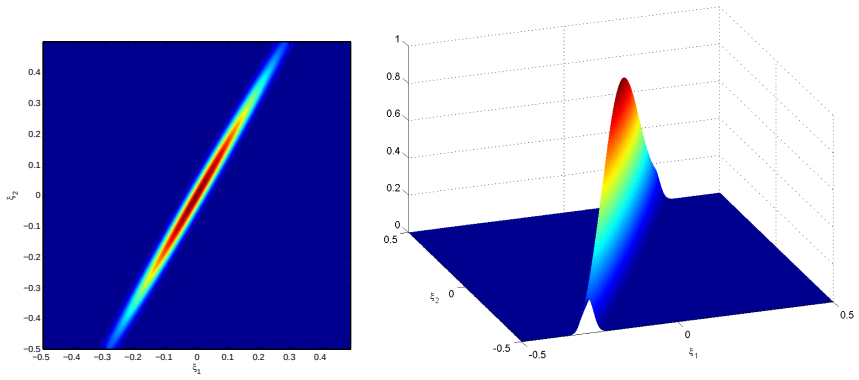

Figure 3.12: Plots with different visualizations of the Gaussian function stated in (3.12) having $\theta = \pi/3$ and $\sigma_{\xi_2}/\sigma_{\xi_1} = 20$

Case B. Gaussian distributed weights

Moving towards more realistic network architectures, let us first vary the weights of connections in the adjacency matrix according to a given (still deterministic) rule. In this way, a hierarchy in synapse efficacy is created. For this purpose, let us introduce the Cartesian coordinates $\xi \in \mathbb{R}^2$. A two-dimensional Gaussian function plays the key role in assigning the weight to each connection. Let us consider the Gaussian function

$$\mathcal{N}_\theta(\xi) = \exp\{-a\xi_1^2 + 2b\xi_1\xi_2 + c\xi_2^2\} \,, \tag{3.14}$$

centred at the origin with

$$a = \frac{\cos^2(\theta)}{2\sigma_{\xi_1}^2} + \frac{\sin^2(\theta)}{2\sigma_{\xi_2}^2} \qquad b = \frac{\sin(2\theta)}{4\sigma_{\xi_1}^2} - \frac{\sin(2\theta)}{4\sigma_{\xi_2}^2} \qquad c = \frac{\sin^2(\theta)}{2\sigma_{\xi_1}^2} + \frac{\cos^2(\theta)}{2\sigma_{\xi_2}^2} \,.$$

A three-dimensional representation of $\mathcal{N}_\theta(\xi)$ is proposed in Figure 3.12.

The parameters σ_{ξ_1}, σ_{ξ_2} are the ξ_1 and ξ_2 spreads of the blob and θ determines its angle with respect to the horizontal axis. In particular, we choose $\sigma_{\xi_2}/\sigma_{\xi_1} = 20$. Let us underline that the Gaussian function (3.14) provides values between zero and one accordingly to the distance from the centre $(0, 0)$. Considering the set $\mathcal{P}$ defined in (3.10) and fixing θ, e.g. $\theta = \pi/3$, the Gaussian function $\mathcal{N}_\theta(x - x_i)$ assigns weights to all neurons lying in the circle of radius r with respect to each cell. Figure 3.13 shows the obtained dynamics. The choice $\theta = \pi/3$ as the direction of the strongest links is reflected by the fact that the pulse triggered by the initial datum presents an axial symmetry with respect to the line $\xi_2 = \tan(\pi/3)\xi_1$ in the domain $B = [0, 1)^2$.

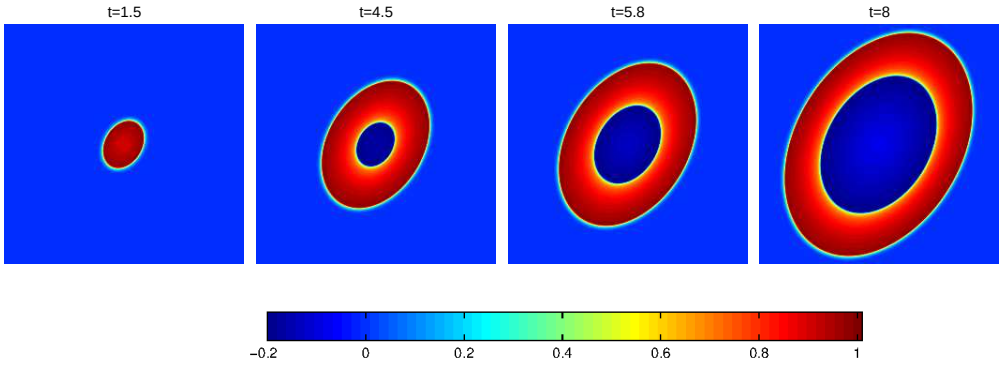

Figure 3.13: Evolution of the travelling pulse in the square lattice with $n = 256$. The Gaussian function (3.14) with $\theta = \pi/3$ determines link weights for each neuron of the lattice. If we considered homogeneous weights, Figure 3.8 (c) would be the result

Differently from the dynamics in Figure 3.8, weights are modified (reduced) according to the Gaussian distribution. By comparing solutions in Figure 3.13 and 3.8 (c), it becomes apparent that the weight reductions turn in a slower pulse.

In order to introduce heterogeneity in the connection rule among neurons, i.e., allowing $\mathcal{P}(i)$ to depend on the neuron i, the angle θ in (3.14) can be determined according to some specific law. For example, let us introduce the vector field $\Phi : X \to (\alpha \sin^2(2\pi\xi_1), 1 + \beta\cos(2\pi\xi_2))$, where $X = (\xi_1, \xi_2) \subseteq [0,1)^2$, $0 < \alpha \leq 1$ and $0 < \beta < 1$. Thus, for the neuron placed at $\bar{X} = (\bar{\xi_1}, \bar{\xi_2})$, we set

$$\theta = \theta_{\bar{X}} = \arctan\left(\frac{1 + \beta\cos(2\pi\bar{\xi_2})}{\alpha\sin^2(2\pi\bar{\xi_1})}\right) . \tag{3.15}$$

By fixing $\alpha = 1$ and $\beta = 0.5$, the corresponding dynamics is shown in Figure 3.14. As another example, the dynamics obtained with the same values of α and β by exploiting the vector field $\Psi : X \to (\alpha\sin(2\pi\xi_1), 1 + \beta\cos(2\pi\xi_2))$ is presented in Figure 3.15. In this case,

$$\theta_{\bar{X}} = \arctan\left(\frac{1 + \beta\cos(2\pi\bar{\xi_2})}{\alpha\sin(2\pi\bar{\xi_1})}\right) . \tag{3.16}$$

Case C. Unidirectional synapsess

We finally reach the notable case of unidirectional synapses. To perform dynamics consistent with the reality, this ingredient is fundamental. We decide to deal with unidirectional synapses by selecting connections lying in half a circle of radius equal to

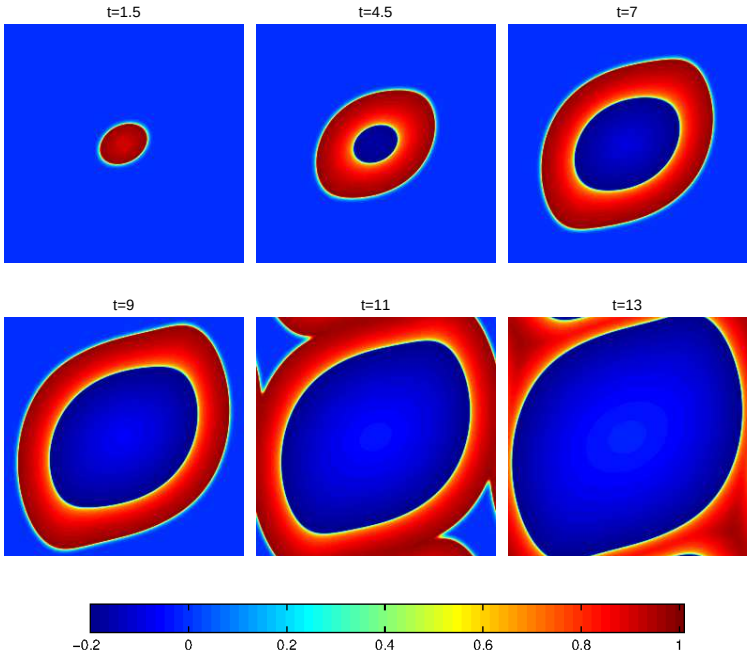

Figure 3.14: Development of the travelling pulse in the square lattice with $n = 256$ in which the angle θ, assigned to each neuron in the Gaussian function (3.14), is determined by (3.15)

the range of interactions for each neuron, which is a subset of $\mathcal{P}$. In formulae,

$$\mathcal{P} = \{p : \|x_{i+p} - x_i\| \leq r \quad \text{and} \quad x_{i+p,2} - x_{i,2} + \frac{1}{\tan\theta}(x_{i+p,1} - x_{i,1}) \leq 0\} \,. \tag{3.17}$$

This choice translates in exploiting the Gaussian function $\mathcal{N}_\theta(\xi)$ given in (3.14) for defining weights of connections, and to impose $\xi_2 - \bar{\xi_2} + \frac{1}{\tan\theta}(\xi_1 - \bar{\xi_1}) \leq 0$ to consider connections in half the plane. In Figure 3.16, snapshots of unidirectional chemical synapses are shown. In this case also, $\theta = \pi/3$. The first four frames should be compared with those in Figure 3.13, where non-directional synapses are taken into account.

3.3.2 Quasi-deterministic dynamics

In order to inject a certain degree of stochastic heterogeneity in the network topology, let us vary the weights in the adjacency matrix according to a non-deterministic rule. Specifically, we exploit the Gaussian function defined in (3.14) and we consider the angle θ as a random variable uniformly distributed in $[0, \pi[$ for each neuron of the lattice. As in Case B above, the corresponding Gaussian function assigns suitable weights to neurons

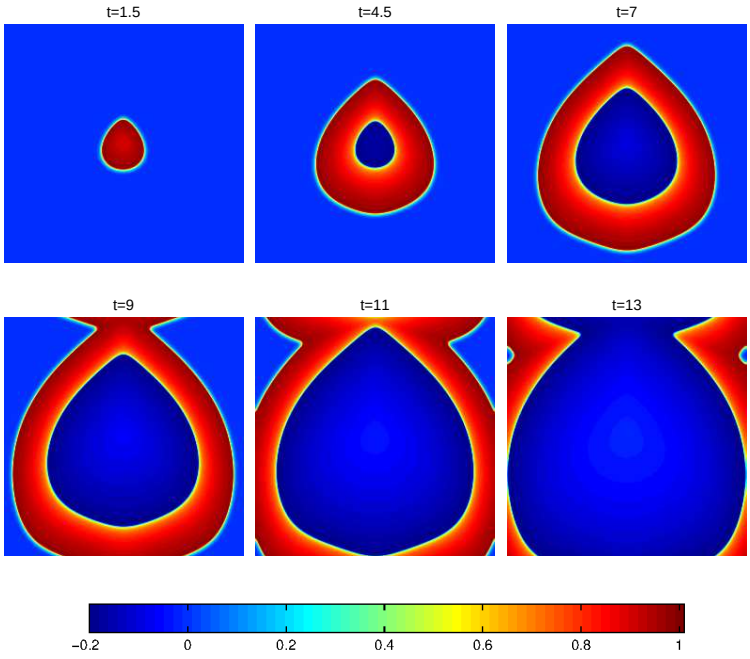

Figure 3.15: Development of the travelling pulse in the square lattice with $n = 256$ in which the angle θ, assigned to each neuron, in the Gaussian function (3.14) is determined by (3.16)

lying in the circle of radius r, but now $\mathcal{P}(i)$ does depend upon i. Figure 3.17 shows the resulting dynamics at the same time instants of Figure 3.8 (c). The random effects on the pattern are apparent. Firstly, contours of the pulse are irregular as highlighted in Figure 3.18. Secondly, since weights in the adjacent matrix are decreased according to the Gaussian function, the pulse travels with a lower speed than in the deterministic case.

To complete the present section, the case of unidirectional random dynamics is presented. As in Section 3.3.1, Case C, the connection weights are assigned by exploiting (3.14) intersected with $\xi_2 - \bar{\xi}_2 + \frac{1}{\tan\theta}(\xi_1 - \bar{\xi}_1) \leq 0$. Moreover, we consider the angle θ as a random variable uniformly distributed in $(\pi/3 - \pi/4, \pi/3 - \pi/4]$ for each neuron of the lattice. Differently from the dynamics in Figure 3.16, it becomes evident that the pulse velocity is significantly lower and that the contour of the pulse are irregular.

3.3.3 The effect of inhibitory neurons

In order to make a parallelism with what done in the one-dimensional case, let us consider both excitatory and inhibitory synapses. The parameters are the same as in

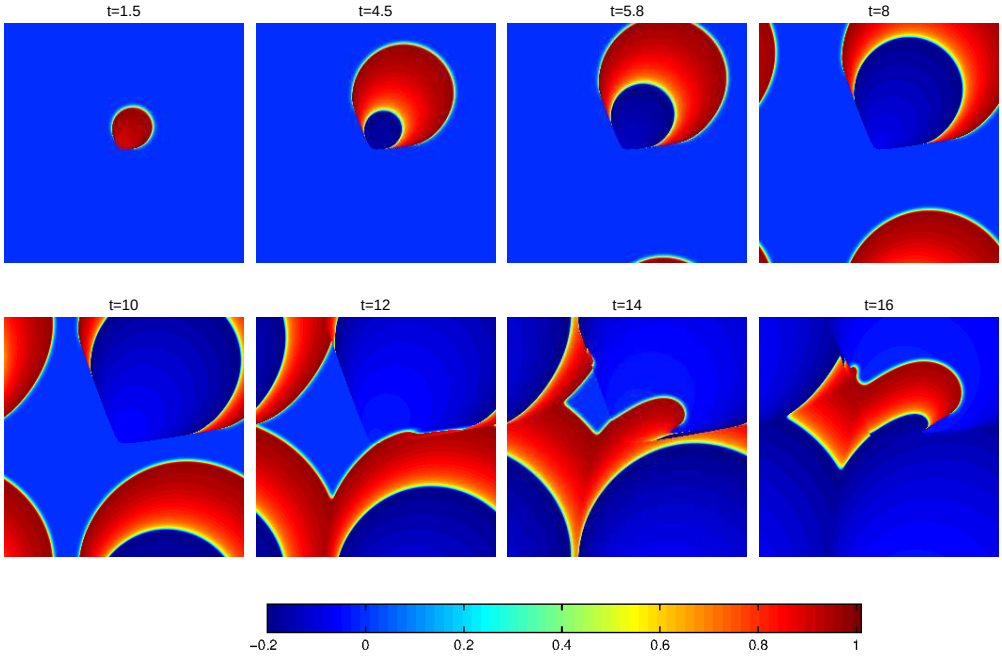

Figure 3.16: Development of the travelling pulse in the square block with $n = 256$. With respect to each neuron, the Gaussian function (3.14) with $\theta = \pi/3$ determines link weights for those connected with it. Furthermore, among them, zero weights are imposed to those neurons lying in $\xi_2 - \bar{\xi_2} + \frac{1}{\tan\theta}(\xi_1 - \bar{\xi_1}) \leq 0$

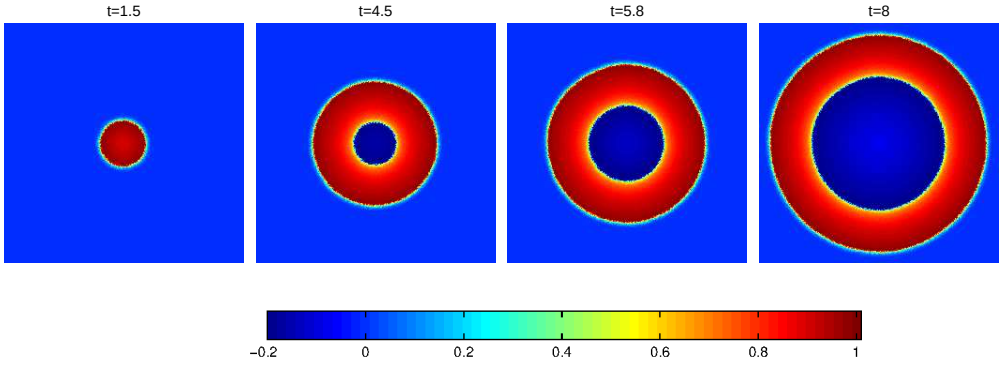

Figure 3.17: Development of the travelling pulse in the square lattice with $n = 256$ in which the Gaussian function (3.14), that determines the link weights, is considered. The angle θ assigned to each node of the lattice is randomly chosen with uniform distribution on $[0, \pi)$

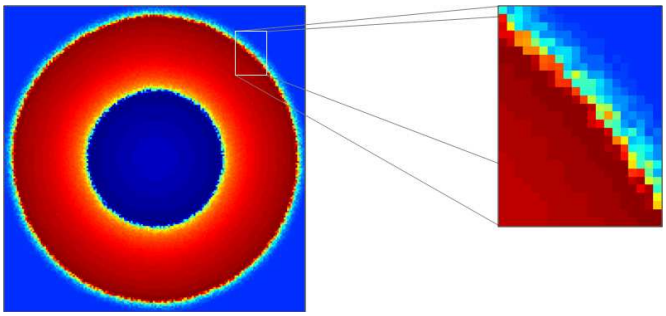

Figure 3.18: To stress the effect of the random ingredient in Figure 3.17, we focus on an enlarged detail of the snapshot at $t = 5.8$: contour of the pulse is irregular

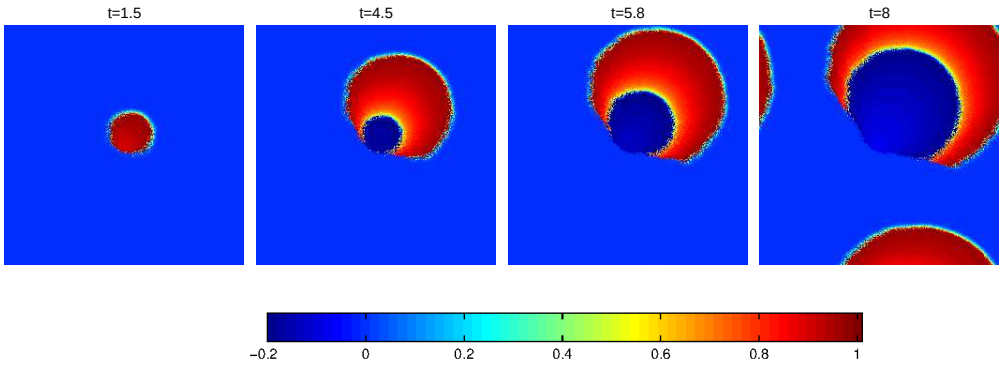

Figure 3.19: Development of the travelling pulse in the square block with $n = 256$. With respect to each neuron, the Gaussian function (3.14), with θ as a random variable uniformly distributed in $(\pi/3 - \pi/4, \pi/3 - \pi/4]$, determines link weights for those connected with it. Furthermore, among them, zero weights are imposed to those neurons lying in $\xi_2 - \bar{\xi}_2 + \frac{1}{\tan\theta}(\xi_1 - \bar{\xi}_1) \leq 0$

(3.13), with the exception of the $v^E_{\text{syn},i}$ now set to 0.93 for each i excitatory neuron. Moreover, the inhibitory reversal potential $v^I_{\text{syn},i}$ is fixed to -0.9 for each i inhibitory neuron.

Figure 3.20 shows dynamics originated in cell populations with different percentages of inhibitory neurons. It becomes apparent that, while the percentage of inhibitory neurons increases, travelling pulses have even less regular boundary shapes and decrease in velocity. In the Figure 3.20 (a) (b) and (c), despite inhibition does not preclude the propagation of the excitation in these dynamics, it clearly reduces the neural excitatory activity. On the contrary, the wider inhibition stops the excitation phenomenon at $t = 17$.

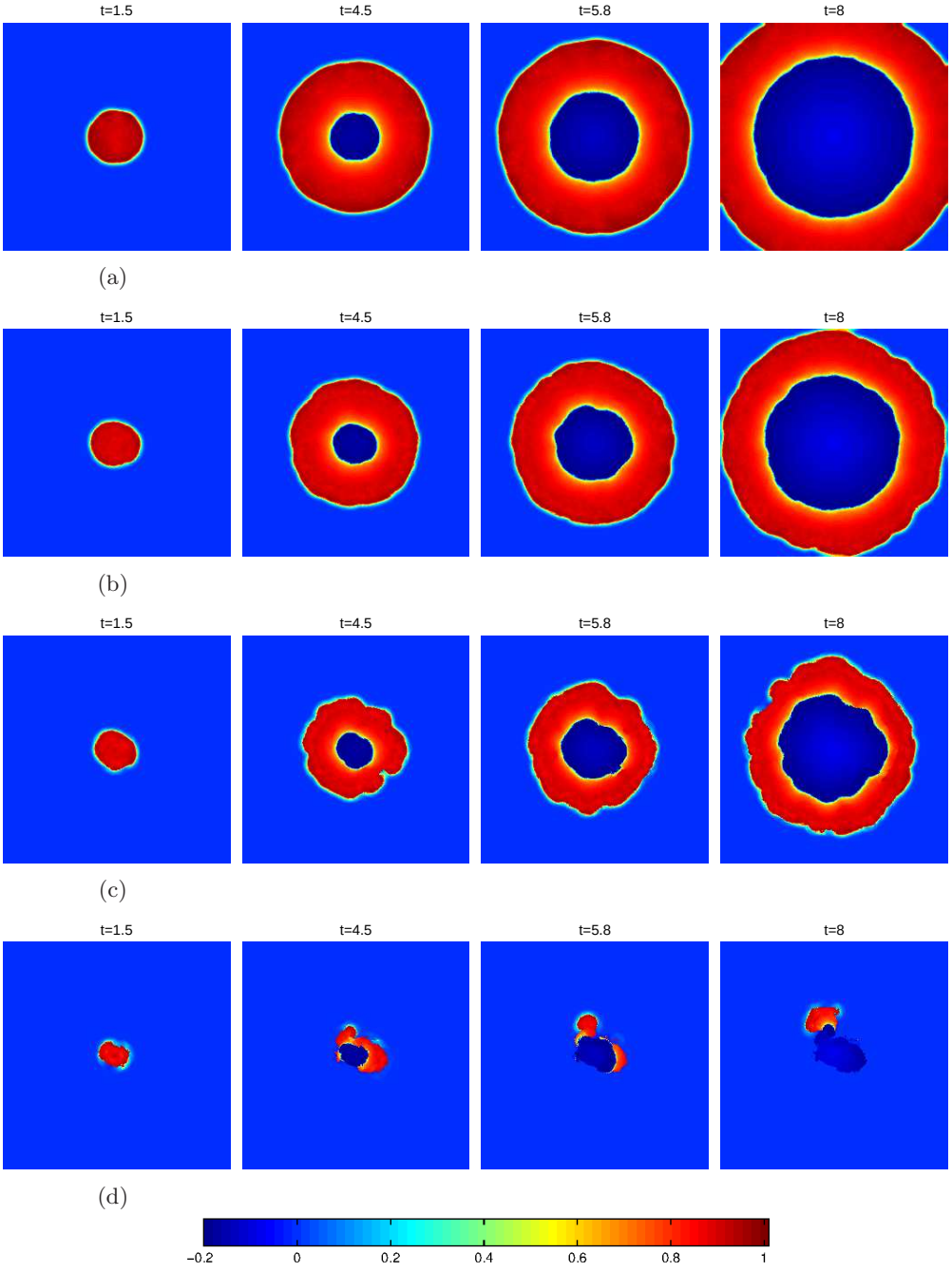

Figure 3.20: Solutions of the discrete model (3.9) by considering different percentage of inhibitory neurons. Notably, evolution of wave pulse for (a) 5%, (b) 10%, (c) 15%, and (d) 20% of them. We considered $v_{\mathrm{syn}^{\mathrm{E}},i} = 0.93$ for each i-th excitatory cell and $v_{\mathrm{syn}^{\mathrm{I}},i} = -0.9$ for each i-th inhibitory one. Snapshots in (a)-(d) show even less regular boundary shapes and the respective pulse velocity decreases. Excitation in dynamics (d) stops at $t = 17$

Chapter 4

Ensemble of electrical and chemical synapses

In Chapters 2 and 3 we investigated the membrane potential dynamics within populations of neurons, assuming that their coupling involve synapses of a single type, either electrical or chemical. This was clearly done in order to highlight the effects due to each type. Since our aim is to study realistic neuronal networks, the fundamental step is to put both the coupling types together. In the following, we will build up the complete model. Afterwards, we will provide a characterization of the synchronization phenomena.

4.1 The complete model

In order to describe a realistic neuronal network, we have to take into account that the input current for each neuron is the result of both electrical and chemical coupling interactions, i.e.,

$$I = I_{\text{gap}} + I_{\text{syn}} \ , \tag{4.1}$$

where I_{gap} and I_{syn} are defined in (2.1) and (3.1), respectively. Referring to each cell, the currents $I_{\text{gap},i}$ and $I_{\text{syn},i}$ assume expressions widely explained in Chapters 2-3.

In order to get across the following treatments, let us consider a generic unstructured decomposition of the domain $B = [0,1]^m$, where $m = 1, 2, 3$. Accordingly, $x_i \in \mathbb{R}^m$ describes the position of that cell i.

Concerning the current due to electrical synapses, $I_{\text{gap},i}$, we define $\mathcal{Q}(i)$ collects the

neurons linked by gap-junctions as follows:

$$\mathcal{Q}(i) = \{q \in \mathbb{Z}\backslash\{0\} : \ i+q \text{ and } i \text{ are nearest-neighbours}\} \ . \tag{4.2}$$

Imposing that each neuron is linked with its contiguous ones, it implies that, as biophysically reasonable, signals flow through gap-junctions in both directions. Furthermore, we let the diffusion coefficient to grow with the number of neurons N (thus, $d = d_N$). In formulae,

$$I^i_{\text{gap}} = d_N \sum_{q \in \mathcal{Q}(i)} (v_{i+q} - v_i) \ . \tag{4.3}$$

The $I_{\text{syn},i}$ current input in (4.1) takes into account currents produced by chemical synapses. Due to the biophysical considerations described in Chapter 3, we set

$$I^i_{\text{syn}} = g_{\text{syn},i} \left(\sum_{p \in \mathcal{P}(i)} w_{i,i+p} s_{i+p} (v_i - v_{\text{syn},i+p}) \right) \ , \tag{4.4}$$

where the set $\mathcal{P}(i)$ collects indexes p such that neurons $i+p$ influence the cell i via chemical synapses. Specifically, with respect to each cell, links exist over a substantial area which remains fixed as $N \to \infty$. One of the possible definitions of $\mathcal{P}(i)$, suggested in (3.10), is

$$\mathcal{P}(i) = \{p \in \mathbb{Z}\backslash\{0\} : \|x_{i+p} - x_i\| \leq r_i\} \ ,$$

i.e., $\mathcal{P}(i)$ collects all the neuron indexes belonging to a circle centred in i and having radius r_i. Let us note that non-homogeneous weights $w_{i,i+p} \ \forall p \in \mathcal{P}(i)$ can be introduced by exploiting, for example, the Gaussian function (3.14) as done in Section 3.3.1, Case B.

Taking into account (4.3) and (4.4), the whole system takes the following representation:

$$\begin{aligned}
\frac{\mathrm{d}v_i}{\mathrm{d}t} &= f(v_i, r_i) + d_N \sum_{q \in \mathcal{Q}(i)} (v_{i+q} - v_i) - g_{\text{syn},i} \left(\sum_{p \in \mathcal{P}(i)} w_{i,i+p} s_{i+p} (v_i - v_{\text{syn},i+p}) \right) \ , \\
\frac{\mathrm{d}r_i}{\mathrm{d}t} &= g(v_i, r_i) \ , \\
\frac{\mathrm{d}s_i}{\mathrm{d}t} &= \alpha_i (1 - s_i) H_\infty (v_i - v_T) - \beta_i s_i \ .
\end{aligned} \tag{4.5}$$

The continuum model can be derived from the discrete one (4.5) by letting the

number of cells tend to infinity. Notably, in the limit case of $N \to \infty$, this model leads to the following integro-differential equation system:

$$\begin{aligned}
\frac{\partial v}{\partial t} &= f(v(x,t), r(x,t)) + d^* \Delta v - g_{\text{syn}} \left(\int_{y \in \mathcal{B}(x)} w(x,y) s(y,t) (v(x,t) - v_{\text{syn}}(y)) \, \mathrm{d}y \right) , \\
\frac{\partial r}{\partial t} &= g(v(x,t), r(x,t)) \ , \\
\frac{\partial s}{\partial t} &= \alpha (1 - s(x,t)) H_\infty (v(x,t) - v_T) - \beta s(x,t) \ .
\end{aligned} \tag{4.6}$$

Here, instead of (2.52) in which a convective term is present as the limit of the electrical discrete coupling, for the sake of simplicity the only diffusive term is taken into account. This means that all gap-junctions are here supposed to be non-rectifying synapses. Moreover, $\mathcal{B}(x) \subseteq B$ is the small fixed area which collects the continuum of cells linked with that in x; notably, it remains fixed as $N \to \infty$. A proof of the well-posedness for the system (4.6) will be presented in Section 4.3.

Despite in the following section an unstructured mesh decomposition will be considered, in order to show membrane potential dynamics produced by the discrete model (4.5), we first consider neurons collected over a periodic lattice contained in $B = [0,1)^m$, $m = 2$, as formalized in Chapter 2.

Let us underline that, thanks to a regular domain decomposition, the definition of $I_{\text{gap},i}$ in (4.3) corresponds to Approach I explained in Chapter 2. This choice implies that if we compare solutions obtained with different N, we would rescale the diffusion coefficient. Here, this selection is due to experimental reasons which underline the high probability of finding gap-junctions among neighbouring cells. In order to avoid the vanishing of the diffusion phenomenon as $N \to \infty$, an alternative way is called Approach II. It involves links among not only nearest-neighbours, which are chosen accordingly to a suitable function of N, together with a fixed diffusion coefficient. Both approaches are fully described in Chapter 2. Furthermore, let us consider the set which takes into account chemical synapses, $\mathcal{P}(i)$, as in Section 3.3.1; in particular, Cases B and C.

By applying an initial stimulus to the neurons lying in the circle of radius 1/32 around the center of the box, a travelling pulse is originated. The strengths of electrical and chemical couplings, i.e., the parameters d_N (4.3) and g_{syn} in (4.4), play a fundamental role in determining the solution. In other words, by varying the parameter values, a hierarchy between the electrical and chemical phenomena is generated.

The dynamics we are showing first involve bidirectional chemical synapses, i.e., $\mathcal{P}(i)$

as in (3.10). In Figure 4.1, the strength of the chemical interactions g_{syn} is maintained fixed to 0.1, while the diffusion coefficient changes; specifically, in the dynamics depicted in Figure 4.1 (a)-(b)-(c), it takes the values $d = 0.05$, $d = 0.01$ and $d = 0.005$, respectively. Comparing these three cases, it becomes apparent that the electrical transmission strength influences the shape and the velocity of the travelling pulses. In the first slot of snapshots, the diffusion coefficient $d = 0.05$ causes the preponderance of the electrical diffusion phenomenon over the chemical one. Thus, since electrical connections involve nearest neighbour neurons as in Figure 3.7, a nearly isotropic dynamics arises. By diminishing the diffusion coefficient d to 0.01, the travelling pulse shape elongates according to the weights assigned to the excitatory chemical connections. When $d = 0.005$, electrical synapses become too weak to cause an isotropic pulse propagation and chemical synapses determine the dynamics: an elongated pulse mainly propagated along one direction, as imposed by the gaussian distributed weights.

As performed in Chapter 3, a notable case is to consider unidirectional chemical interactions. This choice translates into imposing, for each neurons having position (ξ_1, ξ_2), connections lying in the half plane $\xi_2 - \bar{\xi_2} + \frac{1}{\tan\theta}(\xi_1 - \bar{\xi_1}) \leq 0$, as fully explained in Section 3.3.1, Case C. This condition, joined to weights defined by the normal distribution (3.14), leads to the dynamics shown in Figure 4.2. In this particular case, chemical synapses among nearest neighbour neurons and unidirectional chemical synapses co-exist. Here parameters are $\theta = \pi/3$, as in Figure 3.13, $d = 0.01$ and $g_{\text{syn}} = 0.1$. The other values are set as in Section 3.3. Whenever a non-null initial datum is imposed in the center of the domain, the result is a travelling pulse toward the boundaries having a preferred direction due to the chemical synapse unidirectionality. However, it is apparent that the pulse propagation takes place in all directions, different to what is described in Figure 3.16. This is due to the presence of electrical synapses.

4.2 Synchronous and asynchronous states

Synchronization in neuronal network is a widely studied topic. It operates in, among others, the fundamental phenomenon of the synaptic plasticity. In large neuronal networks different dynamics can be observed, from chaotic to spatially or temporally regular patterns. When network activity is uniform on the whole domain at the same time, we say that a synchronous activity arises. In order to mathematically characterize the synchronous phenomenon, we introduce a synchronization measure. There exist many of them in literature. For example, one of those presented in [1] involves a cross-correlation function which compares activity of couples of neurons across different

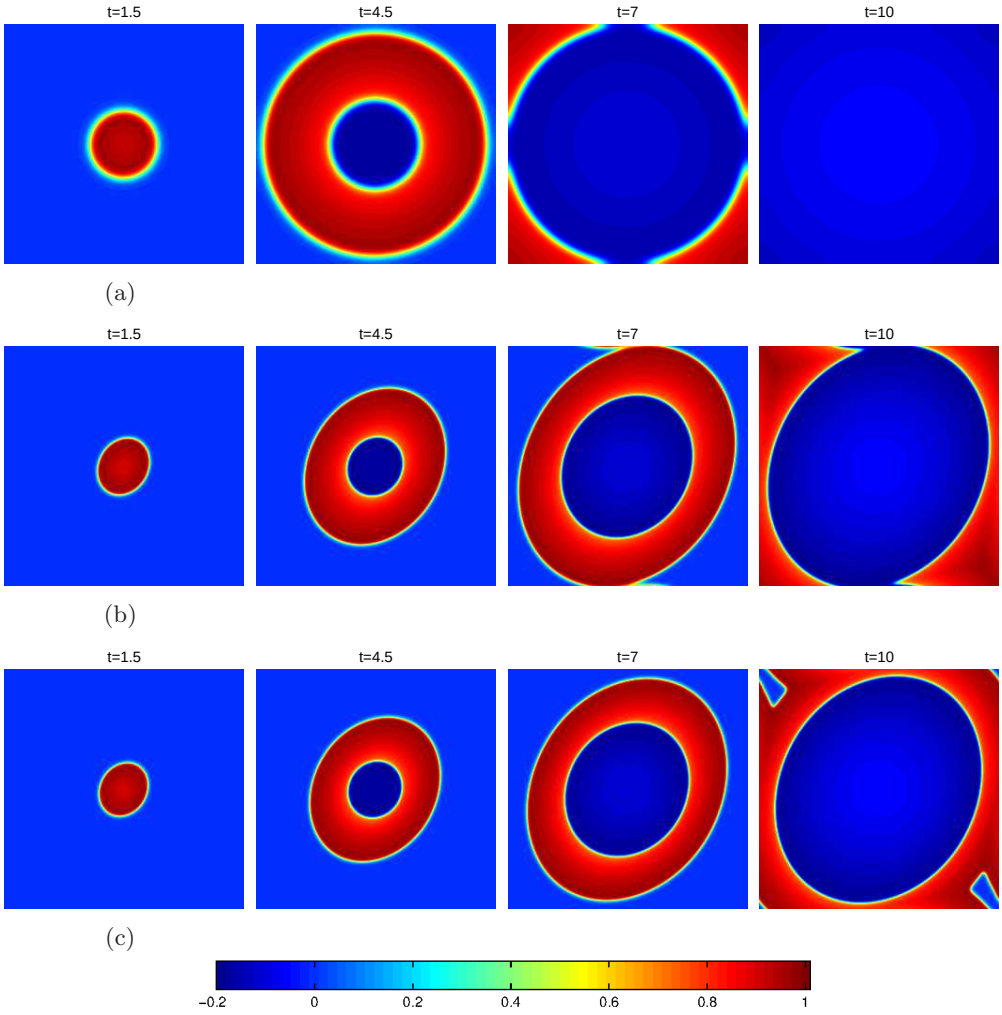

Figure 4.1: Solutions of discrete model (4.5) obtained by considering different values of the diffusion coefficient d while the chemical coupling strength is fixed at $g_{\text{syn}} = 0.1$. Specifically, in (a), $d = 0.05$. In (b), $d = 0.01$ and $d = 0.005$ in (c)

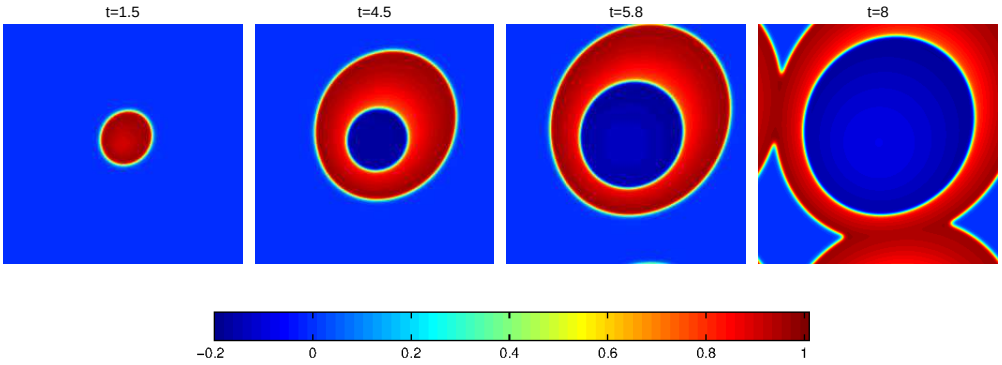

Figure 4.2: Development of the travelling pulse in the square block of $n = 256$. Each neuron is linked to its nearest neighbours by gap-junctions and with those lying in a half circle of radius r by chemical synapses. In particular, chemical synapse weights are imposed by exploiting the Gaussian function (3.14) with the angle $\theta = \pi/3$. In consequence, the active chemical synapses in half circle are determined by imposing $\xi_2 - \bar{\xi}_2 + \frac{1}{\tan\theta}(\xi_1 - \bar{\xi}_1) \leq 0$. The diffusion coefficient d is let to 0.05

time delays. Since this activity is influenced by the synchronization degree, it provides a synchronization measure of the system. Another kind of relevant measure for phase models, fully described in [35], involves the phase coordinate of each single neuron. Within the wide variety of synchronization measures, some of them refer to the fluctuations of the potential v. Our choice, explained in [22], defines the synchronization measure by averaging the fluctuations over a long time and by normalizing the variance value. Specifically, the first step consists in evaluating the average potential $v(t)$ at a given time t:

$$v(t) = \frac{1}{N}\sum_{i=1}^{N} v_i(t) \; .$$

This quantity describes the system behaviour in terms of population-averaged voltage. Furthermore, the variance of the time fluctuations of $v(t)$ is

$$\sigma_v^2 = \Big\langle [v(t)]^2 \Big\rangle_t - \Big[\langle v(t) \rangle_t\Big]^2 \; ,$$

where $\langle \cdots \rangle_t = 1/T \int_0^T \cdots \mathrm{d}t$ denotes the time-averaging over a large time T. At this stage, a normalization of σ_v^2 to the average over the single cell membrane potentials is needed. This leads to the definition of

$$\chi^2(N) = \frac{\sigma_v^2}{\frac{1}{N}\sum_{i=1}^{N} \sigma_{v_i}^2} \; , \tag{4.7}$$